CONTRACT AF (052)-923 28 FEBRUARY 1967

FINAL SCIENTIFIC REPORT

PHYSICS OF AGEING IN THIN FILM RESISTORS: OXIDATION OF CLEAN CHROMIUM FILMS

1 FEBRUARY 1966 - 31 JANUARY 1967

WILLIAM A. CROSSLAND
COLLIN A. MARR
H. THEO ROETTGERS

STANDARD TELECOMMUNICATION LABORATORIES LIMITED
LONDON ROAD
HARLOW, ESSEX,
ENGLAND

THIS RESEARCH HAS BEEN SPONSORED IN PART BY THE ROME AIR DEVELOPMENT CENTER THROUGH THE EUROPEAN OFFICE OF AEROSPACE RESEARCH, OAR, UNITED STATES AIR FORCE UNDER CONTRACT AF 61(052)-923.

ABSTRACT

An attempt has been made to study the oxidation of thin film resistors and its impact on the electrical film properties as an isolated process. Polycrystalline and single crystal chromium films were deposited under extremely clean conditions thus leaving mainly the various gas-metal interactions as possible degradation processes.

Simultaneous measurements of resistance and surface potential as functions of oxygen uptake from atomically clean polycrystalline films up to 20 Å oxide thickness distinguished between the individual oxidation stages, and it was found that the kinetics of incorporation is consistent with the surface potential and the surface structure to be rate controlling. At oxides thicker than 6 Å the oxidation is governed by the Mott-Cabrera mechanism over the temperature range from below -78°C to higher than +50°C. The oxidation appears to affect the resistance merely by the reduction of the cross section of the conductive path, the effective thickness being much less than the measured mass thickness.

Single crystal chromium films without detectable grain boundaries over the substrate area have been prepared on vacuum cleaved rocksalt. A reliable contacting technique has been developed and the rocksalt surface fine structure found to be compatible with meaningful electrical measurements. Preliminary measurements showed the TCR to be equal to the bulk value above room temperature.

Equipment for simultaneous surface potential and resistance measurements during oxidation of single crystal films has been designed and constructed.

TABLE OF CONTENTS

TABLE OF CONTENTS (contd.)

LIST OF FIGURES

LIST OF FIGURES (continued)

Figure

LIST OF FIGURES (contd.)

LIST OF PLATES

LIST OF TABLES

1. INTRODUCTION

Among the numerous ageing mechanisms being in general simultaneously present in commercial thin film resistors, oxidation is considered to contribute most to the long term drift of electrical properties. It is also often the indirect cause of catastrophic failures like "thermal runaway" where a hot spot in the constriction of the film may cause accelerated oxidation and therefore further constriction. Impurity nucleated crystallization in the region of contact lands can result in preferential oxidation due to a reduction in the effectiveness of the protective self limiting oxide (Walker, et al[1]). Other major failure mechanisms include diffusion processes involving material from the contact lands or gaseous impurities, metallurgical changes like annealing processes and precipitation, and also various interactions with the substrate. Many of these processes can be strongly linked with oxidation, as e.g. preferential oxidation of one phase in alloy films can result in precipitation processes (Levinson and Stewart[2]). The strong interdependence of oxidation with other failure mechanisms and the common manufacturing practice of "stabilising" the deposited thin film resistors by either anodisation or exposure to air at elevated temperatures led to the conclusion that oxidation is one of the most important ageing mechanisms.

The published literature illustrates the difficulties of separating oxidation from simultaneous metallurgical and diffusion processes. Almost no measurements of the oxidation kinetics have been made simultaneously with measurements of the electrical proper-

ties, and they can therefore not provide information about the mechanism of oxidation and the rate determining process.

A further difficulty is the emphasis of the present corrosion literature on the heavy oxidation of metals at higher temperature.

The present work is aimed at isolating the oxidation process of a resistive film in order to study its mechanism and the kinetics of the oxide growth under a variety of conditions. Chromium was chosen as resistor material since it represents a major component in commercial resistors and forms their protective oxide. Three conditions have to be met in order to study the oxidation process in detail and to assess its importance to the film stability:

i) The oxidation has to be separated from the other ageing mechanisms which are usually present in thin film resistors.

ii) The various stages of oxygen-metal interactions have to be studied in detail from the coverage of much less than one monolayer of oxygen on a clean surface up to the formation of a distinct oxide phase.

iii) The impact of each interaction stage on the electrical properties of the film has to be known.

In order to meet condition (i) a single crystal film was chosen as resistor thus eliminating precipitation, annealing processes and grain boundary effects. Further, it is possible to exclude the diffusion of contact material into the resistor films by using a thicker layer of the same material as contact lands. This leaves only surface interactions and the interaction with the substrate, the latter being assessed as of minor importance.

Condition (ii) is met by depositing the chromium films from pure sources under ultra-high vacuum conditions, so that their surfaces are initially atomically clean and by using gas handling systems which allow gas quantities equivalent to a fraction of a monolayer to be admitted.

Since the oxidation is a complex process involving physical adsorption of oxygen at the film surface, chemisorption and the eventual incorporation of oxygen into an oxide layer overall kinetic measurements cannot distinguish between the various steps. In this study we use simultaneous measurements of gas pressure, film resistance and film work function change to enable the various processes to be separated, and to observe which is rate determining.

Condition (iii) is met by measuring various physical properties simultaneously with the resistance and by trying to assess theoretically the impact of the various mechanisms on the electrical properties. The experiments on single crystal surfaces should also yield information about the orientation dependence of the oxidation process, its dependence on the defect concentration and should help to determine more precisely the impact of oxidation on the electrical properties of thin films. Additional measurements on polycrystalline chromium films on glass substrates are expected to determine the influence of the grain structure on the oxidation process and represent a link to commercially used resistor material. Furthermore, it is difficult to measure accurately the amount of gas adsorbed on a single crystal surface, since its area is necessarily small compared to other adsorbing areas in the reaction cell. It has to be inferred from the exposure to the gas, work function or

other physical data, whereas it can be determined volumetrically with great accuracy on polycrystalline films. Measurements on these two types of film therefore complement each other.

A kinetic study of the oxidation mechanism over a wide range of temperatures and oxide thicknesses and the study of its impact on the electrical film properties could give the following information under the assumption that the oxidation follows the same rate laws in the presence of other processes:

(a) An estimate of the extent to which resistor degradation is due to oxidation over the normal range of working temperatures.

(b) One or several rate equations which can be advantageously used in life test experiments provided the oxidation rate is analytically correlated with the drift of the electrical properties. The knowledge of the validity of a rate equation over a range of thicknesses and stress conditions would also enable us to predict individual component life with respect to oxidation.

(c) The knowledge of a particular oxidation process would be applicable to similar materials.

(d) The knowledge of the detail processes could suggest means of controlling the oxidation during manufacture either by certain additives in the source material or gas ambient or by altering the temperature-time sequence of the oxidation process.

This report describes the progress that has been made in the first contract year towards the comprehensive programme outlined and the aims listed above.

2. EXPERIMENTAL METHODS

Some of the experimental methods used are unusual in reliability studies, and therefore a brief description will be given before describing the experimental arrangement and data obtained.

2.1 Volumetric kinetic data

The amount of gas taken up by a film, the rate of uptake, and the pressure dependence of the uptake can be measured by adding known volumes of gas to the cell containing the film, and monitoring the fall in pressure.

In the experimental arrangement used for polycrystalline film measurements the apparatus is arranged so that there are virtually no adsorbing surfaces present apart from the resistor film. This enables the uptake of gas by the film to be accurately measured. The gas pressure and film temperature are also monitored so that overall kinetic measurements of the oxidation process can be made. Since volumetric measurements on single crystal films are difficult because of stray adsorption on other surfaces, the exposure (i.e. pressure times time) is used as indication for the coverage which makes pressure measurements over a wide pressure range necessary.

2.2 Surface potential measurements

The work function of metal surfaces is extremely sensitive to very slight changes in the condition of the surface. In respect of oxidation processes measurements of work function change are particularly valuable in two respects:

(a) Adsorption onto the metal film surface may be either weak physical adsorption involving van der Waals forces, or chemisorption involving definite bond formation between the gas and the surface. In the initial stages of oxidation, oxygen molecules strike the metal surface and become dissociatively adsorbed to give a layer of chemisorbed oxygen atoms. Because of the relative electronegativities of oxygen and metals in general (except gold), this results in a double layer of charge at the metal surface with the negative charge directed outwards which results in an increase of work function. This increase is referred to as the surface potential (S.P.) (an increase in work function is conventionally a negative S.P.). Under some circumstances a weak molecular oxygen adsorption occurs where the polarization of oxygen molecules in the surface field results in a positive S.P. Physical adsorption gives always a positive S.P. The transport of a chemisorbed oxygen from the surface into the metal lattice is equivalent to the oxidation process and should result in a decrease of the (negative) surface potential. Hence, work function measurements should allow distinctions to be made between molecularly adsorbed oxygen, atomic chemisorption, and the penetration of oxygen atoms into the metal lattice.

(b) At a later stage in the oxidation when a distinct film of oxide exists on the metal surface, the subsequent growth will be influenced by any field across the oxide layer,

due to the S.P. of the chemisorbed oxygen atoms at the vacuum oxide interface. We have, for example, measured the S.P. of a saturated chemisorbed oxygen layer on chromium as -2.2 V, which could represent a field of 2.2×10^7 volts/cm across a 10 Å thick oxide film. Fields of this order of magnitude are therefore sufficient to control the diffusion of species through the oxide film. The techniques are described in detail in section 3.12(a)

2.3 Film area measurements

One difficulty with polycrystalline metallic thin films is the uncertainty of their structure, which can only be thoroughly studied by depositing them in situ inside an electron microscope under u.h.v. conditions. Since the structure of clean films and the structural changes during oxidation influence the electrical properties, the measurements of the true film area as opposed to the geometric area are useful, as they provide some structural information during the oxidation process. Roughness factors upto 5 are known for 200 Å thick chromium films which had been annealed at 80°C. They would introduce a considerable error into any rate equation containing the oxide thickness. The roughness factor also changes during the oxidation. Therefore, surface area measurements have been carried out in situ on the resistor films by inert gas adsorption measurements, to allow meaningful oxide thickness measurements to be made, and to provide some structural data before and during oxidation. These measurements do not

interfere with the oxidation process. They can be roughly related to the number of metal atoms in the surface and to the crystallite size.

2.4 Electrical properties

Simultaneously to the measurements described above the resistance and its temperature coefficient were determined which gives a close relationship between the physical and chemical phenomena during oxidation and the electrical properties which are in this context of primary importance.

3. POLYCRYSTALLINE FILMS

3.1 Experimental Arrangement

3.11 Vacuum System

A bakeable mercury borosilicate-glass vacuum system has been used, a schematic diagram of which is shown in figure 1. Gas can be admitted from the storage bulbs to a mercury cut-off set incorporating a McLeod gauge. The cut-offs completely isolate the storage section, so that the high vacuum is not exposed to grease taps or unbaked glassware, except the McLeod gauge which can be torched out. From this cut-off set small and accurately measured quantities of gas can be admitted through the cold trap (4) and either valve (2) or the capillary to the reaction cell and the gauge assembly. The reaction cell and gauge assembly plus valve (2) and cold trap (4) were designed to have the minimum possible volume to increase the accuracy of the volumetric measurements, (the total volume being ~ 450 cc), and to have a minimum of stray adsorption

surfaces (the valve V_2 is of all-glass construction except for a glass-encased iron slug which moves a highly polished glass plate, and all tungsten electrodes and supports in the gauges and the reaction cell are glass encased as far as possible). The cold trap V_2 is designed so that the inlet and exit from the cooled region are identical, so that no thermomolecular flow corrections have to be made when measuring the equilibrium pressure in the cell assembly with the McLeod gauge. With this arrangement it is possible to admit measured quantities of gases to a resistor film equivalent to a few per cent of one monolayer of gas on the surface of the film. The pumping arrangement (diffusion pump (1), cold traps (2) and (3) terminating in valve (1)) was used as a fast pumping line to increase the pumping speed during outgassing and film deposition. However, only a polished glass sliding valve could be used for valve 1. Conventional metal ultra high vacuum valves and a specially constructed glass valve using liquid gallium as seal adsorbed large quantities of oxygen, and therefore introduced intolerable errors to the volumetric measurements. Since the conduction of the polished glass valve caused errors above 0.1 micron this system was only used for experiments at low pressures. The system was sealed off at the point marked (A) for experiments at higher pressures. The base line vacuum obtained with either arrangement after thorough outgassing and bakeout was 1 to 2 x 10^{-10} torr. However, in view of the small pumping speed great care had to be taken with cleanliness, and all parts were capable of thorough outgassing.

3.12 The reaction cell

3.12 (a) Surface Potential Measurements

A diagram of the reaction cell based on a design by Pritchard[3] is shown in Fig.2. The resistor film is deposited onto a spherical borosilicate glass bulb, which then forms the envelope of a thermionic diode with the resistor film as the anode. The central directly heated cathode is maintained at constant temperature by placing it in one arm of a very sensitive Wheatstone bridge and by circulating water at constant temperature around the filament lead ins. This avoids any changes in cathode temperature when the cell temperature is changed. The current/voltage relationship in the retarding field region is (Crowell and Armstrong[4]):

$$I = CT_c^2 \exp\left[\frac{-e(\phi_A - V_A)}{k\,T_c}\right] \qquad (1)$$

where ϕ_A = anode work function

V_A = anode-cathode voltage

T_c = cathode temperature

I = diode current

C = constant (depending on the effective cathode area)

The equation

$$I = \frac{(V_B - V_A)}{R_s} \qquad (2)$$

must also be satisfied where V_B is the e.m.f. and R_s the resistance of the diode current source.

Thus at a constant cathode temperature we have from equations (1) and (2)

$$\frac{dV_A}{d\phi_A} = 1 + \left[\frac{kT_c}{e(V_B - V_A)}\right]^{-1} \qquad (3)$$

so an electrometer monitoring the anode voltage will measure changes in the anode work function directly if the resistance R_s of the current source is much greater than the dynamic resistance of the diode. This method is suitable for the measurement of work function changes produced by gas adsorption, since it is insensitive to changes in the cathode work function. The sensitivity is largely determined by the stability of the cathode temperature and by zero point drift in the electrometer. In practice a sensitivity of about 1 mV can be obtained and in the measurements reported here it was usually of the order of a few millivolts. Two types of circuits were used as shown in figure 3. In method (a) I/V plots are obtained before and after changing the work function of the anode, their displacement giving the change in work function under the condition of the characteristics being parallel. Any errors in the design of the diode or any change in the stability of the cathode will be reflected in non-parallel diode characteristics.

In order to operate the diode in intermittent pressures up to approximately 1×10^{-5} torr of oxygen, the cathode must be inert against oxygen pressure up to this range. According to Singleton[5] tungsten cathodes are not suitable, since small quantities of WO_3 vapour are reported to be produced at temperatures above 950°C and pressures below 10^{-4} torr. The rate of production of oxides is reported to decrease beyond ~1600°C. Therefore,

tungsten and rhenium cath'es were coated with lanthanum hexaboride ($La B_6$) to decrease the operating temperature and the rate of oxidation at low pressures. Normally the $La B_6$-coating reacts with the metal to give the metal boride, and lanthanum is evaporated from the cathode. This reputedly does not occur for coated rhenium cathodes.

Two types of cathode filaments were tested:

- 0.075 mm tungsten wire (0.003") coated with a thin layer of zirconium carbide, sintered in vacuum at 1800°C, and then coated with lanthanum hexaboride to a final diameter of 0.0065" (0.17 mm)
- 0.25 mm rhenium wire (0.010") coated directly by cataphoresis from a suspension of lanthanum hexaboride in acetone.

The carbon layer on the first filament reputedly minimizes the reaction between tungsten and the boride coating.

Figure 4 shows I/V curves over a range of cathode temperatures from which it can be shown by the comparison with plain W that the work function of the rhenium basedcathode is approximately the same as bulk lanthanum hexaboride (approx. 2.7 eV, Lafferty[6]). Figure 5 shows the variations in work function of the gold anode around the tungsten based cathode as a function of time and cathode temperature. It is concluded that lanthanum evaporates from these cathodes at temperatures at and above 1150°C. No similar changes could be observed for the rhenium based cathodes below 1800°C. Thus it is con. uded that $La B_6$-coated rhenium cathodes are sufficiently stable for the present purpose.

LaB_6-coated rhenium cathodes were used for some of the measurements described, but plain tungsten cathodes yielded identical results and the following evidence exists that no evaporation of WO_3 occurred:

i) Identical work function changes were obtained with plain tungsten and LaB_6-coated rhenium cathodes when admitting oxygen to the resistor films.

ii) No instabilities could be detected in the cathode bridge circuit as would be expected if the cathode were chemically attacked.

iii) Using the circuit of figure 3(a) the diode characteristics were found to be parallel during addition of oxygen to the resistor films.

iv) The saturation S.P. of oxygen on chromium at -196°C has been measured by Roberts[7] using a vibrating capacitor technique involving no heated filaments. We obtain the same value.

For both cathode materials there exists a minimum temperature below which very small quantities of oxygen cause an almost total drop in diode current, which is due to very severe poisoning by chemisorbed oxygen and does not occur on tungsten at temperatures above 1500°C. The optimum temperature for LaB_6-coated rhenium cathodes was ~ 1200°C. A further complication arises through the dissociation of oxygen molecules at the hot cathode surface and the combined interaction of oxygen atoms and molecules with the anode. The far higher adsorption rate of oxygen atoms renders any inter-

pretation of adsorption measurements problematic even if only a small fraction is dissociated. Therefore we admitted only small doses of oxygen via the capillary system (figure 1) to ensure rapid pressure decrease during adsorption and to prevent an increase of pressure above 10^{-5} torr. At higher pressures the cathode was switched off during oxidation and the pressure decreased for the measurements.

3.12 (b) Resistance Measurements

For resistance measurements two 125μ thick platinum foil contacts were sealed onto the equator of the bulb (figure 2) and spot-welded to the glass-encased tungsten leads. Good electrical contact to the films over the temperature range -196°C to +90°C could only be achieved by lapping the glass over the edges of the platinum foils.

The film resistance was measured by means of an AC bridge (Wayne-Kerr B221) with a sensitivity of ~1 mΩ, although the accuracy of measurements rarely attained this value due to electrical interference and difficulties of precise temperature control. Resistance changes equivalent to approximately 2×10^{-4} of the film resistance could be measured.

Values of film resistance could only approximately be converted to resistivity because of the geometry of the bulb and its appendages and the uncertainty about the precise position and the shape of the contacts.

The film resistance, surface potential, and the gas pressure in the reaction vessel could be displayed versus time on a

three pen chart recorder. Resistance and surface potential could not be simultaneously displayed, since the circuits interfered. Switching between these two measurements took approximately one minute.

3.13 Pressure measurements

The accurate and continuous measurement of oxygen and xenon pressures over the region 10^{-7} torr to 10^{-1} torr and residual gas pressures down to 10^{-10} torr was achieved by using four types of gauges.

(a) A normal Bayard-Alpert ionization gauge was used for monitoring the general background pressure.

(b) A specially constructed McLeod gauge, which could be torched for outgassing, and which exposed no surfaces except glass and mercury to the ambient vacuum, was used for measuring gas pressures in the closed system, and as a standard for calibrating the other gauges. It covered the range 5×10^{-5} torr to 6×10^{-2} torr.

(c) A miniature ion gauge, based on the Schultz-Phelps[8] pattern but with gold electrodes (to minimize stray adsorption) and a LaB_6-coated rhenium cathode was constructed for the measurement of xenon pressures. This gauge had an almost linear response for xenon over the range 5×10^{-7} torr to 10^{-1} torr and probably higher. It could not be used to measure oxygen pressures since the cathode was attacked at oxygen pressures of the order of 10^{-3} torr. The miniature ion gauge was normally operated at a low emission current of about 7μA, so that no errors resulted

from gauge pumping.

(d) An ultra sensitive Pirani gauge was used to monitor oxygen pressures. The filament consisted of 25 cm of 25μ diameter nickel wire that was rolled into tape to increase its sensitivity (Ellet and Zabel[9]).

The gauge was extremely sensitive to very small changes in temperature, and also to the ambient illumination, so it was constructed within a blackened water jacket. Normally the jacket was thermostated at 28°C, and the filament maintained at 120°C. Using a high impedance instrument with a full scale deflection of 1 mV to detect the error signal from the Pirani bridge, pressures down to 1×10^{-6} torr could be measured. The gauge was calibrated up to 6×10^{-2} torr, and when the nickel filament was oxidised by heating to 300°C in oxygen before the gauge was put into service, the calibration did not change over long periods of time.

3.14 Evaporation procedure and purity of materials

The gases used were all of the spectroscopically pure grade and were supplied by the British Oxygen Company Ltd. The purity of the xenon was checked by measuring the vapour pressure at liquid oxygen temperature by means of the McLeod gauge.

Very high purity electrolytic chromium was supplied by Johnson Matthey Co. Ltd. Before mounting it in the vacuum system it was prepared as follows:

i) "Silver boat" purification. This is a hydrogen furnacing technique in a high frequency induction field which reduces non-metallic impurities. At this stage analysis showed the following impurities:
Metallic impurities < 22 ppm, oxygen 6 ppm, nitrogen 2 ppm, hydrogen 1 ppm.

ii) The chromium was then outgassed and partially evaporated under a vacuum of approximately 10^{-8} torr in an ancillary vacuum system. It was then transferred to the reaction cell.

iii) Outgassing of the chromium sample and the vacuum system was then alternately carried out until the chromium could be maintained at a temperature close to the sublimation point in a vacuum of better than 5×10^{-10} torr.

The resistor film was then evaporated onto the bulb, no attempt was made to control the deposition rate, which was in the range 5 to 15 Å per minute. The best evaporation conditions attained were:

Base line vacuum	$1\text{-}2 \times 10^{-10}$ torr
Initial pressure on heating chromium ready for evaporation	4×10^{-10} torr
Pressure throughout deposition	$1\text{-}2 \times 10^{-10}$ torr

On occasions the base line vacuum was higher (5×10^{-10} torr), and the maximum initial pressure on heating the chromium was 5×10^{-9} torr. No influence of these parameters on the surface properties

was observed. This is not surprising, since the true film area was of the order of several hundred square centimetres, and therefore the amount of gas required to contaminate it is high (several litre microns).

3.2 Results and Discussion

3.21 Surface area measurements

Two methods were employed for the measurement of film surface areas,

3.21 (a) Xenon S.P. data

The xenon S.P. versus coverage relationship allows the amount of xenon adsorbed equivalent to one monolayer on the clean metal surface to be determined fairly accurately and represents one method of film area measurement (Pritchard[10]). A typical xenon S.P. plot is shown in figure 6. The detailed shape of the curves up to saturation will be dictated by the complexities of the film structure and the energetics of the adsorption process, which will not be discussed further.

As an oxide layer builds up on the surface the behaviour of xenon becomes complex. The saturation is no longer sharp, a shallow maximum appears in the S.P. plot, and the magnitude of the positive S.P. maximum decreases. This is illustrated in figure 7, which shows the variation of S.P. and pressure as a function of the number of atoms adsorbed for the adsorption of xenon at -196°C onto a chromium surface covered with a 12Å thick oxide layer. In these circumstances it is difficult to read off the monolayer volume, and so the B.E.T. method was applied to the pressure versus amount adsorbed data.

3.21 (b) The Brunauer-Emmett-Teller (B.E.T.) equation

The B.E.T. equation (Brunauer, Emmett and Teller[11]) represents an attempt to extend the concept of an ideal localized (or fixed) monolayer of physically adsorbed gas to a multimolecular adsorbed film. It yields a two-constant equation from which surface areas and heats of adsorption can be calculated. It has been very widely applied to the measurement of surface areas of a wide range of materials with many gases, and the results of the surface area measurements have been very consistent despite doubts about its theoretical validity. It is used as an analytical method for locating the "point B" on a PV isotherm where the affinity of the surface is changing most rapidly. This is the point at which a monolayer of adsorbed gas is formed (see Young and Crowell[12]).

The B.E.T. equation is

$$\frac{p}{v(p_o - p)} = \frac{1}{v_m c} + \frac{(c - 1)}{v_m c} \frac{p}{p_o} \qquad (4)$$

where p = pressure of gas above the film

v = amount of gas adsorbed

v_m = amount of gas adsorbed to form one monolayer

c = a constant, which is related to the heat of adsorption in the original theory

p_o = the saturated vapour pressure of the gas (xenon in our case) at the adsorption temperature.

For xenon adsorption on metal films "c" is high (several thousand), and so a plot of

$$\frac{p}{v(p_o - p)} \text{ versus } \frac{p}{p_o}$$

should yield a straight line of slope $\frac{1}{v_m}$, enabling the amount of one monolayer to be obtained. The equation must be applied in the region of the "point B", and there is justification for treating p_o as an arbitrary constant (Haynes[13]).

The agreement between the two methods is reasonable in the region where both can be applied. It can be seen from figure 7 that the B.E.T. monolayer volume is located where the S.P. commences to level off after the maximum on the S.P. plot.

If the monolayer amount of xenon (v_m) is known, the mean surface area per xenon atom on the surface has to be used to convert this to the film area. To calculate the number of surface metal atoms it is also necessary to make some assumptions concerning the distribution of crystal planes in the surface of the films. The usually accepted value for the mean area per xenon atom is 24 Å^2 (Cannon[14]) and is based on the assumption that the mode of packing of xenon monolayers is largely independent of the adsorbent. There is now evidence that the packing of xenon monolayers is structure sensitive (Brennan, Graham and Hayes[15], Ehrlich and Hudda[16]). If the coverage of oxygen on the metal surface is defined as

$$\theta = \frac{\text{no. of oxygen atoms on surface}}{\text{no. of metal atoms in the surface of the film}}$$

then $$\theta = Q \times \frac{\text{amount of oxygen adsorbed on the surface}}{\text{amount of xenon adsorbed to give one monolayer}}$$

where Q = a constant, depending on the assumptions made concerning the nature of the xenon monolayer, as shown in table 1.

For a diatomic gas Q also depends on whether the gas is disassocia-

tively adsorbed. The table given below gives the variation of Q values for a mean area per xenon atom of 24 $\mathring{A}^2$ (total surface area method), and assuming xenon packs into crystallographic sites on the surface. Values are given for each of the principle crystal planes.

TABLE I

	100 Plane	110 Plane	111 Plane	Mean
Assuming 24$\mathring{A}^2$ for mean area per Xe atom	.69	.49	1.18	.69
Assuming Xe atoms 'pack' into the metal surface lattice	.5	.5	1.5	.695

VALUES OF THE FACTOR Q FOR DETERMINING THE COVERAGES OF DIATOMIC GASES ADSORBED ON CHROMIUM SURFACES BY XENON ADSORPTION.

The absence of evidence of preferred orientation in the electron diffraction pattern suggests it is reasonable to assume the three principle crystal planes are equally prominent, so the mean Q is used.

It can be seen that the average is approximately the same in both cases of table I and this value is used in subsequent calculations. Hence it is assumed that the number of chromium atoms in the surface can be calculated on the basis of equal areas of the three principle crystal planes, and that xenon atoms pack in an orderly array, or occupy 24 $\mathring{A}^2$ each.

When calculating oxide thicknesses from the total amount of oxygen taken up and the amount of xenon adsorbed to give a monolayer

$$X = 1.4 \times \frac{N_{O_2}}{N_{xe}} \text{ (Å)} \qquad (5)$$

is used where X = oxide thickness

N_{O_2} = no. of oxygen molecules adsorbed

N_{xe} = no. of adsorbed xenon atoms required to form a monolayer at the same stage of the interaction.

This relationship assumes that the oxide is the most stable oxide of chromium, Cr_2O_3 with the bulk density of 5 grm/cc.

3.22 The properties of clean films

The resistor films described here were evaporated onto the borosilicate glass "bulb" substrate at 25°C, and annealed at 80°C for 30 to 60 minutes. An electron diffraction pattern and electron micrograph of a typical film are shown in plates (1) and (2). The films are polycrystalline with little or no preferred orientation. The mean thickness of the films studied ranged from 200 Å to 500 Å. Mean thicknesses were measured by chemical mass determination.

Table II shows resistance and thickness data for three films:

TABLE II. DATA ON CLEAN FILMS

Resistor	Weight (mg)	Thickness Å	Vm Xe (atoms 10^{16})	Roughness factor	R(25°C) Ω	TCR(25° and above) /°C	TCR(down to -196°C) /°C
1	1.65	215	15.5	4.2	27.888	$+1.4.10^{-3}$	$+5.65.10^{-4}$
2	1.20	157	12.5	3.3	53.2	$+2.1.10^{-3}$	$+2.10^{-4}$
4	3.32	525	33	8.8	8.827	$+2.0.10^{-3}$	$+4.5.10^{-4}$

For reasons already given in section 3.12(b) resistance values cannot accurately be converted to resistivity values, but the resistivity is considerably larger than bulk chromium if it is calculated on the basis of a 'slab' film, whose thickness is the mean thickness. The TCR value at room temperature is comparable to the bulk value ($+3.0 \times 10^{-3}/^{\circ}C$), but decreases sharply with decreasing temperature. The quoted TCR values are average values since the resistance temperature relationship is not linear. A typical resistance-temperature plot is shown in figure 9. The data for the ideal resistivity of chromium (as deducted from Matthiessen's rule) given by White and Woods[17] indicates a TCR fairly close to the bulk value in the temperature range 25°C to -196°C. Three factors can explain our low TCR at low temperatures:

i) defect scattering in the films

ii) impurity scattering

iii) size effects

(ii) is rejected in view of the materials purity and the cleanliness of film preparation, leaving (i) and (iii) as possibilities.

The measured surface areas indicate the films to be highly defective. They have a large internal surface and must consist of an open agglomeration of crystallites, since the true area per unit geometric area is almost linearly related to the film mass per unit area. This also implies a uniformity of structure with film thickness. Figure 8 shows the relationships between resistance (after annealing), film area and film mass

(the geometric area of the bulb substrates was approximately constant). The square resistance is not linearly related to the film mass per unit area, the dependence decreases at higher film thicknesses.

We have as yet insufficient data to draw firm conclusions, but in view of the open structure of the films the possibility of size effects, even at average film thicknesses larger than the electron mean free paths at temperatures in the range 20°C to -196°C, is strong, since the dimensions of crystallites might be such that electron scattering at their boundaries exercises considerable control over the film resistance which is estimated to be between 63 Å to 220 Å at 20°C depending on the number of conduction electrons assumed per atom of pure chromium (Gould[18])

3.23 Effect of physical adsorption on film resistance

Physical adsorption of xenon caused little, if any, change in film resistance. This is expected: physical adsorption involves no electron exchange and the binding energy is low. Suhrmann[19] observed increases in the resistance of nickel films during xenon adsorption and attributed this to the penetration of the films by xenon, but, possibly due to our films being thicker and the effect smaller, we have found no evidence to confirm. We infer from this that physical adsorption in general is liable to have little or no effect on the resistance of films in this thickness range.

3.24 The chemisorption process

The addition of oxygen to the surface of clean metals results in an initially large negative S.P. change (an increase in work function), followed by a slower decay. The negative S.P. change arises from the adsorbed oxygen atom having a vacant energy level below the Fermi surface of the metal, so electrons are transferred from the metal to chemisorbed oxygen atoms at the metal surface. This results in a surface dipole layer with the negative charge directed from the metal, hence an increase in work function. The chemisorption is dissociative, i.e., the oxygen is adsorbed atomically (see for example Roberts[20]).

Figure10(1) shows a plot of S.P. versus amount of oxygen adsorbed on a chromium film at -196°C. The adsorption was discontinued when the S.P. and therefore the surface was saturated, and the pressure began to rise (i.e. to approximately 10^{-6} torr). The final value attained (-2.15V) is in good agreement with the only other recorded value (Quinn and Roberts[21]), which was obtained using a vibrating capacitor technique. The ratio of the number of oxygen atoms adsorbed to the number of metal atoms in the film surface at this stage was 1.2, indicating that at this temperature (-196°C) the interaction is largely confined to the surface. The high negative S.P. indicates considerable ionicity of the metal-chemisorbed oxygen bond (the comparable value for nickel is approximately -1.5V). If the surface oxygen atoms were totally ionized to O^-, then the surface would not be capable of adsorbing one monc-

layer, since the ionic radius of O^- is 1.76 Å, and the atomic radius of chromium is 1.25 Å. It is not possible to calculate the charge on the oxygen atom from the magnitude of the S.P., since the Helmholtz formula gives

$$S.P. = 4\pi N\theta\, dm \qquad (6)$$

where N = no. of surface sites for adsorption

θ = coverage

dm = dipole moment

This allows only the dipole moment to be calculated, and the distance in the dipole is not known without additional evidence. However, most chemisorbed species are held by largely co-valent bonds with considerably smaller dipoles.

3.25 The incorporation process

3.25 (a) Experimental observation

When the layer at -196°C is warmed to a higher temperature a large positive change in S.P. occurs and is accompanied by a regeneration of the adsorptive capacity of the surface. Figure 11 shows the repeated adsorption at -196°C and subsequent warming up to -78°C and then +25°C which causes the regeneration of the surface and the decrease in dipole moment. The plots labelled (2),(5),(6) and (8) on figure 10 correspond to the subsequent additions on figure 11. Similar behaviour has been observed for other metals (Quinn and Roberts[21], Delchar and Tompkins[22]) and for other strongly electronegative gases (Burshtein and Shurmovskaya[23]). They are usually attributed to incorporation of oxygen into the metal lattice, since a movement of oxygen atoms bearing a negative charge

from the surface into the lattice might result in a positive change in S.P. It is also possible to interpret the positive change in S.P. by a surface migration of oxygen atoms from the outer surface of the film, which exercises the dominant control over the measured work function change compared to its inner surfaces.

Both mechanisms could result in a positive S.P. change and a regeneration of the adsorptive capacity of the surface. The latter is, however, rejected on the following grounds:

(i) Since a coverage of greater than unity is initially attained at -196°C, it would require a large internal surface of the film not accessible to xenon adsorption.

(ii) Although the adsorptive power of the surface is regenerated, the regenerated surface does not respond like the original clean surface in respect of either xenon or oxygen adsorption.

(iii) The large heat of oxygen adsorption on chromium of initially 174 Kcal/mole (Brennan, Hayward and Trapnell[24]) implies a strong binding energy making surface migration unlikely.

(iv) The measurements in figure 11 suggest that the regenerated surface exceeds the total initial surface which can only be explained by incorporation.

(v) As will be seen later, the positive S.P. change is associated with a large resistance change, which might be difficult to account for on the basis of surface migration.

Thus the positive S.P. drifts are associated with the movement of chemisorbed oxygen atoms into the metal lattice, i.e., the incorporation process. This is the initial

stage of oxidation.

The points recorded in figure 10 are in fact the final values attained for each dose of oxygen added. If the S.P. versus time traces are examined for each dose it is observed that incorporation of oxygen atoms occurs even at -196°C and sub-monolayer coverages of oxygen. Figure 12 shows the S.P. versus time traces for the points marked A, B and C on figure10. In each case the pressure falls to zero at approximately the (negative) maximum, so that the positive drift is not accompanied by any change in the number of oxygen molecules adsorbed, but is solely due to the transfer of chemisorbed oxygen atoms to the lattice.

Before the positive S.P. drifts can be used to study the kinetics of the incorporation process it must be established that the number of oxygen atoms incorporated is proportional to the S.P. drift. It is clear from figures10 and 11 that the negative S.P. is not linearly related to the amount adsorbed, but this would not be expected, since the shape of the S.P. versus coverage plot will be influenced by the pronounced structural heterogeneity of the films, and the fact that they have an 'internal' surface. Also the amounts of gas taken up during the successive adsorptions of figure 11 are arbitrary, since atomic oxygen is present and incorporation of oxygen is occurring near saturation. It seems reasonable to identify the amount of oxygen adsorbed at -196°C during the steeply rising negative parts of the adsorption curves of figure 11 with the filling of vacant surface sites, whereas the later shallow part is largely due to incorporation. Thus a plot of adsorbed amount

versus the positive decay during the previous warming from -196°C to +25°C should give the relationship between S.P. decay and the number of chemisorbed oxygen atoms. This is shown in figure 14 to be linear and the slope to be approximately +1.5 volts per 1 x 10^{16} O_2 molecules. Delchar and Tompkins[22] found exactly the same behaviour for nickel films, where the situation was simpler since the extent of incorporation of oxygen at -196°C is very much smaller, and they used a static capacitor method of measurement where the complication due to atomic oxygen did not arise. For nickel the slope was +.66 volts per 10^{16} oxygen molecules. Thus the S.P. drift can be used to follow the kinetics of incorporation.

All curves like those in figure 12 do not fit simple first order kinetics, but for each increment equivalent to a small fraction of a monolayer, they were found to fit an equation of the form:

$$n_i = A \log (t + B) + C \qquad (7)$$

where n_i = the number of atoms of the increment incorporated

t = time

A, B and C are constant.

This can be seen from figure 13.

Two other observations are relevant:-

i) At very low coverage there is little positive decay and the initial negative going S.P. change is smaller, giving rise to a "foot" on the S.P./coverage relationship in figure 9(1). This cannot be explained with stray ad-

adsorption. It was also observed for the nickel-oxygen system and was tentatively explained by Delchar[25]. These non-uniformities largely arose from the use of a cylindrical adsorption cell and the evaporation of the film from a small source situated on the axis of the cylinder. They should not be present in our experimental arrangement, where the film is thrown from a "point" source at the centre of a spherical bulb substrate. The overall shape of S.P./coverage relationship at -196°C is, apart from the "foot", almost certainly dictated by the ratio of inner to outer surfaces of the film. The initial adsorption is occurring on the outer surfaces, which exercises most control over the work function, and the subsequent adsorption on the inner surfaces. The reason for the "foot" however is not understood, since an explanation based on surface migration from the outer to the inner surfaces would seem unreasonable.

ii) There is a small tendency for the positive decay to increase with coverage up to a coverage of close to unity. If the adsorption is continued further the behaviour changes, since second layer adsorption of oxygen occurs at high coverages and low temperatures, and the transfer of second layer oxygen to the chemisorbed layer begins to dominate the S.P. plot. This is discussed in 3.27(d). The slope of the surface potential versus log (time)-plots

such as figure 13, does not vary considerably with increasing coverage or increasing total S.P. The major change with increasing coverage is a fall in maximum negative S.P. attained per dose.

TABLE III

Total S.P.	Coverage	Slope of S.P. versus log (time) plot	"Normalised" slope
-0.880	.25	3.7×10^{-2} volts/ time decade	9.2×10^{-2}
-1.461	.60	3.62×10^{-2}	5.4×10^{-2}
-1.551	.64	3.9×10^{-2}	5.5×10^{-2}
-1.756	.75	3.5×10^{-2}	4.4×10^{-2}
-1.893	.86	2.7×10^{-2}	3.1×10^{-2}

SLOPE OF S.P. VERSUS LOG (TIME) PLOTS AS A FUNCTION OF COVERAGE AND TOTAL S.P. FOR THE ADSORPTION OF OXYGEN ON CHROMIUM AT -196°C.

The apparent activation energy of the incorporation process was measured at about unit coverage of chemisorbed oxygen. The initial rates were

-160°C	.156 V/min
-78°C	.685 V/min

These figures yield an apparent activation energy of approximately 0.75 Kcal/mole.

3.25 (b) Kinetics and mechanism of the incorporation

Equation (7) can be derived on the assumption that the activation energy E for the incorporation increases linearly with amount incorporated, i.e. for each increment n_i let the activation energy

$$E = E_o + \alpha n_i \qquad (8)$$

where α and E_o are constants

since if the rate is

$$\frac{dn_i}{dt} = \text{const} \exp\left(-\frac{E}{kT}\right) \qquad (9)$$

we obtain again

$$n_i = A \log (t + B) + C$$

Equation (7) is a form of the Elovich equation, which has been found applicable to many surface processes requiring activation, and can be derived in a variety of ways (Roberts[20]).

We have recently offered the following mechanistic explanation in this case (Crossland and Roettgers[26]): Oxygen strikes the surface at random from the gas phase and is chemisorbed with a high sticking probability. The surface of the film is heterogeneous, and there exist adsorption sites with a range of activation energies for the incorporation process, so that at a given low temperature incorporation is only possible on a particular percentage of the total number of sites occupied. For a particular increment of gas the activation energy will rise with the number of atoms incorporated. Further increments may change the distribution of sites

since oxygen chemisorbed onto sites with insufficient activation energy for incorporation will block them, whereas sites with sufficient energy may be capable of further incorporation processes. This would give rise to increase of incorporation with coverage, would depend on the probability of incorporation at sites on which incorporation had already occurred, and would probably cause a decrease in the maximum negative S.P., since in the later stages some of it is due to chemisorption onto sites above incorporated oxygen atoms. We rejected a model based on the field existing between the adsorbed layer and the metal surface as an explanation of the behaviour especially at low coverages, since a uniform field does not exist within a partial monolayer and we had observed extensive incorporation at low coverages of chemisorbed oxygen (e.g. see Table III).

However, Delchar and Tompkins[22] have interpreted their data for nickel, which is very similar to our own for chromium by means of the surface potential field model. They assume that each oxygen atom has a potential energy of $\frac{1}{2}qV$ resulting from its position in the electrical double layer. The potential difference V is encountered by the atom on moving across the oxygen-metal dipole layer, and q is the charge on each oxygen atom. The potential difference V is then identified with the measured S.P., especially at high coverage which gives the linear increase of activation energy with coverage required to explain the S.P. versus log (time) plots, with the rate equation being

$$\frac{dn}{dt} = \text{const. exp} - \frac{\Delta E_F - \frac{1}{2} qV}{kT} \qquad (10)$$

where ΔE_F = the most probable barrier height

and n = the no. of oxygen atoms incorporated.

This rate equation can be written as

$$\frac{dV}{dt} = -\beta \exp \alpha V \qquad (11)$$

which on integration under the condition that V_o is the S.P. at $t = 0$ gives

$$V = -\alpha^{-1} \log \left[t + \frac{\exp(-\alpha V_o)}{\alpha \beta} \right] - \alpha^{-1} \log \alpha \beta \qquad (12)$$

A plot of log (t + constant) versus V should give a straight line of slope

$$\frac{1}{\alpha} \quad \text{where} \quad \alpha = \frac{q}{2kT} \qquad (13)$$

This relationship was used by Delchar and Tompkins[22] to determine q, the charge on an oxygen atom chemisorbed at a nickel surface. A value of 0.3e was obtained where e is the electronic charge. This value is very reasonable, since it implies a metal-oxygen bond distance of approximately .35 Å, which would be the case if the chemisorbed oxygen atoms were located in the potential wells between surface metal atoms, rather than mounted directly above them.

We can apply the same formalism to our data if we assume

i) a uniform chemisorbed layer, and

ii) the potential energy of the dipoles to be correctly described by $\frac{1}{2} qV$ over the range of our data.

The slope of the S.P. versus log (time) plots for chromium gives a value of .4 e which is in good agreement with the value for nickel, since its ratio to the Ni value corresponds to the ratio of the measured saturation S.P. values of chemisorbed oxygen on the two metals. This is required by the Helmholtz formula (equation (6)) if the adsorption processes and the metal lattice constants are similar. Since the apparent activation energy is .75 Kcal/mole at approximately unit coverage, E_p, the barrier height, can be calculated since at unit coverage according to eqn.(10)

$$.75 = E_p - \tfrac{1}{2} qV$$

giving E_p = 10.8 Kcal/mole compared with 7.3 Kcal/mole for nickel. On the basis of the above assumptions the slope of the S.P. versus log (time) plots will not depend on V_o, the initial S.P., and hence on coverage.

Both assumptions are however open to criticism:

i) The distribution of oxygen atoms over the total area of the resistor film will depend on the reaction cell and inlet geometry, and the measured S.P. will be an average over the whole surface. The two extreme cases are a perfectly distributed uniform array as above and the case where admission of oxygen to the bulb results in saturated chemisorption on a limited film area while only little adsorption occurs on the rest of the surface. For the latter case the measured S.P. gives only the average surface charge density. The data can in this

case be corrected by multiplying all the S.P. data for a given dose by a scaling factor to make V_o equal to the saturation S.P. which for chromium is -2.2 V. This will change the slope of the S.P. versus log (time) plots by the same factor, and the last column of Table III shows the values obtained by this "normalisation". Delchar and Tompkins[22] obtained for nickel reasonable agreement between the interaction with large oxygen doses at temperatures higher than -196°C, and values obtained by forming a monolayer of chemisorbed oxygen at -196°C (where little or no incorporation occurs) and then warming the monolayer to a higher temperature. It can be seen that in our case no approximately constant value is obtained. It is difficult to determine the distribution of incident oxygen molecules over the film surface. An inlet consisting of a small hole at the bulb surface would result in a cosine distribution at the pressures used in these experiments which should give a very uniform distribution. Our inlet tube has the form of an annular ring (see figure 2), whose length is comparable to the ring size. The resulting distribution however should be more uniform than in the cylindrical cell used on nickel (Delchar, Eberhagen and Tompkins[27]) and it appears unlikely that, e.g. at 0.25 coverage and an S.P. of -0.880 V practically all the gas admitted should be adsorbed over one small area of film giving an S.P. of -2.2 V in this limited region.

ii) For a uniform distribution of dipoles at the surface it is not reasonable to expect the potential energy of the dipoles to be correctly described by $\frac{1}{2}$ qV over a wide range of coverage. The formula for the interaction energy of a closely spaced array of dipoles consisting of point charges is

$$\Delta Q = -\tfrac{1}{2}\, qV \tag{14}$$

and this energy is clearly comparable to the measured activation for the incorporation process. If the dipole layer is not ideal, the deviations from this relationship may be expressed by

$$\Delta Q = -\tfrac{1}{2}\, qfV \tag{15}$$

where f is a structural factor representing the fraction of V effectively acting on the dipoles. Mignolet[28] has calculated the variation of ΔQ with the distance d between the centre of gravity of the charges and the area a^2 occupied by a dipole on the surface. This gives

$$f = \frac{2}{1 + \operatorname{tg}(\frac{1}{2} \operatorname{arc\ tg} \frac{\sqrt{7}}{\rho})} - 1 \tag{16}$$

where $\rho = \frac{d}{a}$

The factor f therefore varies considera with the distribution of charges, and f = 1 is only obtained for large values of ρ, i.e., for long and closely spaced dipoles, with the charges spread continuously on the two planes. For small values of ρ it reduces to

$$f = \frac{2\rho}{4\pi} \qquad (17)$$

An approximate calculation of the value of f can be made on the following assumptions:

(α) The chemisorbed oxygen is not ionically bonded, but held by co-valent bonds with an ionicity sufficient to give the measured S.P.

(β) The chemisorbed oxygen atoms are situated at lattice sites between the metal atoms in the surface. This position of minimum potential energy is more likely than oxygen atoms situated directly over surface metal atoms. The perpendicular distance between the two layers of charge would then be in the region of d = 0.5 Å. Assumptions (α) and (β) are in agreement with the values deduced by Delchar and Tompkins[22].

(γ) a^2 will be different for the different principle crystal planes. For (110) as the most closely packed plane of chromium $a^2 = 5.87$ Å^2, hence a = 2.42 Å.

Substituting these values in equation (16) and assuming the coverage to be unity gives f = 0.115 which falls to 0.07 for a coverage of $\frac{1}{2}$, and if 2.5 Å is assumed for d, an f-value of .56 is obtained for unit coverage. Gross defects in the dipole structure due to the non-uniformity of the metal surface will lead to a further lowering of f.

Whilst we are aware that the application of simple dipole calculations represents a considerable over-simplification, es-

pecially when applied to data on polycrystalline materials, these figures do suggest that the potential difference V that an atom encounters on moving across the oxygen-metal double layer may be considerably smaller than $\frac{1}{2}$ qV, especially when the distance between the charges is low.

Since the slope of the S.P. versus log (time) plots is approximately constant with coverage, it might be argued that in fact the local S.P. in regions where incorporation is taking place is higher than the measured average (due to a lack of a uniform distribution of surface oxygen atoms), but that the potential difference that an oxygen atom encounters on moving across the oxygen/metal double layer is only a fraction of this because $f < 1$. If these two effects were to largely cancel each other, this would justify the approximately constant slope, and the reasonable values observed for q. This does not however account for the fact that equation (16) predicts values very much less than $\frac{1}{2}$ qV for the potential energy, and does not explain why equation (10) is applicable to the data on nickel over quite wide ranges of coverage, when f is itself sensitive to coverage changes. Such an interpretation would also require the build-up of high local concentrations of chemisorbed oxygen atoms over limited regions of our films at coverages as low as $\frac{1}{4}$.

If an effect due to surface heterogeneity were present a rate equation of the same form as equation (10) would arise, but ΔE_f would be a function of coverage and $\frac{1}{2}$ qV may be replaced by $\frac{1}{2}$ qfV where $f \leq 1$ and is sensitive to coverage changes.

$$\frac{dn}{dt} = \text{const} \exp - \left[\frac{E_o - (\alpha - \frac{1}{2} qf)V}{kT} \right] \qquad (18)$$

where E_o is constant

and α is a constant dependent on the distribution of surface sites.

Thus depending on the relative magnitudes of α and $\frac{1}{2} qf$, linear V versus log (time) plots might be obtained over small or larger coverage ranges, and the reasonable values obtained for q and the metal-oxygen bond distance assuming equation 10 to hold may be fortuitous. Measurements on single crystal film surfaces, whose structure is uniform and defined, and on which a completely uniform distribution of oxygen atoms can be obtained will help in establishing the dominant mechanism.

The preceding discussion has been concerned with the energy barrier of the incorporation process, and the way in which it may be lowered by the dipole interaction energy. No mention has been made of the mechanism of the incorporation process. Lanyon and Trapnell[29] have suggested two types of mechanism for the incorporation process.

In the first type oxygen molecules assist interchange of oxygen and metal atoms by means of a liberation of the heat of chemisorption. This type of mechanism cannot be operative on chromium since we have found that incorporation proceeds without any oxygen in the gas phase.

The second type of mechanism proposed by Lanyon and Trapnell[29] involves defect sites in the metal surface. Two cases are distinguished here, one results in the removal of the defect

sites and one does not. Since the incorporation appears not to be limited to defect sites the second case is considered most likely. A third possibility has been advanced by Delchar and Tompkins[22]. Despite the very low activation energies measured, the rate of incorporation is extremely slow. This is true for nickel and for our data on chromium. Assuming first order kinetics and using the measured activation energy Delchar and Tompkins[22] estimated that the rate on nickel is a factor of approximately 10^{12} times too low. They propose a model in which oxygen atoms at the metal surface move between the surface metal atoms in a similar way to that occurring during interstitial diffusion of oxygen. This occurs only when those metal atoms surrounding a given chemisorbed oxygen atom are all moving away from the oxygen atom as a result of their thermal vibrations. The probability of this occurring is small, and it gives a low probability factor to the rate equation, thus explaining the low rate. A calculation of the probability factor of a simple cubic crystal of nickel using a value for the size of the oxygen atom based on a charge of .3e gives a probability factor of the right order to explain the experimental rates. A mechanism of this type could equally well apply to our data. It is interesting to note that the mechanism leads to a variation of activation energy with the crystallographic nature of the adsorption sites.

Thus it has been demonstrated that the processes of chemisorption and incorporation of oxygen can be separated on chromium films by surface potential measurements at low temperatures. The kinetics of incorporation have been studied down to low

coverages of chemisorbed oxygen, and a rate equation of the form of equation (9) is operative with initially a low activation energy and a low probability factor as observed by Delchar and Tompkins[22] on nickel films. The rate may be controlled by the surface field and/or surface heterogeneity, and the important parameters are the surface potential of chemisorbed oxygen and the crystallographic nature of the surface (e.g. the crystal planes presented, defects, etc.) Observations on single crystal surfaces are expected to clarify this situation.

3.26 Structural changes during oxidation

TABLE IV. TRUE FILM AREA DURING OXIDATION

True area, cm^2	Amount of oxygen taken up (molecules x 10^{-16})
Film 1	
780	0
340	134
320	165
Film 2	
410	0
310	43
192	110

Table IV shows some variations in the true area of two films as a function of the amount of oxygen taken up. In both cases the geometric area of the film is approximately 100 cm^2. As already

noted the clean films consist of an open agglomeration of crystallites. This structure must undergo drastic changes during oxidation, and the area changes shown above must be due to a doubling of the crystallite size. Such changes have been observed by other workers (Roberts[30], and Brennan, Hayward and Trapnell[24]) and attributed to the heat liberated during oxidation. If oxygen is chemisorbed at -196°C and the chemisorbed layer warmed to a higher temperature so that incorporation occurs, no large change in the true film area occurs. This implies that the heat of chemisorption can be dissipated at -196°C, and that the above area changes are largely due to the heat of chemisorption of oxygen and not to the incorporation process.

It has already been noted that such changes must be taken into account when deriving an approximate value for the oxide thickness. They will also affect the resistance changes accompanying the oxidation.

3.27 The growth of thin oxide layers

3.27 (a) Distinction between the oxidation stages

If after adsorption at -196°C the film is warmed to a higher temperature the activation energy for further incorporation becomes available, sites become unblocked, and further adsorption can occur. This process can be carried out continuously as illustrated in figure 11 until a definite oxide layer exists. If the adsorption is carried out at a higher temperature without temperature cycling (e.g. figure 16), then the entire interaction is con-

veniently divided into 3 stages:

i) A build up of negative S.P. The maximum negative S.P. will occur at amounts adsorbed equivalent to coverages higher than unity at temperatures above -196°C, since extensive incorporation takes place simultaneously. This is illustrated in figure 15 at -78°C.

ii) A fast process by which a thin oxide film grows on the metal surface.

iii) A slow process once a certain oxide thickness is reached.

At some time during stages (i) and (ii) the growth mechanism changes from a place exchange or incorporation mechanism to a diffusion process controlled by the diffusion rate of species through the oxide film. Nucleation of an oxide phase must occur between stages (i) and (ii). During the growth of the thin oxide film various factors may be rate determining, and various rate equations have been derived in the literature. Some properties of the system oxygen plus polycrystalline chromium films may however complicate the application of theoretical rate laws:

(α) It is observed that the structure of the film changes during oxidation.

(β) The polycrystalline nature of the films will always give deviations from theory, since in general it assumes a homogeneous surface and oxide, and polycrystalline films are heterogeneous in nature.

We have attempted to avoid an error due to changes of film structure by computing the oxide thickness on the basis of the film area as measured at the point in question. While this reduces the effect of film structure changes it does not necessarily remove them, since a reduction in film area due to oxidation induced sintering is always related to changes in the nature of the metal-oxide interface (e.g. shifts in the predominance of surface planes, changes in the defect structure of the films and any re-arrangements of the oxide that may be necessary as the underlying metal sinters).

(٢) To test a given kinetic law it is necessary to obtain data over a large range of oxide thicknesses which is difficult since initial rates are too fast to be measurable, and the oxidation at the temperatures we are considering slows down rapidly. Two further difficulties should be mentioned. The first is an uncertainty with regard to zero time in our experiments which does not necessarily correspond to zero oxide thickness as our kinetic measurements start when the rate becomes slow enough to be mensurable. The integrated form of some of the rate equations requires a fairly arbitrary choice of to where the integrated rate equation has the form

$$X = f(t + t_o)$$

where X = oxide thickness

and t = time

The choice of t_o can influence the slope and linearity of graphical tests of the rate equation. Secondly, if a fit is obtained with one kinetic law it is not itself of conclusive evidence that only this is applicable. It is often the case that more than one rate law can describe a given set of data over a limited range of oxide thickness (Roberts,[30]).

The oxide thicknesses with which we are now concerned are in the region of a few Angstroms to several tens of Angstroms. The thickness of the oxide is appreciably less than the characteristic space charge depth existing in thicker oxide films, and it is therefore generally assumed that space charge effects can be ignored. Different types of rate equation are obtained depending on the rate determining reaction, e.g. electron tunneling, ionic transfer or interface reactions. For the reasons given above, kinetic data alone is not sufficient to distinguish between these possibilities.

3.27 (b) Measurements of the oxide growth

Figures 15 and 16 show the variation of S.P. and film resistance during the interaction of oxygen with a chromium film at -78°C. After the S.P. has saturated, the interaction is still fast, and an appreciable oxide thickness is built up with little change in S.P. The rate then suddenly slows down, and oxidation proceeds at a slower rate, again accompanied by little change in

S.P. The effect of warming to 22.6°C is also shown. The negative S.P. falls, and then more oxygen can be rapidly adsorbed, before the rate slows down again. The meaning of the higher maximum negative S.P. attained at 22.6°C is obscured by the fact that small doses of oxygen were admitted initially with a hot cathode filament, and hence atomic oxygen was present. The behaviour at 58°C is very similar. On cooling back to 25°C the rate is then immeasurably slow over 8 hours at 10^{-2} torr pressure, and increasing the pressure to one atmosphere causes no discernable change in the film resistance.

Figure 17 shows the dependance of oxygen uptake and film resistance on time at -78°C, the plots are basically similar at 22.6°C and 58°C. At various points on these plots the pressure was suddenly changed so that the pressure dependence of the oxidation could be ascertained. No dependence of uptake on pressure could be observed. Attempts have been made to fit the curves similar to figure 15 to logarithmic, inverse logarithmic and parabolic equations, but the results are indecisive. At all these temperatures it is difficult to say which gives the better fit, since fits can be obtained with both log and inverse log equations. Data on other films is similar, but we shall not attempt to discuss it in detail until it is more extensive.

3.27 (c) The Mott-Cabrera Model

The fact that the S.P. appears largely constant at the oxide layer grows suggests that the Mott-Cabrera mechanism for the growth of thin films is operative.

Cabrera and Mott[31] suggested the following model: a chemisorbed film exists on the oxide, and ions and electrons move independently through the oxide film. At low temperatures the ions cannot diffuse under the influence of the concentration gradient of ions, but the electrons can pass from the metal to the oxygen at the film surface. This process results in cations at the metal-oxide interface, and anions at the oxide-gas interface, setting up a strong electric field across the oxide which is sufficient to pull cations through the oxide. The type of growth law obtained depends on the thickness region considered and the characteristic space charge depth in the oxide. If for an oxide of thickness X

$$X > X_1 = \frac{ZeaV}{kT}$$

where Ze = charge on the cation

a = cation jump distance

V = potential across the oxide,

then $\frac{dX}{dt} = \frac{const}{X}$ at constant temperature, which gives a parabolic rate law on integration.

A cubic law can also be derived for a p-type semiconducting oxide, if the number of cation vacancies is dependent on the field strength and therefore inversely proportional to the oxide thickness.

However, for chromium Ze is likely to be 3e, V ≈ 2 volts

and $a \approx 2.5$ Å giving $X_1 \approx 150$ Å, which is much larger than the oxide thicknesses with which we are presently concerned. At thicknesses very much less than X_1 the electric field across the oxide is so great that the migration rate of cations is no longer proportional to the field strength, and the oxidation is controlled by non-linear ionic diffusion. This gives the following rate equation

$$\frac{dX}{dt} = N'\Omega \nu \exp\left(\frac{-W + qa'FN}{RT}\right) \qquad (20)$$

where N' = the number of special sites per unit area at the metal surface from which a metal ion moves into the oxide layer

W = the energy barrier which a cation has to surmount in moving from the special site into an interstitial position or cation vacancy, with

W = U + S where U = the activation energy for diffusion within the oxide

S = the heat of solution of the cation in the oxide

a' = the distance between the special surface site and the top of the energy barrier

q = the charge carried by a mobile cation

Ω = the volume of oxide containing one metal ion

ν = the frequency of vibration of the cation

R = the gas constant

N = Avogadros number

F = the field existing across the oxide layer

$= \frac{V}{X}$ where V = the potential across the oxide layer

X = the oxide thickness

This equation has previously been found applicable to the oxidation of iron films (Roberts[32]), the anodic oxidation of niobium (Adams and Kao[33]), the oxidation of barium (Bloomer and Cox[34]), and the nitridation of calcium films (Roberts and Tompkins[35]).

The fact that the S.P. of chemisorbed oxygen on chromium is approximately -2.2V, and that the S.P. appears to be approximately constant as a thin oxide layer grows suggest that this rate equation might apply here. The observation that the uptake versus time (figure 17) does not give a uniquely good fit with an inverse logarithmic plot as predicted by the above equation is not considered a serious difficulty for the reasons outlined in section 3.27(a).

The high constant S.P. during the growth of the oxide however is not conclusive proof that the above mechanism holds, since the measured potential might not appear across the oxide to cause cation diffusion. Apart from a potential appearing between chemisorbed oxygen atoms and the metal, other double layers of charge are possible which would contribute to the measured S.P. but not the field across the layer. Grimley and Trapnell[36] have considered the case where chemisorbed oxygen bonds to oxide surface metal ions, which change their valency in order to give

electrons to the chemisorbed layer. This process may give a field that is localised within an ion pair and does not act across the oxide layer. Neutral pairs may be converted into adsorbed ions by an electron transfer from the metal, thus creating a field but the proportion of such ions may well be small because transfer involves a great reduction in the Coulomb energy of attraction between metal and oxygen ions. They treat two cases, one where the surface is saturated with field creating species, (p- or n-type oxide) and the case where an equilibrium exists between neutral pairs and field creating ions. The former results in a linear law, and the latter can lead to a variety of laws under different circumstances.

We have observed that if an oxide layer is saturated with oxygen by allowing the slow adsorption at -78°C to proceed until the rate is almost immeasurably slow at an oxygen pressure of several microns with the cathode filament cold, the oxide surface is not saturated with field creating species. This was ascertained by pumping out the residual gas, switching on the diode and admitting a small quantity of oxygen. The S.P. at this point was close to the saturation value. The small increment was rapidly adsorbed with a negative S.P. change which decayed back to the initial S.P. at a rate implying that the rate of oxidation was much faster than during the slow uptake at -78°C. The cathode was then cooled and a further small increment was slowly adsorbed at the same rate as the slow adsorption (confirming the lack of

pressure dependence). After 12 minutes the S.P. had not measurably changed. These observations imply that a full monolayer of chemisorbed oxygen contributing to the measured S.P. does not exist at the oxide surface, since by supplying the energy required to dissociate oxygen molecules further oxygen can be chemisorbed, leading to an increased field and increased rate of incorporation.

Contrary to our previous statement (Crossland and Roettgers[26]) this phenomenon is in full agreement with the assumptions of the Mott-Cabrera theory: In the theory the constant potential arises in the following way: electrons pass through the oxide layer from the metal to the oxygen adlayer (probably by electron tunneling) at a rate that is fast compared with ionic motion. The adsorbed oxygen is then assumed to be partly ionised, creating a field across the oxide layer until a quasi-equilibrium of electron flow in both directions is established over a period shorter than the diffusion time of a metal ion. The electrostatic potential V built across the oxide layer is then independent of thickness, and the field

$$F = \frac{V}{X}$$

is thickness dependent. Since the field is also given by the Coulomb formula

$$F = 4\pi Ze\,n$$

where Ze = the charge per oxygen atom

n = the number of field creating species per unit area

and Ze can be assumed to be constant, the assumption of a constant V means that

$$n = \text{const.} \times \frac{1}{X}$$

i.e. the layer is not saturated with field creating species. The experimental observation is in fact in disagreement with Grimley and Trapnell's[36] assumption of a saturated adlayer.

The most direct evidence for the Mott-Cabrera mechanism would be to demonstrate a direct dependence of the oxidation rate on the field across the oxide layer, as measured by the S.P. divided by the oxide thickness. This would establish that the potential is in fact appearing across the oxide, and any potentials contributing to it from either a "contact potential" between metal and oxide, or from oxide surface effects such as those postulated by Grimley and Trapnell[36] must be small. We describe this proof below using data similarly attained as in figure 11.

From the final rate of incorporation at -78°C, and the initial rate at 25°C (using the S.P. change as a measure of the incorporation process) activation energies can be calculated. This method is particularly valuable since it allows the S.P. and the oxide thickness to be varied. At each point where the

activation energy is measured we also measured the area of the film by xenon adsorption, so that at these points we know

i) the film surface area

ii) the S.P. of chemisorbed oxygen

iii) the amount of oxygen taken up by the film

iv) the activation energy for incorporation

This allows $\frac{S.P.}{X}$ to be calculated, and if the Mott Cabrera mechanism holds, this quantity should be directly related to the measured activation energy ΔE, since according to eq.(20)

$$\left.\begin{aligned} \Delta E &= W - qa' FN \\ \text{and } F &= \frac{S.P.}{X} \end{aligned}\right\} \qquad (21)$$

TABLE V. ACTIVATION ENERGIES DURING OXIDATION

Observed activation energy (K cal/mole)	Oxide thickness X (Å)	$\frac{S.P.}{X}$ (Volts/Å)
3.4	2.1	.60
5	4.6	.45
2.75	8.1	.32
5.5	10.7	.27
8	12.5	.23
6.6	12.7	.24

Table V shows the data obtained, and figure 18 shows a plot of ΔE versus $\frac{S.P.}{X}$. The plot should be a straight line, whose

intercept with the activation energy axis is W, the entry barrier for cation diffusion. This is clearly not so for the first two points of table V but the remaining points lie on a straight line whose intercept corresponds to W = 24 Kcal/mole. This value is very similar to the figure of 22 Kcal/mole derived from volumetric kinetic data for the nitridation of calcium films (Roberts and Tompkins[35]), and 20 Kcal/mole also derived from volumetric kinetic data for the oxidation of iron films (Roberts[32]). In this case an S.P. of approximately 2 volts was assumed whereas the correct value for iron is probably lower (~ -1.6 volt, Quinn and Roberts[21]) so that the estimated 20 Kcal/mole is probably too low. Since W = U + S and the measured value of W is comparable to the activation energy for diffusion within oxides, the heat of solution of the cation in the oxide must be small.

The fact that the initial points at equivalent oxide thicknesses of 2.1 and 4.6 Å do not lie on the line is not surprising, since a definite oxide phase over the metal surface might not be expected at such low effective oxide thicknesses. It is also evident from table V that the activation energy is dependent on $\frac{S.P.}{X}$ and not on $\frac{1}{X}$, as a plot of ΔE versus $\frac{1}{X}$ does not give a straight line.

The slope of figure 18 represents a very small value for a' if the diffusing species is Cr^{3+} (near 1 Å), suggesting

that $\frac{a'}{a} \sim 2$ where a = the distance between planes of oxide ions, as had to be assumed for the nitridation of calcium films. However, a value derived in this way would be in error if the oxide layer was not entirely Cr_2O_3.

The data therefore indicates:

(i) The S.P. is initially constant as the thin oxide layer grows.

(ii) There is a direct dependence of the rate of oxidation on $\frac{S.P.}{X}$, and therefore the S.P. must appear largely across the oxide.

(iii) The oxide surface is not saturated with field creating species. We therefore conclude that thin oxide films in the region 0 to 20 Å thick at temperatures up to around room temperature grow by the Mott Cabrera mechanism, and that the rate equation (20) holds.

Roberts[20] has listed the important parameters in an oxidation process based on the Mott-Cabrera mechanisms.

(α) The structural characteristics of the metal surface, since N' is related to surface defects.

(β) The surface potential V of the chemisorbed gas: the larger the S.P., the more extensive will be the incorporation.

(γ) The value of W. This will be small when the heat of solution and the energy for cation diffusion

are small. Thus an open type oxide structure involving a cation of small radius will give a small activation energy.

(γ) Electrons must be able to establish an equilibrium between metal and adsorbed oxygen on the oxide in a time short with respect to that required for a cation to diffuse through the oxide.

In this latter context it is interesting to note that Fromhold and Cook[37] have recently shown that "Hauffe-Ilschner" transition from electron tunneling to a Mott-Cabrera type mechanism in the thin oxide film region is not feasible. This is in agreement with our findings, since we have found the latter mechanism operative from the earliest stages. They have also shown that a reverse transition from non-linear ionic current controlled oxidation to electron tunneling controlled oxidation might be expected at a higher oxide thickness in the region of 30 Å.

Present work is aimed at extending the range of temperature and oxide thickness to verify the predictions of the Mott-Cabrera theory regarding the temperature dependence of the limiting oxide thickness and the onset of "catastrophic" oxidation, and to find its limitations.

3.27 (d) "Second layer" oxygen adsorption

At low temperature (-196°C) and when the surface of the films had reacted with more than one monolayer of oxygen a series of effects were observed that indicate the existence of a weakly bound state of oxygen with a positive dipole.

i) Close to unit coverage of oxygen at -196°C, the admission of an increment of oxygen gives an initial positive transient S.P. which decays to give the saturation value. If the adsorption is continued well beyond unit coverage the saturation S.P. falls (as found on nickel), the adsorbed O_2, giving rise to this +S.P., can be pumped off and hence is weakly held. Similar behaviour occurred when oxygen was admitted at -196°C during the adsorptions marked 2,3,4, etc. on figure 11, a positive transient preceded the normal negative change. The magnitude of this transient (a few mV to several tens of mV) increases as the surface becomes more oxidised, and the decay time increases from a few seconds to several tens of seconds.

ii) At high coverage of oxygen on an oxide surface at -196°C the normal positive drift is replaced by a slow negative drift following the negative maximum which is due to the transfer of oxygen from the weakly adsorbed state to the strongly chemisorbed state with negative S.P. This has no effect on the incorporation, since the film resistance steadily increases at the expected rate during this process.

iii) On warming such a layer from -196°C to -78°C a negative transient S.P. occurs before the normal positive decay

which is due to a transfer of oxygen from the weakly bound state to the chemisorbed state on increasing the temperature.

Oxygen molecules do not strike the surface and instantly dissociate into atoms to give the negatively charged chemisorbed species. They must approach this state via a weakly bound state of adsorbed species involving oxygen molecules which we appear to have observed. A positive dipole might be expected by analogy with other observations of weakly bound species, e.g. physical adsorption gives a positive S.P., as does weakly bonded hydrogen. This 'second' layer oxygen has not been observed to be stable at temperatures above -78°C, but at low temperatures it becomes more stable as the oxide layer thickens.

3.28 The effect of oxidation on the film resistance.

It is difficult to separate the ways in which chemisorption of oxygen and oxidation might influence film resistivity, some possible ways are listed below:

i) A simple decrease in film thickness caused by the growth of the oxide.

ii) Electrons are transferred from the metal to chemisorbed oxygen atoms at the surface. A number of attempts have been made to treat qualitatively the

conduction changes during chemisorption by considering the number of electrons removed from the conduction band. A parameter α is defined as

$$\alpha = \frac{\Delta\lambda}{\lambda_o}\frac{z}{n}$$ (see for example Gundry and Tompkins[38])

where $\Delta\lambda$ = change in film conductance

λ = initial conductance

z = total number of metal atoms in the film

n = number of chemisorbed atoms

Although α has been identified with N_c/N_B (N_c = number of bonds per chemisorbed entity, N_B = number of bonds necessary to remove a surface metal atom from the conduction process) we reject this as being not applicable since it ignores the structural heterogeneity of the films and all other effectsexcept the electronic one, (Gundry and Tompkins[38]).

iii) On polycrystalline films preferential adsorption and oxidation might occur at grain boundaries etc. In any case adsorption and oxidation at grain boundaries might give a larger contribution to the resistance change than adsorption and oxidation on the crystallite surfaces.

iv) Oxidation might result in a change of surface properties which could influence the way in which electrons are scattered at the surface.

v) Oxidation may introduce impurity scattering centres into the films to a depth sufficient to affect the resistance.

vi) It has already been observed that changes in film structure accompany the oxidation, this will be reflected in a resistance change.

It should be possible to assess the contribution of some of these processes by measurements on single crystal films. In the meantime we shall use the parameter α simply as a normalised resistance to describe the behaviour of the polycrystalline films, where N = the total number of oxygen atoms that have reacted with film.

Resistance variation during the build-up of the negative surface potential is shown in figures 10 and 15. The average values of α are 2.3 at -78°C and 1.1 at -196°C. α is lower at the lower temperature, because there is considerably less sintering and the partitioning of the adsorbed oxygen is much more in favour of the chemisorbed state, since the incorporation process is activated.

Figure 19 illustrates this point in more detail. Adsorption was carried out initially at 20°C and the film then cooled to -196°C. The surface potential changes much more rapidly at -196°C with adsorbed amount and the resistance much less than at 20°C. When the film is warmed to +20°C with no

oxygen in the gas phase, there is a positive change in S.P. and an increase in resistance, showing that oxygen is being transferred from the chemisorbed state into the metal lattice. The effect of briefly warming to 65°C is shown earlier in the plot, and illustrates the same effect in reverse. Average α at 20°C is 5.9.

The resistance versus coverage curves of figures 11 and 16 are convex to the coverage axis because initially chemisorption and incorporation occur at the outer surface of the film, with less effect on the resistance than subsequent additional interactions at the inner surface. The curvature is more marked at -78°C as a correspondingly larger amount of oxygen can interact with the outer surface.

It can be seen from figure 16 that once the large negative S.P. increase has finished, the increase in resistance with the extent of oxidation is approximately linear, and at -78°C gives $\alpha = 3.5$. All the oxygen taken up is now being incorporated, hence the larger α. This linear relation and the fact that the T.C.Rs of the films were not appreciably changed during the course of the interaction suggest that the decrease in film thickness with oxidation accounts for the increased resistance.

If we define the film thickness X_{film} to be

$$X_{film} = \frac{m}{\rho \times a}$$

with m = film mass

ρ = film density

a = geometric film area

we find $X_{film(4)} = 525$ Å. With the oxide thickness $X_{oxide} = 8.9$ Å, we have

$$\frac{X_{oxide}}{X_{film(4)}} = 1.7 \times 10^{-2}$$

which should be equal to the relative resistance change $\frac{\Delta R}{R}$ due to oxidation. Since, however, we measured $\frac{\Delta R}{R} = 12.8 \times 10^{-2}$, we have to assume an effective film thickness $X_{film(4)} = 70$ Å.

If the film thickness is calculated from the mass and the area as measured by xenon adsorption, values in the range 60 to 120 Å are obtained. These results suggest that the film resistance may be controlled by regions of low thickness. Quantitative results will only be obtained from measurements on smooth single crystal films.

4. SINGLE CRYSTAL FILMS

4.1 Preparation and Structure of Single Crystal Chromium Films

Two types of single crystal films with different orientations would allow the dependence of oxidation on the orientation to be studied. The growth of such oriented single crystal films depends very much on the type of substrate used (Pashley[39]). Numerous substrates were considered and the two most useful ones

were selected that would give films of two different orientations. They were: mica which would give either a (110) or (111) orientation, and rocksalt (NaCl) that should give a (100) orientation. Another requirement was that these films should be grown in U.H.V. under clean conditions. This has been known to present problems with other metals (Matthews[40]).

4.11 Chromium on mica substrates

The substrate material used was high quality ruby mica, the surface prepared by splitting the mica sheet, this process exposing a cleaved surface. Initially chromium was deposited onto these air cleaved surfaces over a range of substrate temperatures from 25°C to 500°C. These films were examined by reflection electron diffraction, transmission electron diffraction and microscopy after stripping the films off their mica substrates. Polycrystalline results were obtained with some preferred orientation.

On the basis of experience with other metals it was thought that cleaving the mica in vacuum would improve the chance of obtaining single crystal films. An apparatus was constructed that enabled this to be done thus exposing a fresh clean mica surface to the chromium source. The vacuum system used for all these experiments with single crystal films was a Varian V.1.15 ion pumped U.H.V. system fitted with a similar evaporation source to that described in section 3.14. The rest of the apparatus is described in section 4.2.

Films were deposited under the following conditions: Substrate temperature was varied between 25°C and 500°C and deposition rates from 1Å/sec up to 10Å/sec. The best film crystallinity was obtained at substrate temperatures of 450°C. The deposition rate was not found to be critical over the range used.

Examination of these films by transmission electron diffraction and microscopy after stripping from the mica showed them to be composed of small crystallites whose average diameters ranged from a few hundred up to thousand angstroms in the best films (plate 4). The diffraction patterns showed a pronounced preferred orientation, and in the case of the better films a spot pattern was obtained (plate 3). All the low order reflections were present except the (310) and it was concluded that these films consisted of three $\{110\}$ orientations (figure 20). The $\langle 001 \rangle$ directions of the crystallites were parallel to the [010], $[\bar{3}3\bar{1}]$ and $[\bar{3}31]$ directions of the mica.

This structure can arise as follows:- The positions of the atoms in a chromium (110) plane are shown, relative to the positions of the potassium ions of the (001) plane of the mica in figure 21. Three [001] spacings of the chromium atoms fit to within about 4% the spacing of the potassium ions in the mica [010]direction. There is a misfit in the [100] mica direction of about 23%. It is probable that epitaxial growth is determined by a process of nucleation, each chromium nucleus will become oriented independently so that its [001] direction will be

parallel to one of the three equivalent <010> mica directions.

This situation only applies to the isolated nuclei. When the latter grow and impinge on their differently oriented neighbours, low angle boundaries will be formed between them (plate 5). From the electron diffraction patterns it is seen that there is a misorientation from perfect epitaxy of about $\pm 5^{\circ}$. This misorientation could arise during coalescence. Two adjacent nuclei, with their <001> directions parallel to the [010] and $[\bar{3}\bar{3}1]$ mica directions, will each have a <112> direction that is at an angle of about $10\frac{1}{2}^{\circ}$ to the other. If they rotate towards each other by this amount, a coherent (112) twin boundary will be formed (figure 22). The boundaries marked T in plate 4 are probably twins. The twin will have a lower energy than a low angle boundary and will be stable. The diffraction pattern shows that a substantial number of crystallites must be oriented in this way. All other misorientations between crystallites will be taken up by dislocations which will tend to be perpendicular to the film surface and be immobile.

Thus it would seem that chromium films deposited onto mica substrates will always show this type of structure with three (110) orientations. However at the surface only the (110) configuration is present and therefore surface potential measurements and oxidation studies are still of interest.

4.12 Chromium on NaCl cleavage surfaces

It has been shown by Shirai[41] that chromium can be deposited epitaxially onto rocksalt surfaces to give a (100) orientation. Attempts to produce similar films deposited at U.H.V. onto air cleaved substrates were not successful, only polycrystalline films with some preferred (100) orientation were observed. Following the experiences of other workers with other metals (Pashley[39]) the rocksalt substrates were prepared by cleaving in vacuum, and good single crystal films were obtained by depositing onto these freshly cleaved surfaces. In order to determine the optimum deposition conditions for the perfection of crystallinity a detailed investigation was carried out over a wide range of deposition conditions and substrate preparations.

The apparatus used consisted of a Varian V.1.15 ion pumped U.H.V. system capable of providing vacua of 10^{-9} torr, fitted with an electron bombardment heated chromium source as described in 3.14. The substrate crystal was mounted in a clamp and could be heated by a small furnace up to 500°C. A rotary feedthrough was connected via a lever to the substrate protruding above the clamp, so that the top half of the substrate could be cleaved off under vacuum. The results are summarised below:

(a) Initially films were deposited on air cleaved substrates between room temperature and 300°C, either in U.H.V. or

at 10^{-6} torr and were essentially polycrystalline with a preferred (100) orientation (plate 6). The best films were those deposited at approximately 250°C and 10^{-9} torr pressure. These films had crystallite sizes of approximately 200 Å and possibly 50% preferred orientation.

(b) Films deposited at 10^{-6} torr on vacuum cleaved NaCl were again polycrystalline over a large temperature range but with a more highly preferred orientation then previously (plate 7).

(c) Air cleaved substrates were cleaned by heating under vacuum to approximately 480°C for five minutes and then cooling to the usual deposition temperatures between 250°C and 300°C. Films deposited at either 10^{-9} torr or 10^{-6} torr were more perfect than the earlier films but still with some polycrystalline material present (plate 8).

(d) Films deposited at 10^{-9} torr on vacuum cleaved NaCl were single crystal, very sharp spot diffraction patterns were obtained (plate 9). The best films were those deposited at substrate temperatures between 250°C and 300°C.

In all cases the orientation was:-

$$(001)_{Cr} // (001)_{NaCl} \qquad [110]_{Cr} // [100]_{NaCl}$$

Only in the depositions at 10^{-6} torr was there slight evidence of $[100]_{Cr} // [100]_{NaCl}$

The deposition rate was varied between 2Å/sec and 10Å/sec but did not seem to be critical, usually a rate of approximately 3Å/sec was used.

These single crystal films have been found to be continuous at average thicknesses down to 100 Å. At such low thicknesses the surface to bulk ratio is high and it might be expected that surface effects might be detectable in the film resistivity measurements (see section 4.2).

Electron microscopy and diffraction on the single crystal films showed them to be single crystalline over the whole area of the substrate with no evidence of grain boundaries, stacking faults or twins. The only defects observed were dislocations and dislocation clusters (plate 10). This was much more marked on films deposited at substrate temperatures of 100°C where in the diffraction pattern the (110) spots had broadened into arcs subtending angles of up to 14°. The most perfect films, those deposited at temperatures between 200°C and 300°C had very sharp spot patterns, but micrographs taken in the region of extinction contours did not show a smooth intensity variation across the contour but a rather patchy configuration indicating that there were still large numbers of dislocations present. These probably originate during the

growth process when coalescing islands cannot reorientate themselves completely and dislocations form at the coherent boundary. The pattern formed by extinction contours in regions of high symmetry is shown in plate 11.

4.13 Nature of the Rocksalt Cleavage Surface

When examining films on rocksalt cleavage surfaces by multiple beam interferometry in order to measure the film thickness it was discovered that these surfaces were far from optically flat and were traversed by many cleavage steps. The features on typical cleavage surfaces which may effect the film resistance were examined by polarization interferometry, gold decoration and shadow replication.

The polarization interferometer attachment fitted to a Reichert Zetopan optical microscope was used to examine what were considered good cleavage surfaces on air cleaved rocksalt crystals after coating the cleaved surface with a reflecting film of aluminium. A typical micrograph taken with this instrument is shown in plate 16. The plate was taken using white light so as to locate the 'black' fringe, measurements were taken with 0.6μ monochromatic light, where a displacement of one fringe width corresponds to a step height of 0.3μ. All the surfaces examined were similar in that they showed steps of height between 0.1μ and 1μ and spaced on average approximately 100μ apart. Between these large steps a background fuzz was visible, but not measurable by this technique.

A technique developed by Basset[42] was used to reveal these fine structure steps. It consists of evaporating a very small quantity of gold (sufficient to give an average film thickness of approximately 5Å) onto the surface. The gold nucleates preferentially on steps and features on the substrate and these nuclei grow to form discrete small islands. A carbon film was then deposited onto the surface which fixes the islands in position and after floating off the substrate acts as a support film for examination by transmission electron microscopy. The outline of these steps and terraces are clearly revealed (see plate 12). This does not give any measurement of the step height although according to Bassett[42], these steps may be monoatomic. Thus a terrace of steps as in plate 12 may together form a sloping step of approximate height 100 Å and the separation of these terraces may be typically 10μ.

Surfaces decorated in this way were examined after different substrate treatments: Plate 12 shows a typical sinuous pattern on air cleaved NaCl, plate 13 shows a much more ordered pattern found on substrates cleaved in vacuum, and plate 14 shows how the surface is changed by heating under vacuum. This latter effect is probably due to the onset of thermal etching. The results are similar to those observed by Sella and Trillat[43] and Bethge[44] and thus indicate that our surfaces are similar to those found by other workers.

It may be concluded that even the best rocksalt cleavage surfaces are not atomically flat but are covered by many small steps of height up to 100 Å spaced up to 10μ apart and larger steps of between 0.1μ and 1μ in height spaced up to 100μ apart.

We must now consider whether this type of surface is likely to present any problems with resistivity measurements which depend on the film being continuous and uniform over the area of film between current and potential contacts, bearing in mind that the thinnest continuous film available is approximately 100 Å thick.

The 100 Å type steps are seen from decoration to be composed of terraces of smaller steps and it is reasonable to suppose that a 100 Å chromium film would be continuous over these steps. To determine the profile of the larger steps, gold-palladium shadow replication was used. With a shadowing angle of 45° in a direction perpendicular to the step edge the film was seen to be continuous over both leading and trailing edge of the steps (plate 15) which shows that these steps are probably also composed of much smaller terraces giving the larger steps an average sloping surface. This indicates that a 100 Å chromium film might again be expected to form continuously over these large steps.

Thus we may conclude that these surfaces although stepped are not likely to present any problem in getting

film continuity for resistivity measurement. If problems do arise later with the large steps then this may be avoided by using more than one source and depositing at different angles onto the substrate.

4.2 Electrical Measurements on Clean Single Crystal Films

To determine the effect of oxidation on the electrical conduction process in the films it is first necessary to measure the resistance, resistivity and T.C.R. as a function of film thickness under clean conditions at U.H.V. This will help to define the electrical conduction process in the clean films, and serve as a starting point for assessing the manner in which chemisorption and oxidation change the film resistance. We hope to separate the possibilities outlined in section 3.28 by a comparison of the behaviour of these films with the polycrystalline films. It has been noted in the previous section that the thinnest single crystal films available are approximately 100 Å thick, which is thin enough to show effects connected with surface scattering (Choppra and Bobb[45]). To get electrical contacts onto a film deposited on a vacuum cleaved substrate without breaking the vacuum presents some experimental problems. These have been only partially solved for the case of mica substrates, but a satisfactory system has been devised for films on NaCl substrates.

For measurement of film resistance it is undesirable to

use a two terminal method since the contact resistance between the contact leads and the film may be comparable with the film resistance. A four terminal method was preferred, with two current contacts and two potential contacts thus eliminating any contact or lead resistance.

4.21 Chromium on mica substrates

High quality muskovite ruby mica plates of ~ 0.012" thickness were machined into a cross shape (figure 23a) with shallow grooves cut across two arms of the cross. These arms, centre section and grooves were covered with a gold film of approximately 500 Å thickness. A blade was inserted into the edge of one of the other arms, at about half the groove depth, the flap raised slightly so that the cleave propagates as far as the junction with the side contact arms. The substrate was then clamped onto its heater in the vacuum system, gold pressure contacts placed on the gold contact arms and the raised flap connected with a fine wire to the rotary feedthrough. The rotary drive thus cleaved the mica by pulling the flap back (figure 23 b) and the freshly cleaved surface was exposed to the chromium source mounted above. The current contacts were made to the film at the junction between the gold film on the machined grooves and the chromium film which overlap in this region. After deposition a pair of independently sprung probes (figure 2 3 c) were carefully lowered onto the film

by the rotary feedthrough. These probes of known spacing were positioned in line with the current contacts just inside the grooves. Thus knowing the current through the film, film and probe dimensions, measurements of the potential drop across the probes would give the film sheet resistivity.

Considerable difficulty with this apparatus was mainly due to the film rupturing at the point of contact with the probes. Although several different probe designs were used with either radiused or pointed ends, the 'welding' effect between clean probe and film surfaces caused tearing by any slight subsequent movement of the probes. Four-probe measurements as proposed by van der Pauw[46] will be carried out with the present current contacts.

4.22 On NaCl substrates

The substrate material used was obtained from Harshaw Chemical Company in the form of rectangular blanks 38 x 20 x 6 mm and was described as being of "good cleavage quality".

45° cuts were taken out of opposite sides so that a plane joining the apex of each cut bisected the crystal along a (100) plane. These cut faces were cleaned and polished and gold was evaporated through a mask onto these sloping faces and through another mask to form 0.5 mm wide stripes up the large face of the crystal (figure 24). The crystal was clamped in a copper block with liquid gallium in the recess to ensure good thermal

contact to the block. Glass terminal plates were mounted on the sides of this block with 0.010" gold leads attached. The gold leads were fixed to the gold contact areas by a room temperature setting 50% alloy of gallium-gold (Harman[51]). Soldering and thermal compression bonding were found to be unsatisfactory due to thermal damage to the substrate or weak bonding to the rocksalt over small areas of contact. This assembly was then mounted on the substrate heater and cooling tank in the vacuum system (figure 25).

The cleavage technique was then to operate the rotary drive connected to the round nosed cleavage hammer so as to strike the centre of the upper half of the crystal with a sharp tap. The top half then cleaves off along a (100) plane at the narrowest section i.e. at the top of the sloping faces.

The chromium film was then deposited onto this cleaved surface to overlap the gold current contacts on the sloping faces. Potential contacts were made by the gold stripes on the sides of the crystal making contact over the sharp cleavage edge to the chromium film. The substrate configuration then consisted of the current contacts across the full width of the substrate providing parallel current flow along the film with the edge potential contacts providing contact to parallel equipotential lines running across the film. The resistance measured is therefore over a region

defined by the width of the substrate and by the distance between the inside edges of the potential contacts.

The circuit for the resistance measurement consisted of a constant current source connected to the current contacts of the film, in series with a standard decade resistance box. The potentials across the standard resistor and the potential contacts on the film were measured on a 100 mV digital voltmeter. The procedure was to measure the potential across the film, then the potential across standard resistance, reverse the current in the circuit and repeat. Any thermal e.m.f's could be measured at zero current and compensated for. From the average of these measurements, the film dimensions and the potential contact spacings, the film resistivity was calculated.

These measurements were first taken at deposition temperature as the film annealed and subsequently as the film was cooled to room temperature and below. Several resistance versus temperature runs were made from which the T.C.R. was calculated. Also the resistance change was measured as the vacuum system was let up to atmospheric pressure.

So far the major problem encountered has been the poor nature of the cleavage surfaces obtained; these have been so badly faulted that the film geometry and hence any resistivity measurements have been meaningless. This is surprising because preliminary experiments with cleaving on the bench produced

results at least as good as the more usual blade type cleave and surfaces obtained were similar to those discussed in section 4.13. It was thought that these problems might arise due to plastic deformation of the crystal at high temperatures (Stirland[47]). However, even cleaves at room temperature have produced the same badly faulted surface.

Attempts have also been made to anneal out the strain in the crystals prior to cleavage by heating them to temperatures up to 450°C. This made very little difference. Recent work has been directed towards modifying the method of cleaving the crystal to enable cleaved surfaces to be obtained comparable to those that are easily produced outside the vacuum system, and the method has been modified, so that cleaving is accomplished by a slow bending force with a slight tensile and shearing component transmitted by a clamp on the top part of the rock salt crystal. Cleavage surfaces produced by this method have been consistently good, comparable to those described in section 4.13. At the time of writing films are being deposited on these surfaces for evaluation. It has been verified that meaningful resistivity measurements can be made on films deposited onto rocksalt cleavage surfaces of the type described in section 4.13, by depositing chromium onto such a surface cleaved in air prior to mounting in the vacuum system. A film of average thickness 40 Å (almost continuous) had a resistivity of only three times the bulk value, which may be

attributed to size effects and shows that the films are continuous over the substrate steps.

Because of the problems mentioned above the only meaningful results so far available are the measurements of T.C.R. on films of approximately 200 Å thick. The T.C.R. values are not dependent on the film geometry and are comparable to the value for bulk chromium of $+3.0 \times 10^{-3}$ deg.C^{-1}

e.g. T.C.R. ($0^{\circ}C \rightarrow 200^{\circ}C$) = $+3.05 \times 10^{-3}$ deg. C^{-1}

T.C.R. ($0^{\circ}C \rightarrow -50^{\circ}C$) = $+2.36 \times 10^{-3}$ deg. C^{-1}

The difference between these results and those on polycrystalline films reported earlier (section 3.22) may be due to their more highly defective structure. These results are much nearer the bulk value than those of Young and Lewis[48] and the value found by Gould[18]. The latter reported work on glass substrates under comparable conditions to ours and found a T.C.R. of approximately $+1.6 \times 10^{-3}$ deg. C^{-1} for films of 200 Å thickness.

The lower values found at low temperatures may indicate the onset of size effect, as the mean free path of conduction electrons becomes larger at low temperatures or they may indicate a high residual resistivity in the films due to defects, but further experiments will reveal more information.

On letting the vacuum system up to atmospheric pressure the resistance increased consistently by 13% for films

approximately 200 Å thick, which is to be compared with 20 to 25% for polycrystalline films on glass reported in section 3.28. After solving the cleavage problem oxidation studies will now be undertaken. They will be carried out in the vacuum system described in section 4.31, and simultaneous work function measurements will be made using the methods described there.

It is concluded that it will be shortly possible to make meaningful measurements of resistance, resistivity, and temperature coefficient of resistance as a function of film thickness.

4.23 Film thickness measurements

In order to relate electrical measurements to film structure or surface phenomena it is necessary to have accurate knowledge of the film thickness. The techniques suitable for this work can be divided into three categories:

(a) Optical methods that give an average geometric thickness.

(b) Chemical methods that give a mass thickness.

(c) X-ray and electron beam methods giving predominantly mass thickness.

(a) Optical methods

Multiple Beam Interferometry is frequently used for film thickness measurements and is capable of high accuracy at low film thickness (Scott and McLoughlan[49]), but has a number of disadvantages:

(1) Masking is necessary to produce a step function in the film, which is experimentally difficult on vacuum cleaved substrates.

(2) Difficulty in positioning the step so as not to interfere with the geometry for the resistivity measurement.

(3) The cleaved surface has steps and features of comparable height to the film step height, thus upsetting the fringe pattern and making interpretation difficult.

(4) These single crystal substrates are not in general as flat as the usual glass substrates and consequently the comparator plate as used with the F.E.C.O. (Fringes of Equal Chromatic Order) system cannot be placed sufficiently close to the film surface in the step region to obtain low order number fringes that are necessary for high accuracy.

Points (1) and (2) could be avoided by use of a second control substrate but in view of the other limitations method (a) was not considered to be a practical proposition.

(b) Chemical Methods

Mass thicknesses only can be determined by chemical methods. Geometric thicknesses can then be calculated assuming a value for the film density. The methods considered differed only in the technique used for the mass determination. The lower limit of sensitivity was found from known solutions and

the relative accuracy found by using known standard solutions.

TABLE VI

Technique	Accuracy at lower limit	Accuracy at 1 p.p.m. standard solution
Flame adsorption spectrophotometry	0.2 μg ± 50%	± 10%
Spectrophotometry with diphenylcarbazide	0.06 μg ± 25%	± 10%
Polarograph	0.2 μg ± 25%	± 10%

Rectangular sections of the substrates were cut out, and the film area measured by means of a travelling microscope. The films were then dissolved for analysis.

(c) X-ray and electron beam methods

(1) X-ray fluorescence has been used for film thickness determinations, but is not applicable for films on NaCl substrates due to the characteristic X-ray emission from the substrate being outside the measurable range, and the need of accurately known standard thickness films.

(2) A technique using an Electron Probe Microanalyser (Hutchins[50]) for mass thickness determinations has been developed but at this stage has not been capable of providing sufficient accuracy.

In conclusion, the chemical method of spectrophotometry

using diphenyl carbazide was selected as the most reliable and accurate technique. A further development incorporating isotope dilution analysis is being investigated and may give a further increase in accuracy.

4.3 Measurements of Work Function Changes on Single Crystal Films

The importance of work function measurements on single crystal films has been outlined in section 2.2 and is emphasized by the measurements on polycrystalline films in section 32. Two types of measurement system have been constructed for this purpose, a slow electron gun diode, and a vibrating capacitor, so that the most suitable method could be selected. The vibrating capacitor arrangement is now being assembled in conjunction with the rest of the equipment (vacuum cleavage apparatus, evaporation source, substrate heater and holder etc.) so that measurements can begin. Work towards this end has been divided into three categories.

4.31 The vacuum system for the study of the oxidation of single crystal films

The single crystal films have a low area and a roughness factor close to unity, the actual area being approximately 1 cm^2. They are therefore much more susceptible to surface contamination than the polycrystalline films, whose actual area is several hundred square centimetres. To be certain that these

films can be kept clean for periods of many hours requires a baseline vacuum in the 10^{-11} torr decade. A special vacuum system is required to achieve this, and also a special method of measuring the pressure, since this is below or close to the X-ray limit of conventional Bayard-Alpert ionization gauges.

A schematic diagram of the vacuum system constructed is shown in figure 26. It is a borosilicate glass-mercury system based on the design of Venema and Bandringa[52]. A conventional two-stage mercury diffusion pump backs a large two-stage mercury diffusion pump, the top part of which is bakeable at 400°C. The pumping speed at the top of the large pump is 50L/sec. The tubing diameter beyond the last diffusion pump is two inches, and the cold traps are of the concentric ball type for maximum efficiency and conduction. The pumping speed at the top of the last cold trap is 5L/sec. The whole apparatus from the last diffusion pump onwards is bakeable to 400°C with two ovens which can be cooled independently, one covering the diffusion pump and the first cold trap, and one covering the second cold trap, gauges, etc. After outgassing, apparent pressures of 1×10^{-10} torr and less are indicated by a Bayard-Alpert gauge, which is close to the X-ray limit.

To increase the measurable pressure range beyond the X-ray limit a hot cathode magnetron gauge was constructed after

the design of Lafferty[53]. The electrode arrangement employed is shown in figure 27. The axial magnetic field was arranged by placing a cylindrical magnet over the gauge. A field of about 250 oersted was used, but the value is not critical. The filament was connected to a bridge circuit similar to the diode bridge circuit described in section 3.12(a). The gauge is set up by setting the anode current at about 10^{-7} Amp, and then applying the magnetic field. The anode current then falls to 10^{-8} to 10^{-9} Amp, since electrons go into orbits in the anode enclosure. This gives them a very high ionization efficiency, but the anode current is very small, which prevents instabilities in operation and gives a maximum ratio of ion current to X-ray current. The calibration of the gauge should be linear down to 5×10^{-14} torr. Ions are collected at the top disc, and the ion current measured with an electrometer amplifier. The bottom plate prevents the escape of electrons, but is not as negative as the ion collector with respect to the cathode, so that most ions are collected at the ion collector.

Since we are only interested in making certain that the baseline pressure of the system is of the order of magnitude required, the hot cathode magnetron was simply calibrated directly against the Bayard-Alpert gauge over the 10^{-10} and 10^{-9} torr decades, and the sensitivity deduced from this calibration was used to convert ion current measurements to pressure. A calibration curve is shown in figure 28. The points plotted with

different symbols were obtained on different occasions. It can be seen that the X-ray limit of the Bayard-Alpert gauge is just becoming evident in the low 10^{-10} torr region. On the basis of this calibration the baseline pressures of between 5×10^{-12} torr and 1×10^{-11} torr have been achieved with this system. This should be adequate for the purpose in hand.

4.32 Slow electron gun diode

The difficulty with the retarding potential diode method for measuring S.P. changes occurring on the single crystal film is that the diode has to be arranged so that all the diode current is taken by the small single crystal film area. To ensure this a low energy electron gun has to be used to provide a relatively narrow beam of low energy electrons to be collected by the crystal surface. The electron energy must be kept below 50 volts to avoid ionizing oxygen in the reaction cell. The construction of a suitable gun and the design considerations have been described by Mitchell and Mitchell[54] and we have adopted their design. A schematic diagram of the gun and the target assembly used for testing are shown in figure 29, which also gives the various electrode potentials. The magnetic field was provided by a coil wound on the glass envelope of the gun. The small target T_1 is of the same size as the single crystal film surface and is situated approximately 3.5 cm from the end of the gun. In the final design of the reaction cell, which

has not yet been built, the single crystal surface can be moved to within a few millimetres of the end of the gun to avoid the tedious compensation procedure adopted by Mitchell and Mitchell[54]. This is similar to the arrangement used by Anderson[55]. With the test arrangement shown it was found that over 95% of the gun current could be focussed onto T_1 over the range of target voltage 0 to 60 volts. The magnetic field was essential. This is considered adequate in view of the distance between T_1 and the gun in the test arrangement.

4.33 The vibrating capacitor

Tests on a vibrating capacitor arrangement for monitoring changes in work function of single crystal films have been conducted in conjunction with a company-sponsored programme aimed at measuring grain boundary diffusion of gold through thin polycrystalline chromium films. A schematic diagram of the test assembly is shown in figure 29 and the circuitry used in figure 31. The principle of the method is to observe the contact potential difference between a gold reference surface which will not change during oxidation and the metal film (or the test surface) as follows:

The two surfaces take the form of capacitor plates: the gold plate is earthed and electromagnetically made to vibrate normally to the plates at the resonant frequency (Ca.25 Hz) of a tungsten rod to which it is attached. The film (or test

surface) is held at 10^9 ohms from earth. The a.c. signal generated by this capacitor is amplified and detected by means of a phase sensitive detector. The rectified output voltage from the phase sensitive detector is smoothed and used to nullify the potential difference between the plates by negative feedback. The nulling potential is measured by a digital voltmeter and equals the contact potential difference to within 0.1%. The reference signal for the phase sensitive detector originates from a signal generator, and the same signal is fed via a frequency divider to the power amplifier that energises the electromagnet which excites the vibration. A stainless steel bellows arrangement allows the gold plate to be accurately positioned, and moved away from the test surface. Tests have been conducted with this arrangement at atmospheric pressure on the bench, and sensitivities of a few millivolts achieved. It has also been operated under vacuum with the same result.

One difficulty with this arrangement for S.P. measurements during oxidation is that the reference plate shadows the single crystal film, and does not allow uniform access of the gas to the surface. The importance of this can be seen from the discussion in section 3.25. To avoid this, the final design for measurements on single crystal films allows the reference plate to vibrate in a plane parallel to the two plates with a large amplitude so that the test surface is only shadowed for a small

percentage of the time. A schematic diagram of the layout of the reaction cell under construction for films on vacuum cleaved rocksalt is shown in figure 30.

Cleavage is accomplished by accelerating the stainless steel slug along its tube by means of external coils. The force required is not great, and the springs prevent fracture of the glass. This cleavage arrangement is now being modified in the light of section 4.22.

Electrical connection is made to the film, via the six leadthroughs (4 for resistance measurement, two for a thermocouple), using the same techniques as those described in section 4.22.

The substrate heater is mounted outside the u.h.v. system, and the substrate is heated by conduction through the stainless steel block. To minimize heat losses the tube containing the heater can be pumped out with a rough pump. The substrate can be cooled to temperatures approaching liquid nitrogen by circulating liquid nitrogen through the tube.

The vibrating arm and reference plate can be moved out of the way during deposition by means of the stainless steel bellows arrangement.

During measurements all metal parts except the film are earthed, as is the glass envelope, which is rendered conducting by coating with tin oxide.

The electron bombardment evaporation source has been described in section 3.14. At the time of writing this reaction cell is still under construction and will soon be operational.

5. SUMMARY AND CONCLUSIONS

Surface potential measurements on polycrystalline chromium films have enabled us to distinguish three species of surface oxygen reacting with chromium films:

(a) a weakly bound state with a positive dipole which is found at low temperatures and is probably molecular oxygen, being the precursor to the chemisorbed state,

(b) the tightly bound chemisorbed state,

(c) oxygen atoms incorporated into the metal lattice.

The latter is associated with the largest resistance changes. Chemisorption and oxide formation on polycrystalline chromium films result in profound changes in film structure resulting in a large change in the total area of the films. This must be taken into account when calculating oxide thicknesses and when considering the impact of the oxidation of the film resistance.

Incorporation of oxygen occurs on chromium even at -196°C and submonolayer coverages, and follows a logarithmic law indicating that the activation energy increases linearly with increasing oxide thickness. The behaviour up to unit coverage may be due to a range of surface sites with different activation energies and/or a surface field effect. Our data supports the former view.

The oxide thickness formed by exposing the films to oxygen at tempe_atures in the region of room temperature is approximately 20Å, and the oxidation is not dependent on oxygen pressure. These thin films grow by the Mott-Cabrera mechanism, the S.P. of chemisorbed oxygen being approximately -2.15 volts and the entry barrier for cation diffusion 24 Kcal/mole.

The implications of this mechanism for the stability of resistance values are discussed: The oxidation rate and therefore the resistance drift will decrease with the number of defect sites on the metal surface and the field across the oxide which is proportional to the S.P. The activation energy W for cation diffusion should be large for a slow oxidation rate which is equivalent to a compact oxide structure and large cations. The optimisation of the above parameters would permit the growth of a very thin limiting oxide film which protects the resistor stability better than a thick oxide layer for which the parameters listed above are not optimised.

The oxidation results in little change in TCR of the films, and apart from the initial stages the film resistance increases almost linearly with oxide thickness. To account for the magnitude of the changes an effective thickness much thinner than that deduced from film mass measurements has to be assumed.

The crystallinity of chromium films deposited in uhv on air cleaved and vacuum cleaved mica and rocksalt surfaces are described. The conditions necessary to grow good single crystal

chromium films with a (100) orientation and no evidence of grain boundaries and also highly oriented (110) films have been derived. Techniques are described to allow resistance and temperature coefficient measurements to be made on these films under uhv conditions. A study of the nature of rocksalt cleavage surfaces and electrical measurements on thin polycrystalline films deposited on air cleaved surfaces indicate that meaningful resistivity measurements can be made on single crystal films down to low thickness and that sufficiently good rocksalt cleavage surfaces can be obtained while cleaving in uhv, thus establishing that these films will make a useful vehicle for a study of the basic mechanisms of resistor degradation due to oxidation. Measurements of the TCR of clean single crystal films reflect the fact that they are structurally more perfect than the polycrystalline films. Preliminary measurements indicate that the TCR is not changed by oxidation and the resistance increases less than polycrystalline films of comparable thickness.

Tests are described of two methods of measuring the surface potential changes occurring on single crystal films, and of an ultra high vacuum system giving a baseline vacuum sufficient to eliminate any danger of contamination.

6. SUGGESTIONS FOR FUTURE WORK

The immediate continuation includes the extension of data towards higher oxide thicknesses and temperatures, in order to determine when the Mott-Cabrera would break down, and what type of mechanism takes over from it. The influence of presorbed gases and surface treatments on subsequent oxidation will also be investigated in order to assess the possibility of minimizing long term oxidation by these means. The equipment for vacuum cleavage, resistance measurement, and work function measurement on single crystal films are now being combined in a single reaction cell which will give information concerning electrical conduction processes in clean thin film structures, the way in which they are modified by oxidation, and on the structural dependences of oxidation processes.

Further work would be directed towards the determination and control of oxide and metal surface structures since they influence considerably the oxidation rate (see sections 3.25 and 3.27). Since only Low Energy Electron Diffraction (LEED) and Reflection High Energy Electron Diffraction (RHEED) are suitable methods for studying surface structures, LEED is suggested to be applied to our particular problem because it allows extremely thin surface structures to be measured, particularly since it can be combined with the experimental arrangement described in sections 4.12, 4.22 and 4.3.

7. REFERENCES

1. Walker, McKelvey, Schnable and Sharp, "Accelerated ageing and failure mechanism analysis of thin tantalum RC networks", Philco 1966

2. Levinson and Stewart, "Experimental confirmation of oxidation in evanohm thin films", 3rd Symp. Physics of Failure in Electronics, Chicago 1964.

3. Pritchard, Trans. Farad. Soc. 59, p.437, 1963.

4. Crowell and Armstrong, Phys. Rev. Vol.114 No.6 p.1500 1959.

5. Singleton, J.A.P. p.2819, 1966.

6. Lafferty, J.A.P. 22, 299, 309, 1951.

7. Roberts, Trans. Farad. Soc. Vol.60 p.899, 1964.

8. Schultz and Phelps, Rev. Sc. Instr. Vol.28, No.12 1957.

9. Ellet and Zabel, Phys. Review 31, p.1102, 1931.

10. Pritchard, Nature, 194 p.38, 1962.

11. Brunauer, Emmett and Teller, J. Amer. Chem. Soc. 60, 309, 1938.

12. Young and Crowell, "Physical adsorption of gases", Butterworths, London 1962.

13. Haynes, J. Phys. Chem. 66, p.182, 1962.

14. Cannon, Nature Vol.197, 1000, 1963.

15. Brennan, Graham and Hayes, Nature 199, p.1152, 1963.

16. Ehrlich and Hudda, J. Chem. Phys. 30, 493, 1959.

17. White and Woods, Phil. Trans. Ser. A.251, 273-302, 1959.

18. Gould, P.A., Brit. J. Appl. Phys. 16, p.1481 (1965)

19. Suhrmann, J. Chim. Phys. 54, p.15, 1957.

20. Roberts, Quart. Revs. Chem. Soc. XVI No.1., p.76, 1962.

22. Delchar and Tompkins, General Electric Research Report No.66-C-327, Sept. 1966.

23. Burshtein and Shurmovskaya, Surface Science 2, p.210, 1964.

24. Brennan Hayward and Trapnell, Proc. Roy. Soc. A.256, p.81, 1960.

25. Delchar, Ph.D. Thesis, Imperial College of Science and Technology, University of London 1962.

26. Crossland and Roettgers, Physics of Failure Symp., Columbus, Ohio, 1966.

27. Delchar Eberhagen and Tompkins, J. Sci. Instr. 40, 105, 1963.

28. Mignolet, Bull. Soc. Chim. Belg. 64, 126, 1955.

29. Lanyon and Trapnell, Proc. Roy. Soc. A227, p.387, 1955.

30. Roberts, Trans. Farad. Soc. 56, 128, 1960.

31. Cabrera and Mott, Rep. Progr. Phys. 12, p.163 1948.

32. Roberts, Trans. Farad Soc. 57, Pt.I, 1961, p.94.

33. Adams and Kao, AECU-3769, 1957.

34. Bloomer and Cox, Brit. J.A.P. 16, p.1331, 1965.

35. Roberts and Tompkins, Proc. Roy. Soc. A251, 369, 1959.

36. Grimley and Trapnell, Proc. Roy. Soc. A254 p.405, 1956.

37. Fromhold and Cook, J. Chem. Phys. 44, No.12, 1966, p.4564.

38. Gundry and Tompkins, Quart. Rev. Chem. Soc. XIV No.3, p.257, 1960.

39. Pashley, D.W., Adv. in Physics 14, 55, 1965.

40. Matthews, J.W., J. of Vac. Science and Technology, 3, 3, 1966.

41. Shirai, S., Proc. Phys. Maths. Soc. Japan, 21, 1939.

42. Bassett, G.A., Proc. Fourth Int. Conf. on Electron Microscopy, Vol.1, p.512, Berlin, 1958.

43. Sella, C. and Trillat, J.J., Single Crystal Films, edited by M.H. Francombe and H. Sato (Oxford: Pergamon Press, 1964).

44. Bethge, H., Phys. Stat. Sol. 2, 775, 1962.

45. Chopra, K.L. and Bobb, L.C., Single Crystal Films, edited edited by M.H. Francombe and H. Sato (Oxford: Pergamon Press, 1964).

46. van der Pauw, Philips Tech. Review, 20, 8, 1958.

47. Stirland, D.J. and Campbell, D.S., J. of Vac. Science and technology, 3, 5, 1966.

48. Young, I.G. and Lewis, C.W., 10th A.V.S. Nat. Vac. Symp, 1963.

49. Scott, G.D., McLauchlan, T.A., and Sennett, R.S., J. App. Phys, 21, 9, 1950.

50. Hutchins, G.A., The Electron Microprobe, John Wiley, 1966.

51. Harman, G.G., Rev. Scientific Inst., 31, 7, 1960.

52. Venema and Bandringa, Phillips Technical Review, 20, No.6, p.145, 1959.

53. Lafferty, J. Appl. Phys., 32, No.3, 1961.

ACKNOWLEDGMENTS

The authors would like to thank Mr. D J. Ellis who performed some of the experimental work described, and Mr. D.J.D. Thomas who performed the electron microscope investigation into the structure of the films deposited onto mica substrates, and gave assistance with the electron microscopy in general.

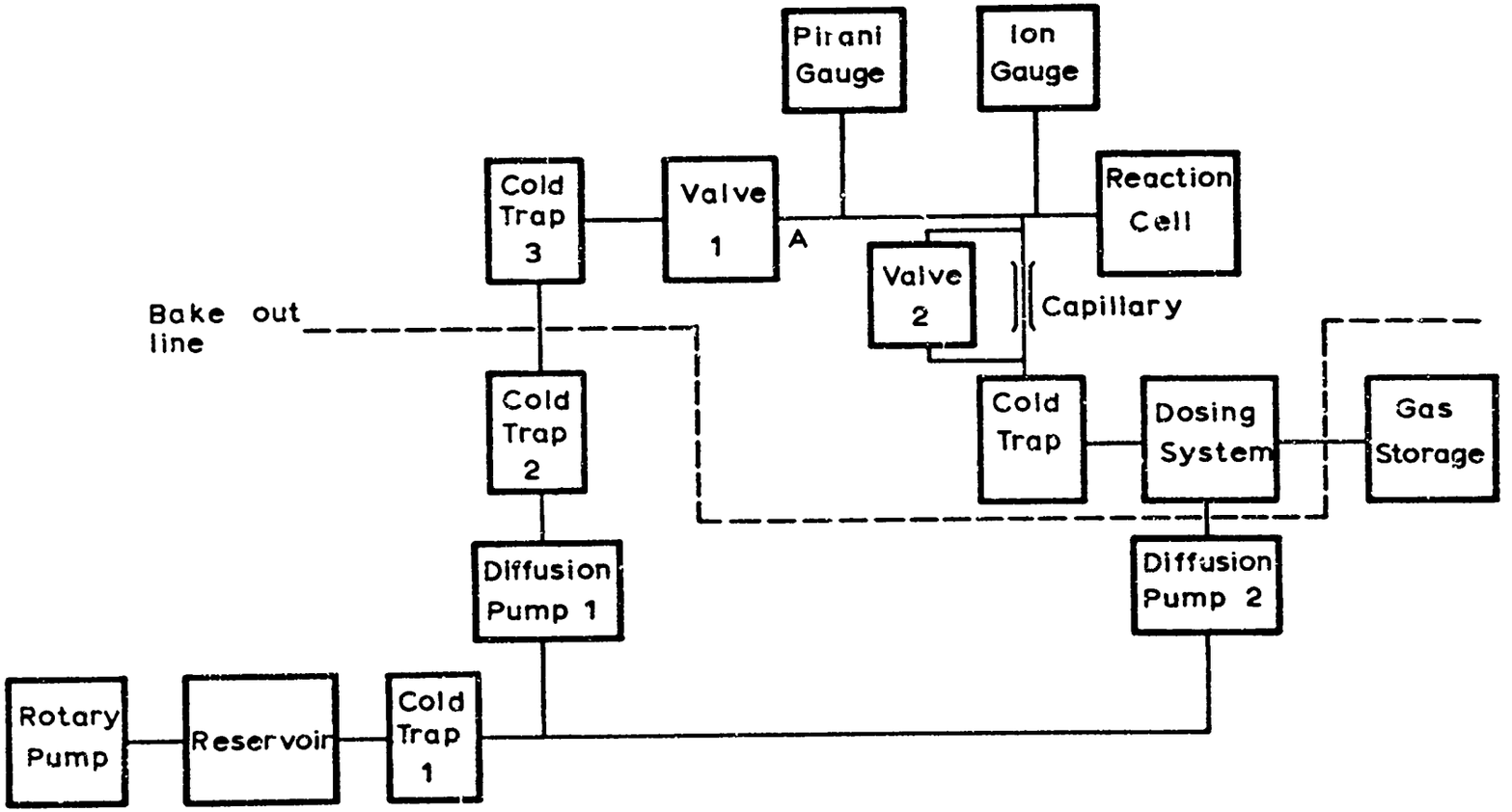

Fig.1 Schematic Diagram of Vacuum System for Measurements on Polycrystalline Chromium Films

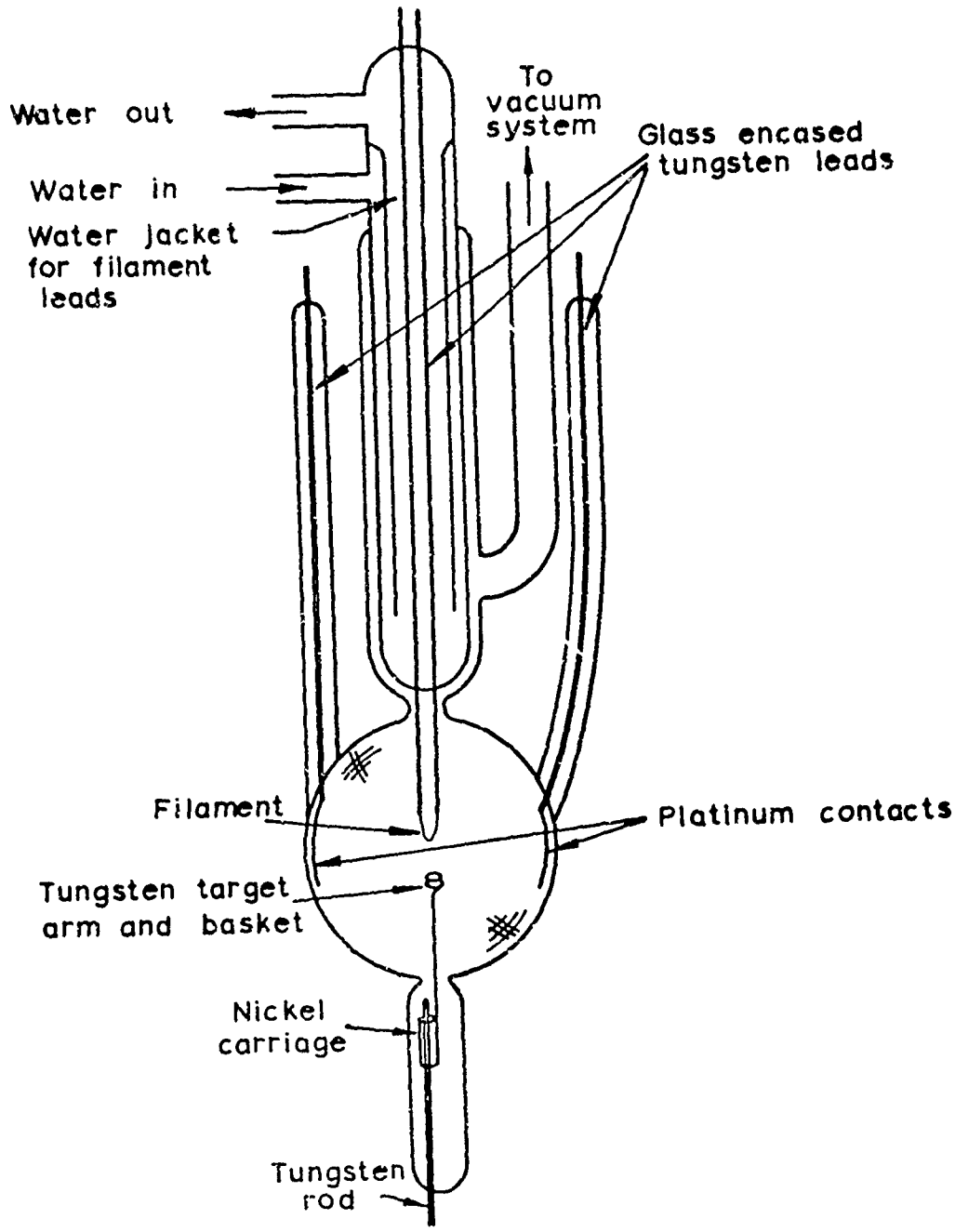

Fig.2 The Reaction Cell Used for Adsorption and Work Function Measurements on Polycrystalline Chromium Films

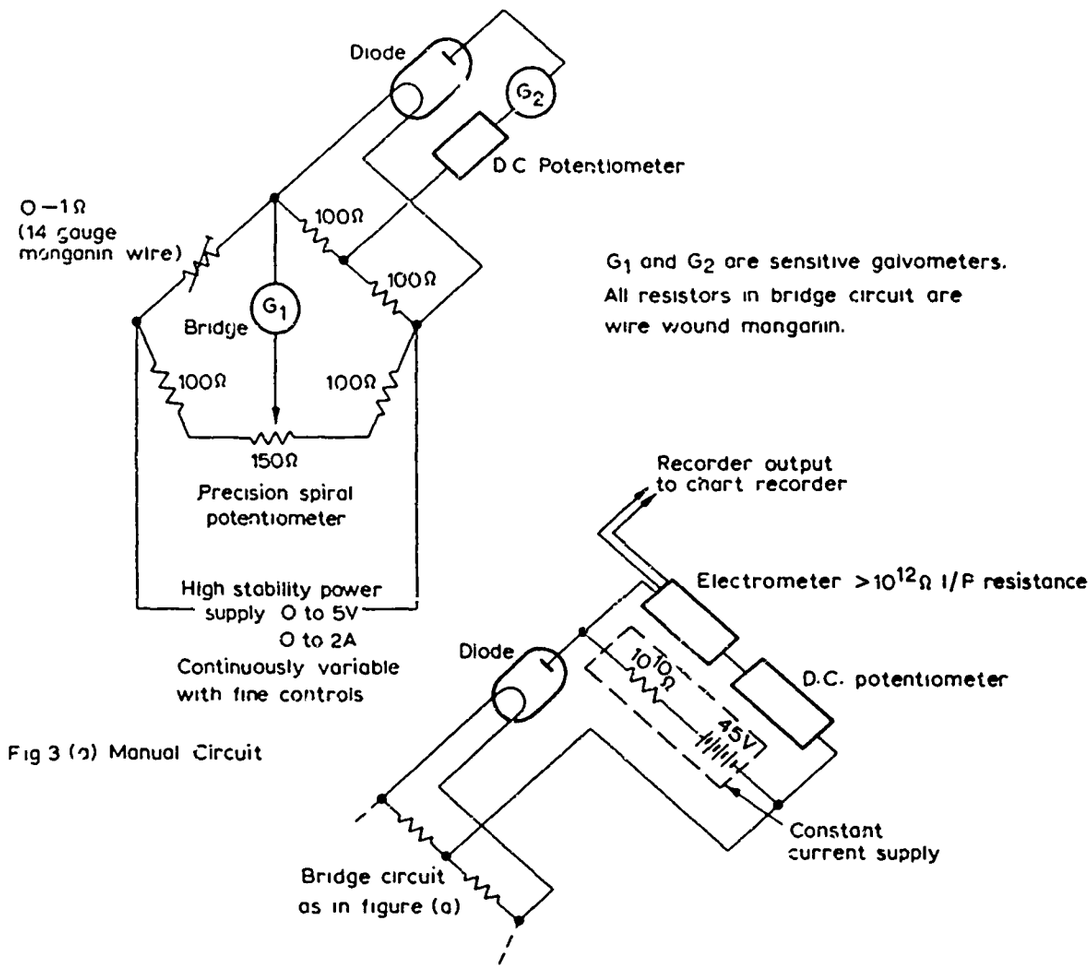

Fig 3 (a) Manual Circuit

Fig 3(b) Automatic Recording Circuit

Fig. 3. Schematic Diagram of Circuits used for the Measurement of Work Function Changes by the Diode Retarding Field Method

(a) Manual Circuit

(b) Automatic Recording Circuit

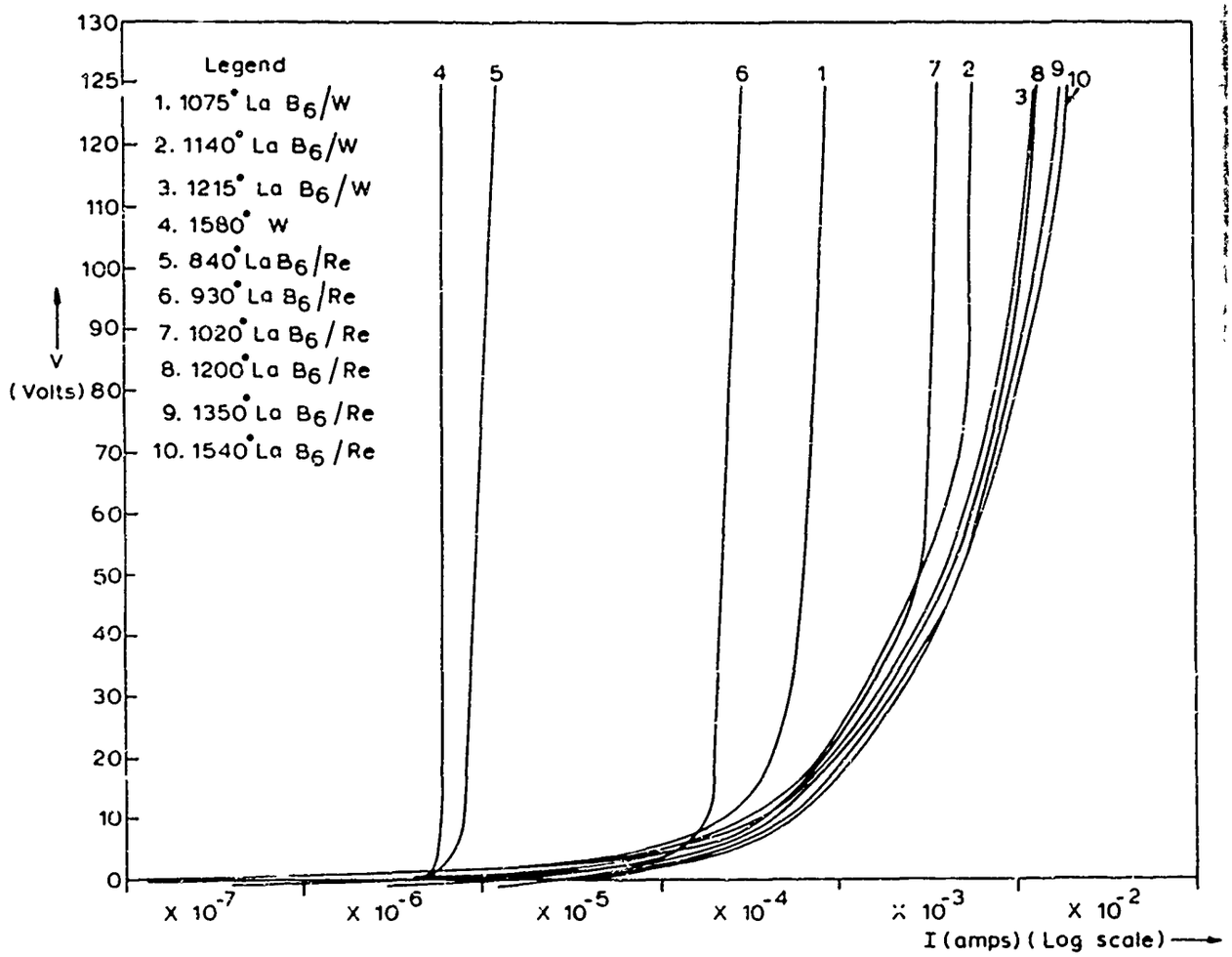

Fig. 4 Electron Emission from Tungsten (Curve 4), Compared with Lanthanum Hexaboride Coated Cathodes. I V Curves are Shown as a Function of Cathode Temperature

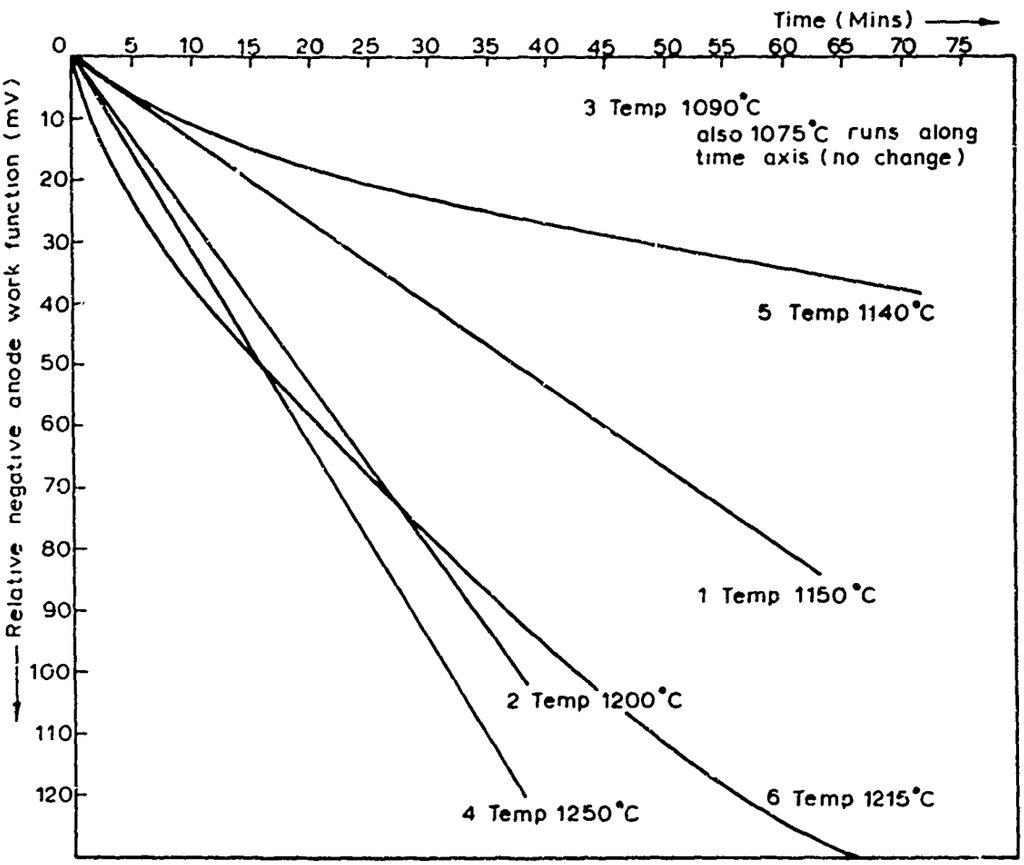

Fig. 5. Evaporation of Lanthanum from LaB_6 / ZrC / W Cathodes.
The Graph Shows Changes in the Work Function of a Gold Anode in the Vicinity of the Cathode as a Function of Time at a Number of Temperatures.

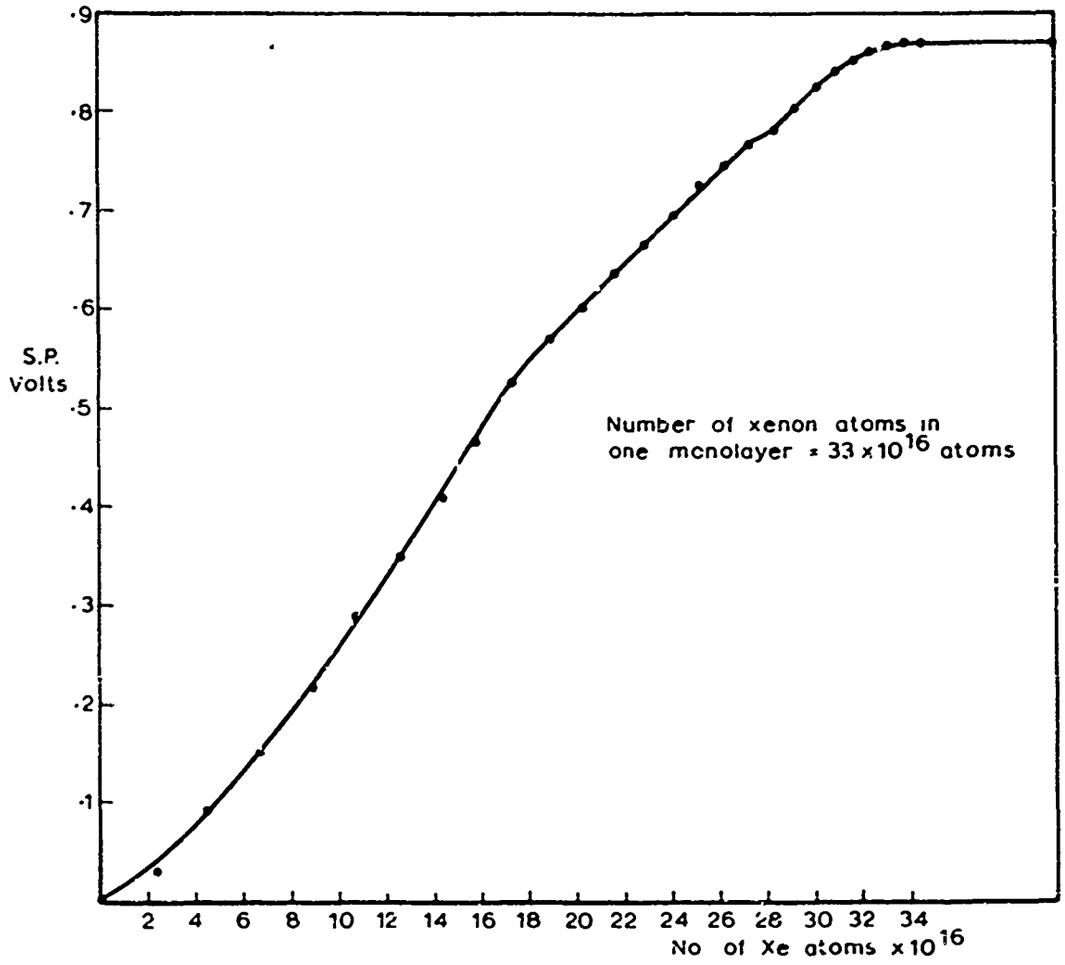

Fig.6. The Adsorption of Xenon onto a Clean Chromium Film at -196°C. The S.P. is Shown as a Functions of Amount of Xenon Adsorbed. The Saturation Point Indicates the Formation of One Monolayer.

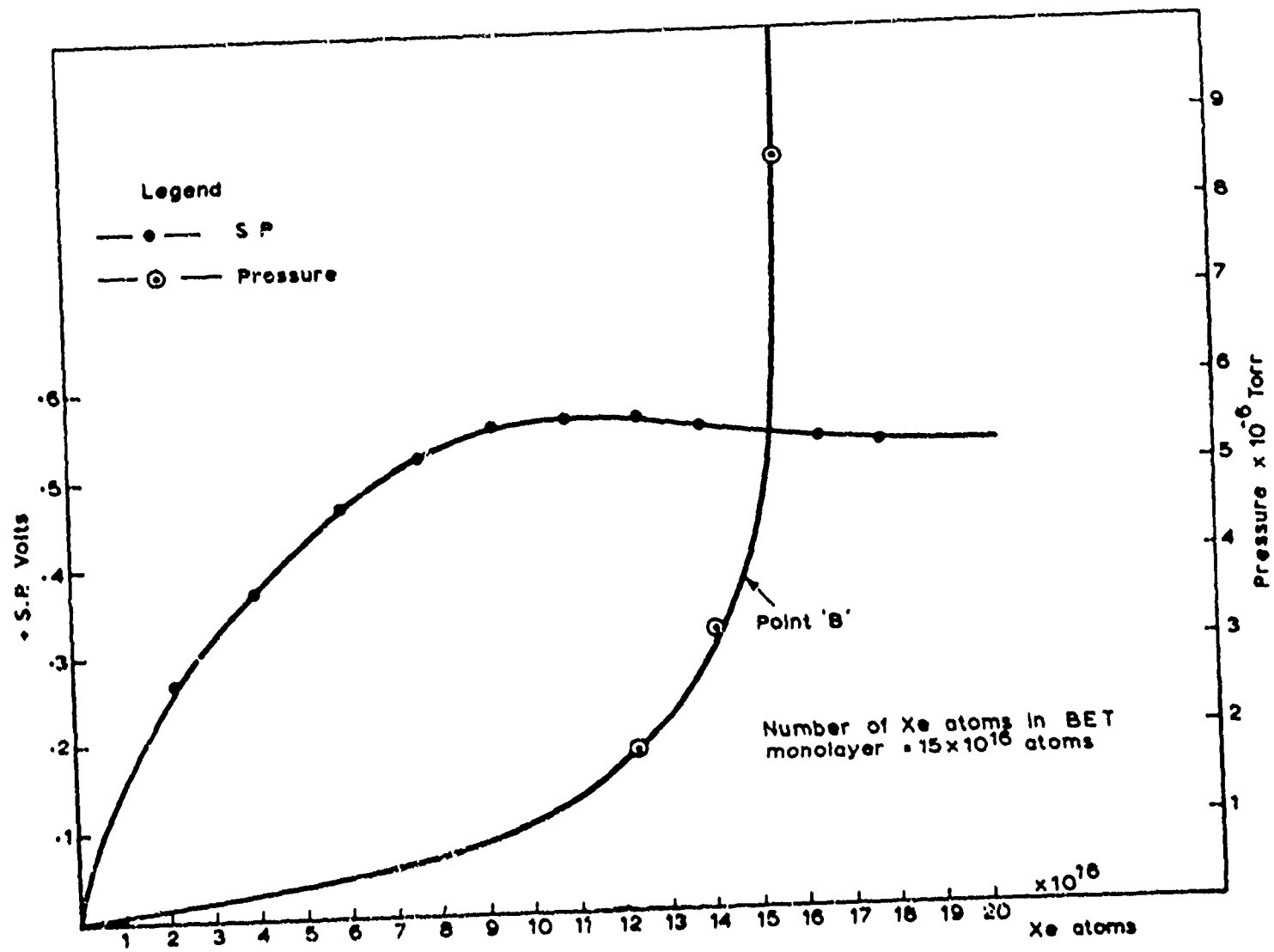

Fig.7. The Adsorption of Xenon at -196°C onto a Chromium Film with a 12 Å Thick Oxide Layer. The S P and the Pressure in the Region of the Mono Layer Point are Shown as a Function of Amount of Xenon Absorbed.

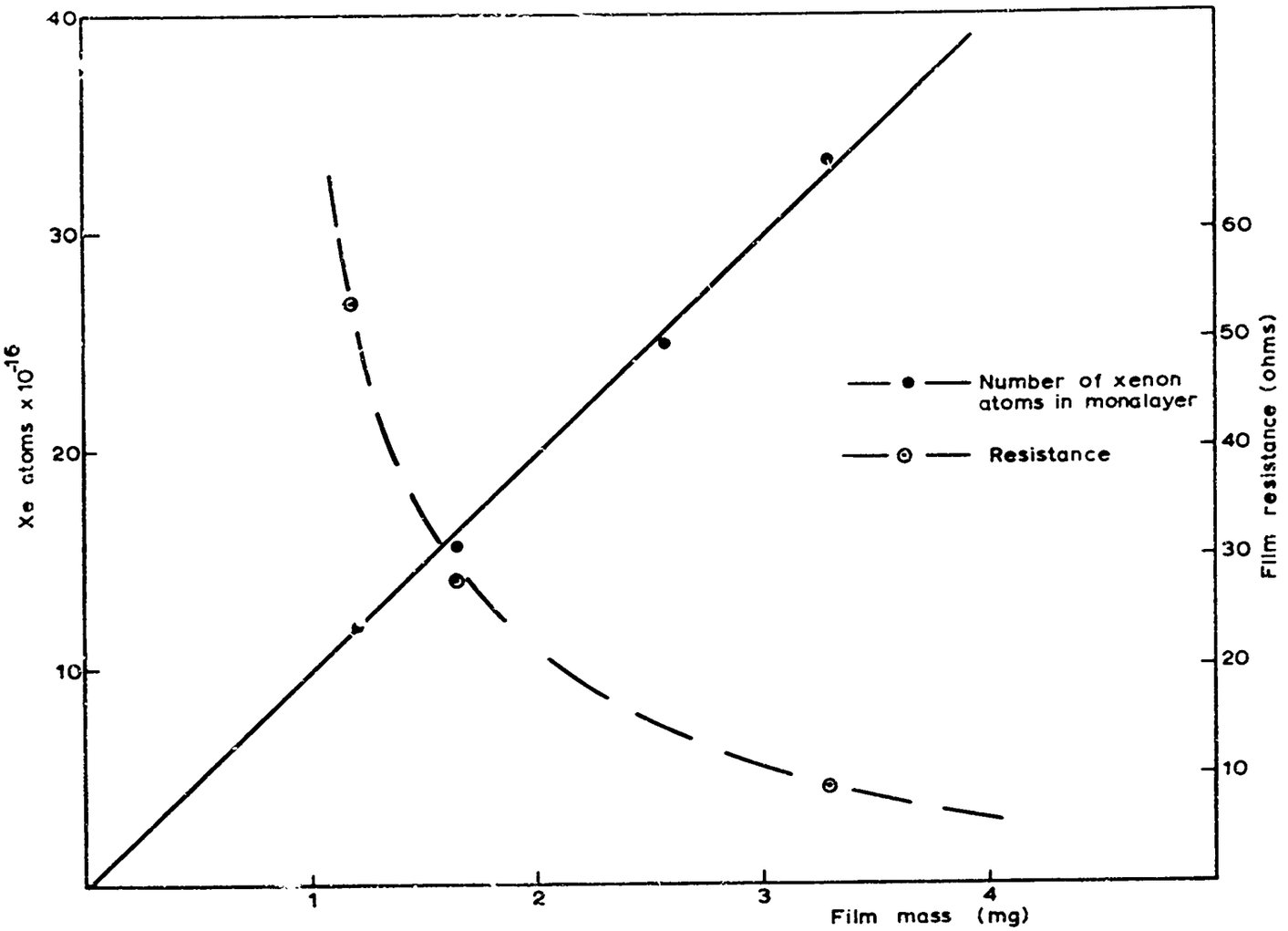

Fig.8. The Dependance of Film Area as Measured by the Xenon Monolayer Volume and Film Resistance at 25°C on Film Mass ,(For a Fixed Film Geometric Area).

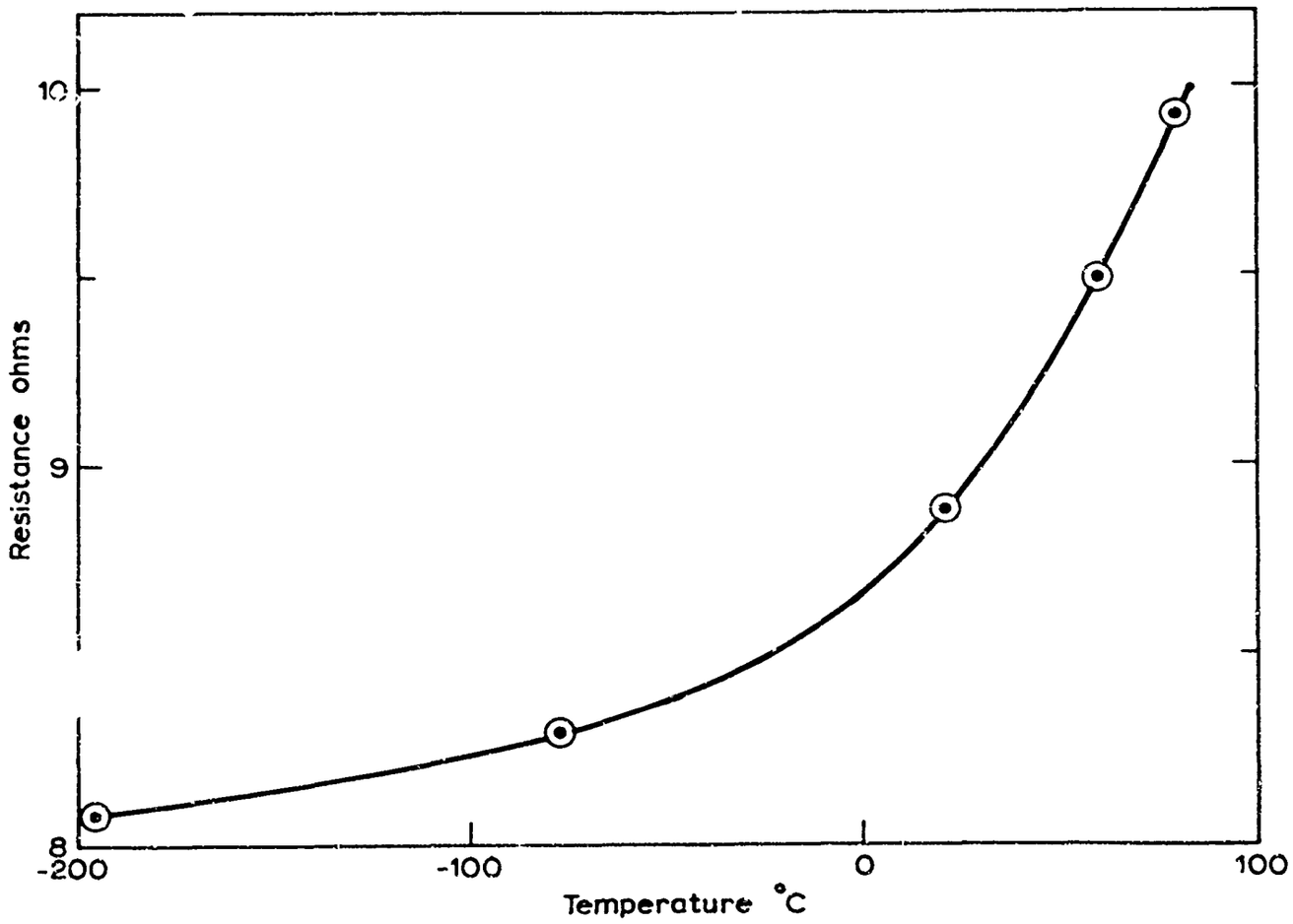

Fig.9 . Changes in Resistance with Temperature for a Clear Chromium Film of Thickness 500Å after Annealing at 80°C

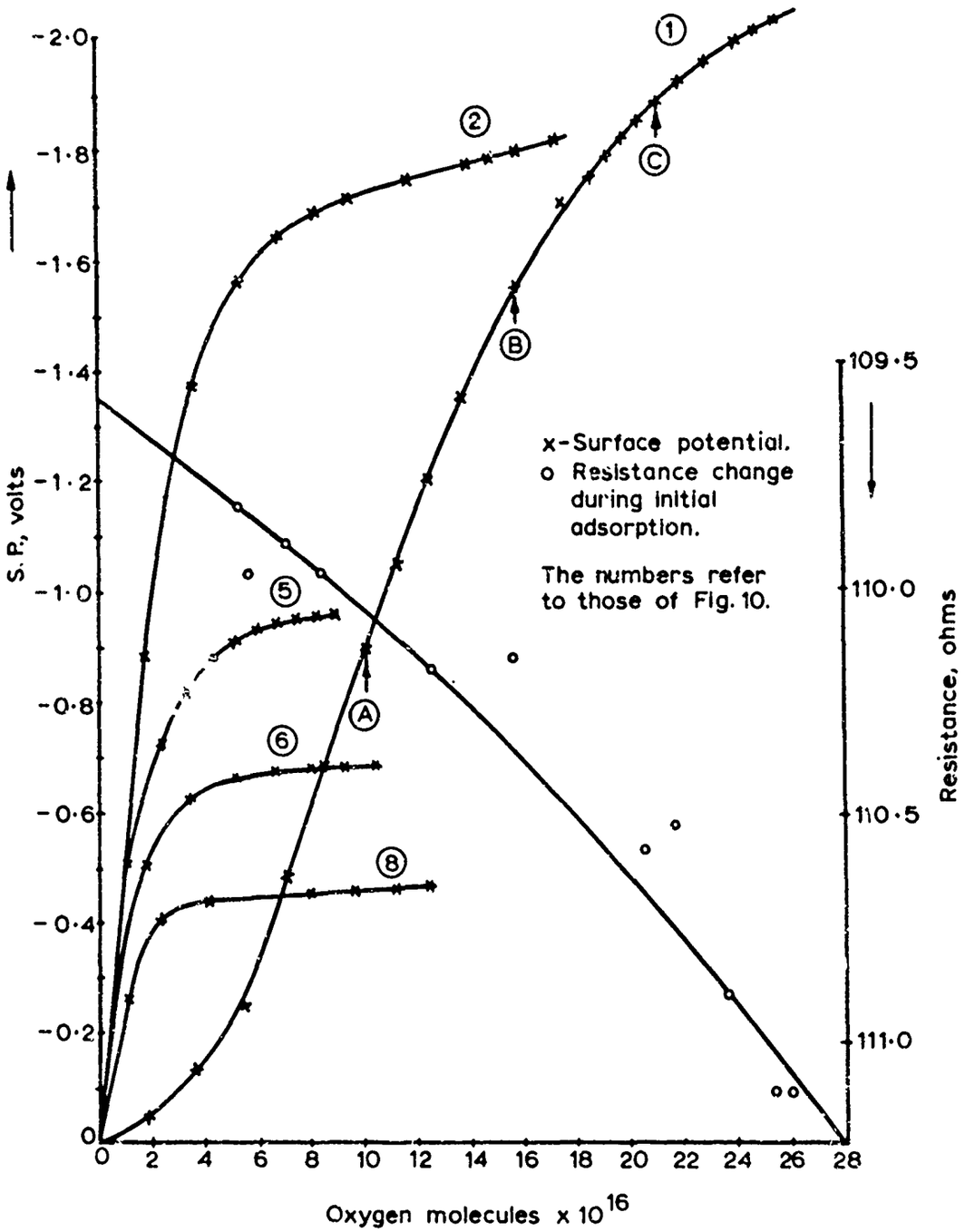

Fig.10 ① The changes in S.P. During the Interaction of a Chromium Film with Oxygen at −196°C. The Resistance Change is Also Shown ② ⑤ ⑥ ⑧ Show Adsorption of Oxygen Onto the Same Film Surface at −196°C After it has been Successively Regenerated by Warming to 20°C The Points Ⓐ Ⓑ and Ⓒ refer to Fig.12

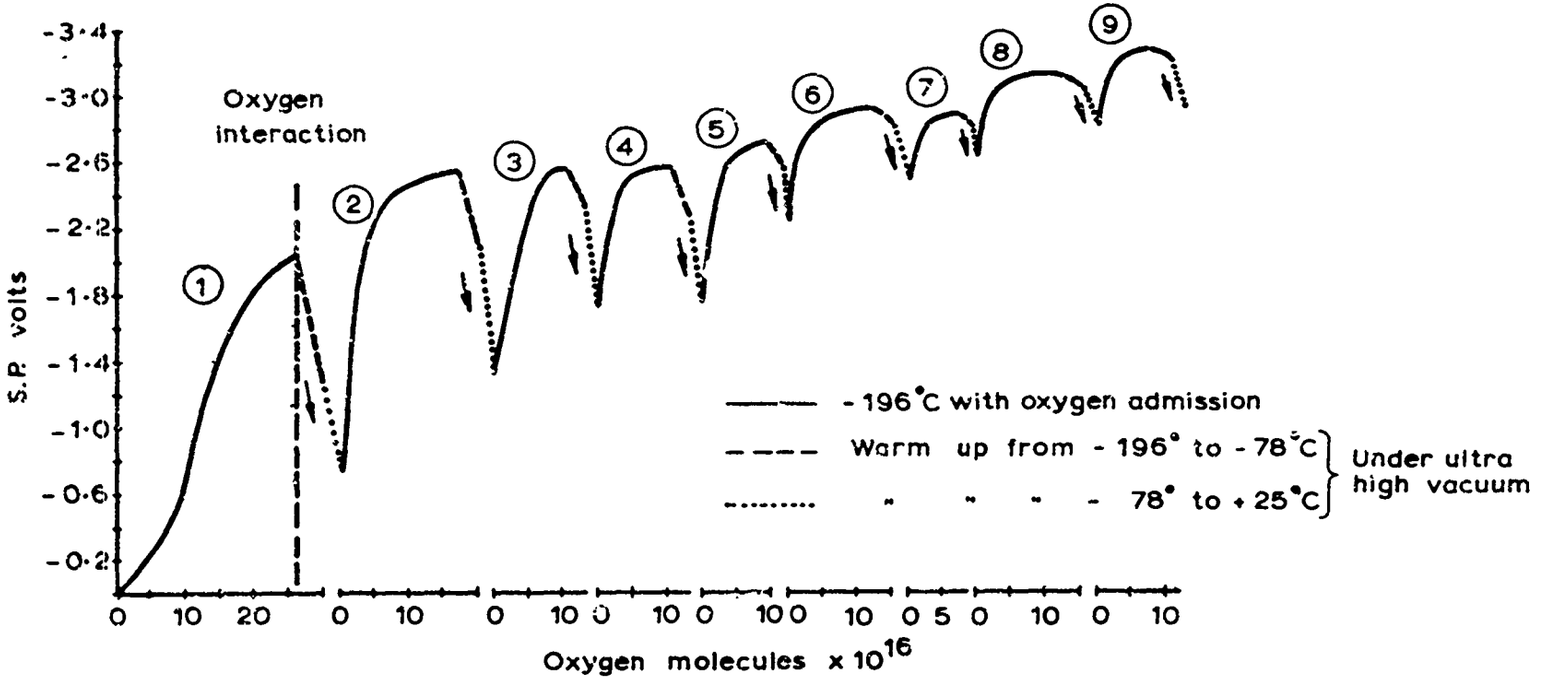

Fig.11 The SP Changes Occurring During Repeated Adsorption of Oxygen on a Chromium Film at -196°C Followed by Warming to -78°C and +25°C. The Numbers on Fig.10 Correspond to Those on Fig.11

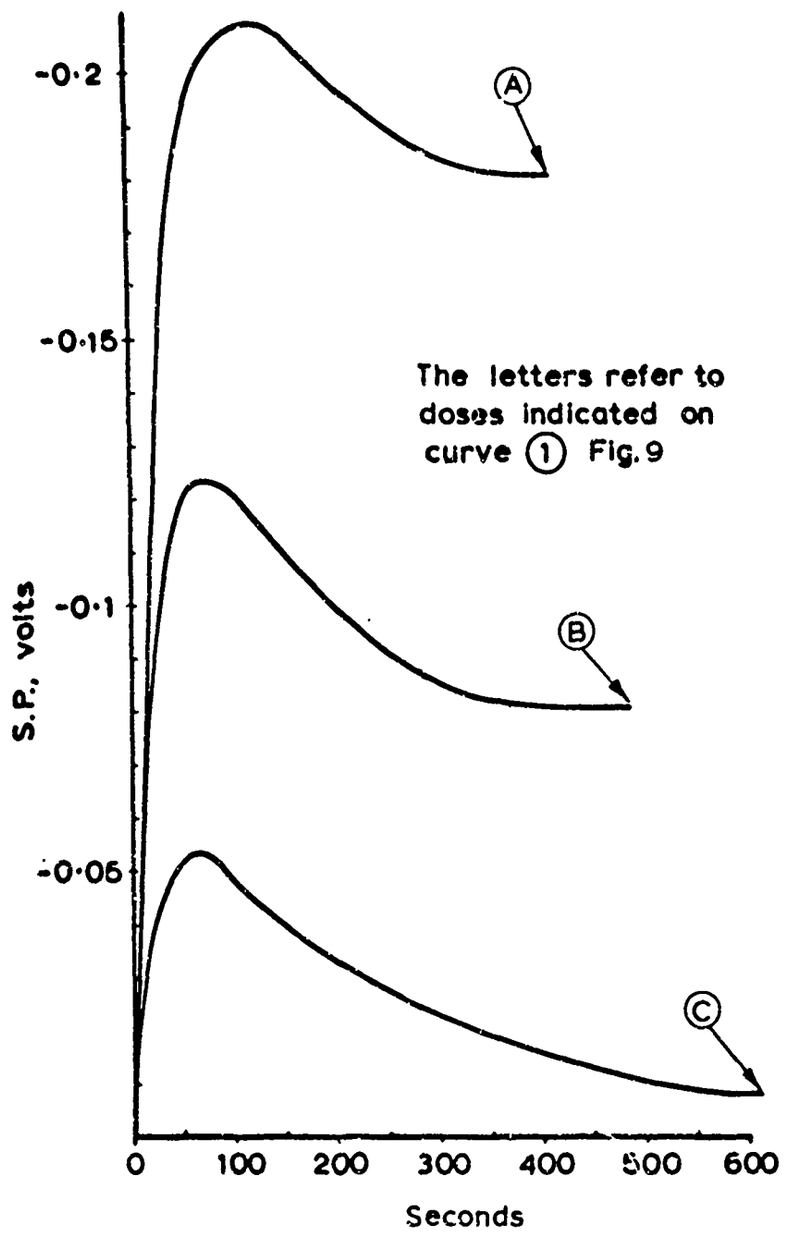

Fig.12 The S.P. Versus Time Traces for the Doses Marked (A) (B) and (C) on Figure (10)

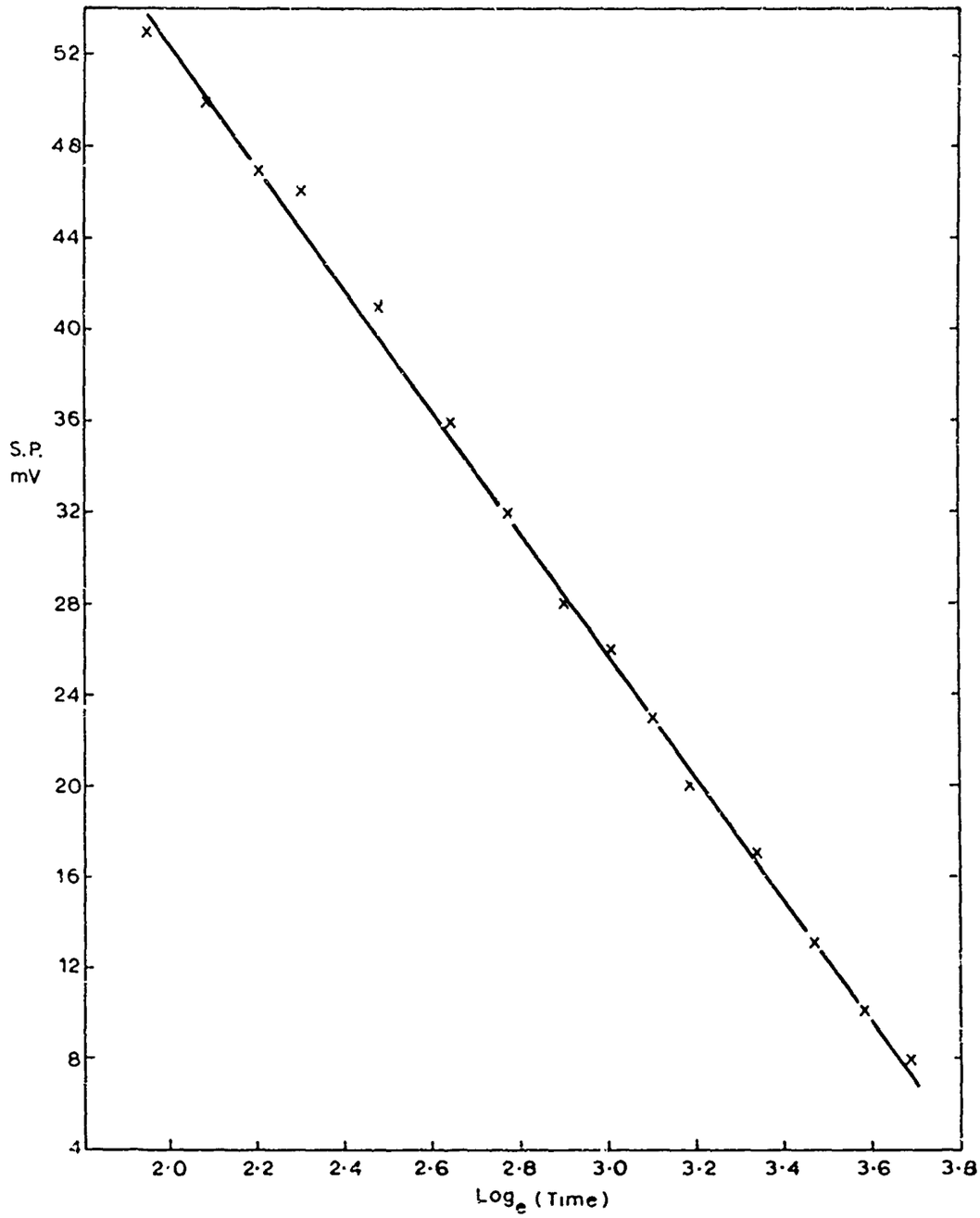

Fig.13 Log (Time) Plot for the Dose Marked C on Fig.12

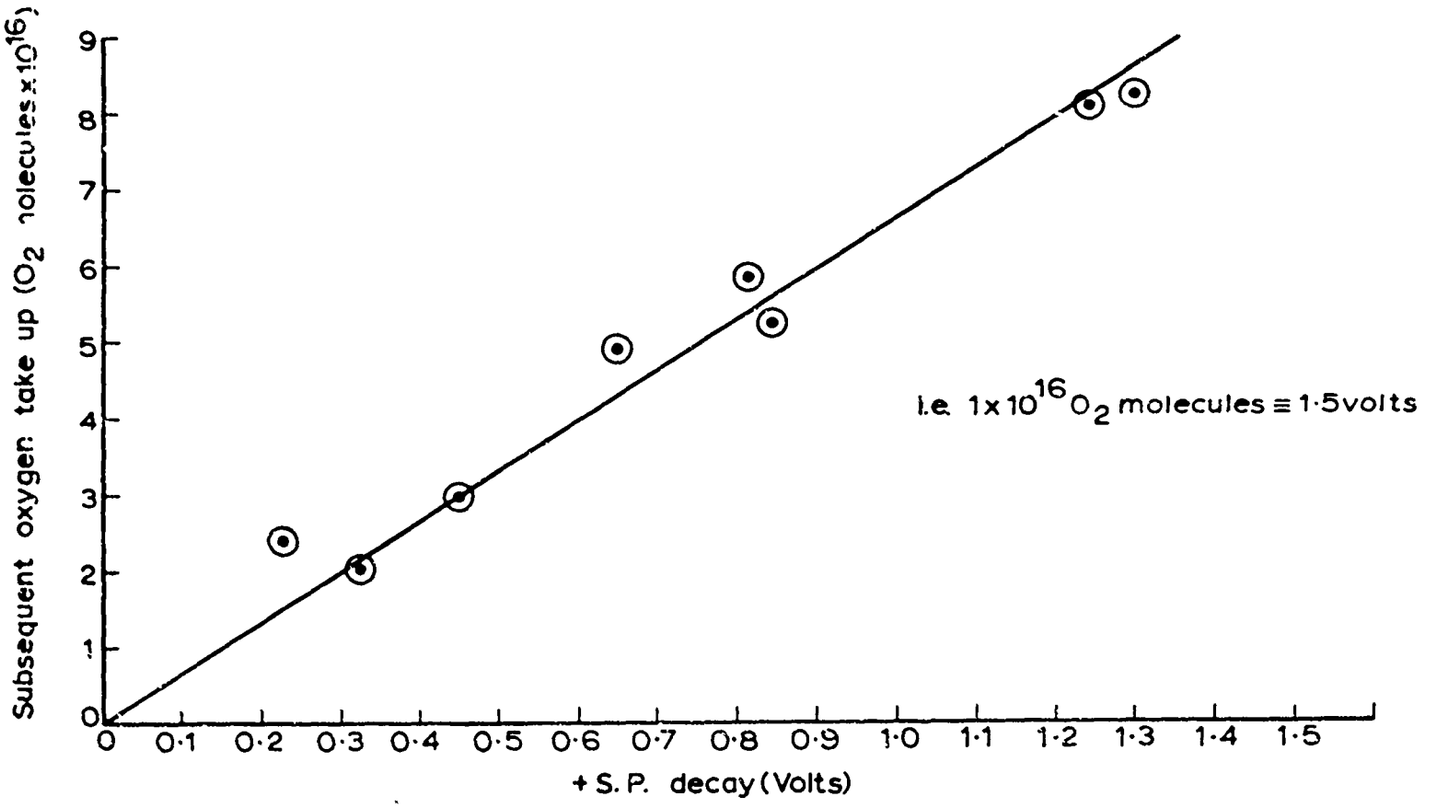

Fig.14 Relationship Between S.P. Change and the Number of Oxygen Atoms Incorporated into the Chromium Lattice (Deduced from Figure. 10.)

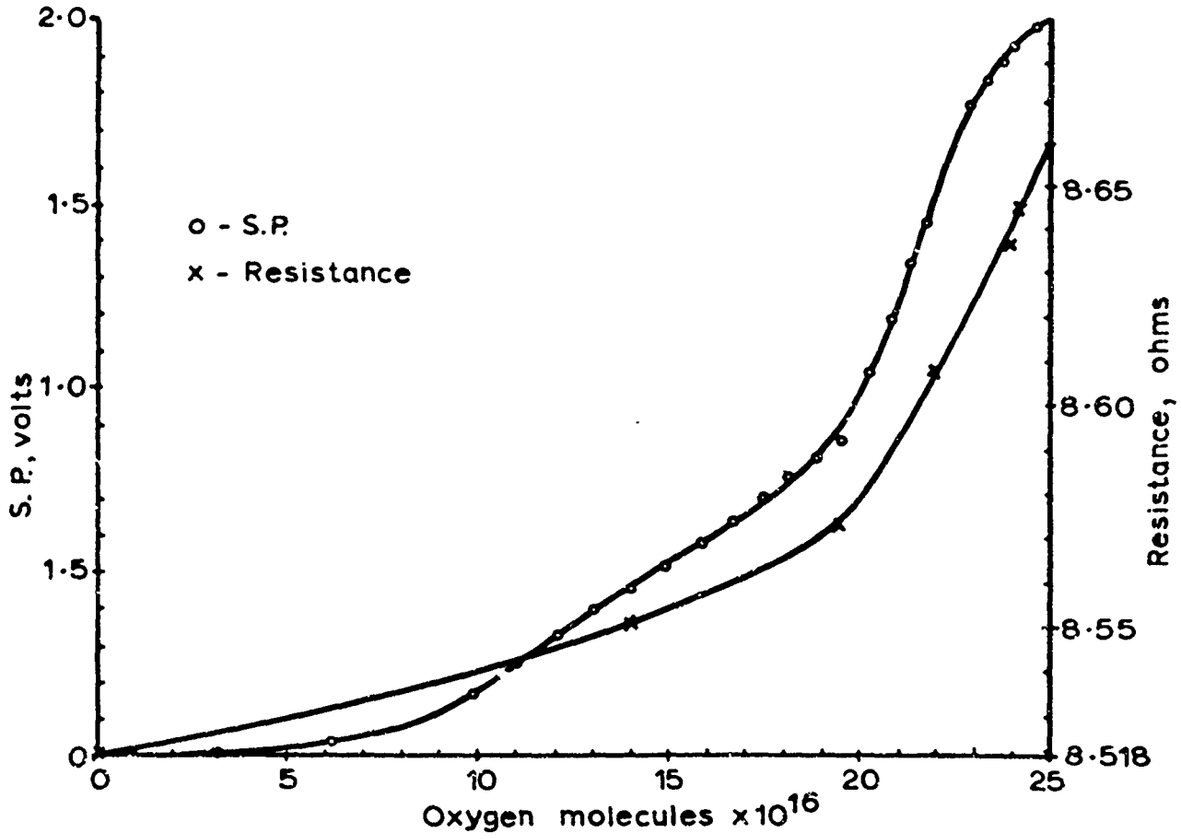

Fig.15. Resistance and S P Changes Occurring During Adsorption and Incorporation of Oxygen on a Chromium Film at -78°C as a Function of the Number of Oxygen Molecules Adsorbed

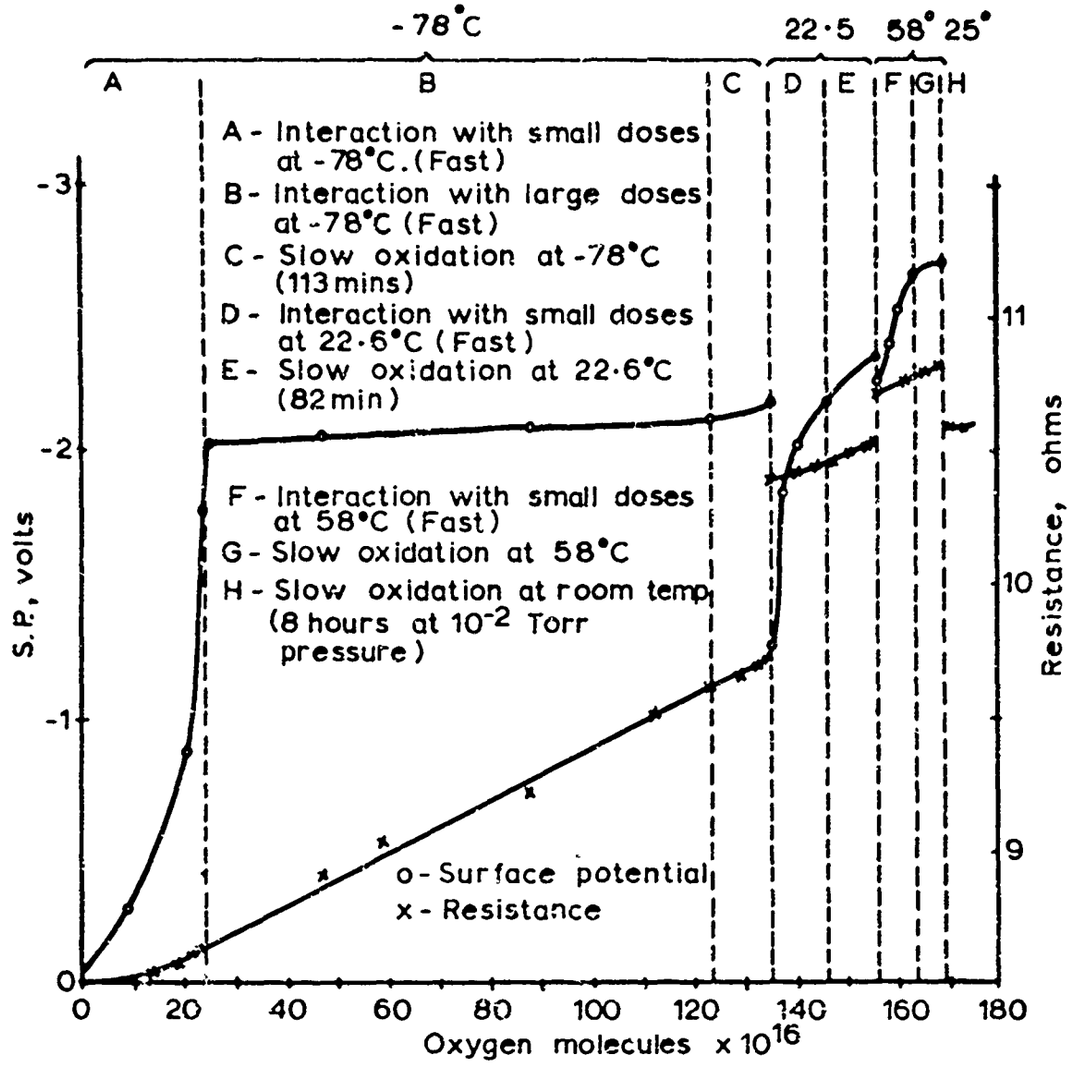

Fig.16 The Resistance and SP Changes Occurring During the Growth of an Oxide Film on Chromium at -78°C. The Effect of Warming to 22·6°C and 58°C when the Limiting Oxide Thickness is Formed are also Shown

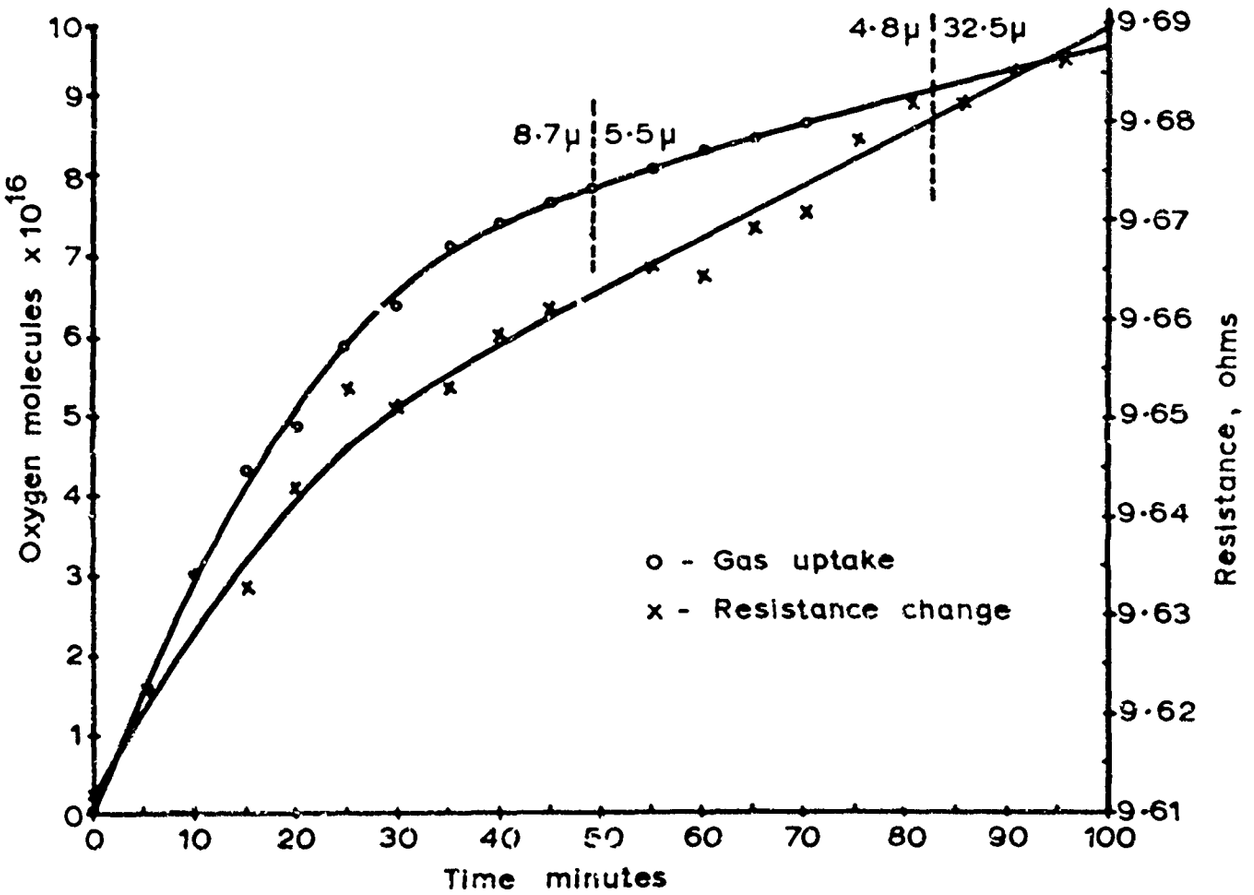

Fig.17 The Slow Uptake of Oxygen on Chromium at -78°C and the Resistance Change Versus Time. Changes of Oxygen Pressure (in microns) are Shown.

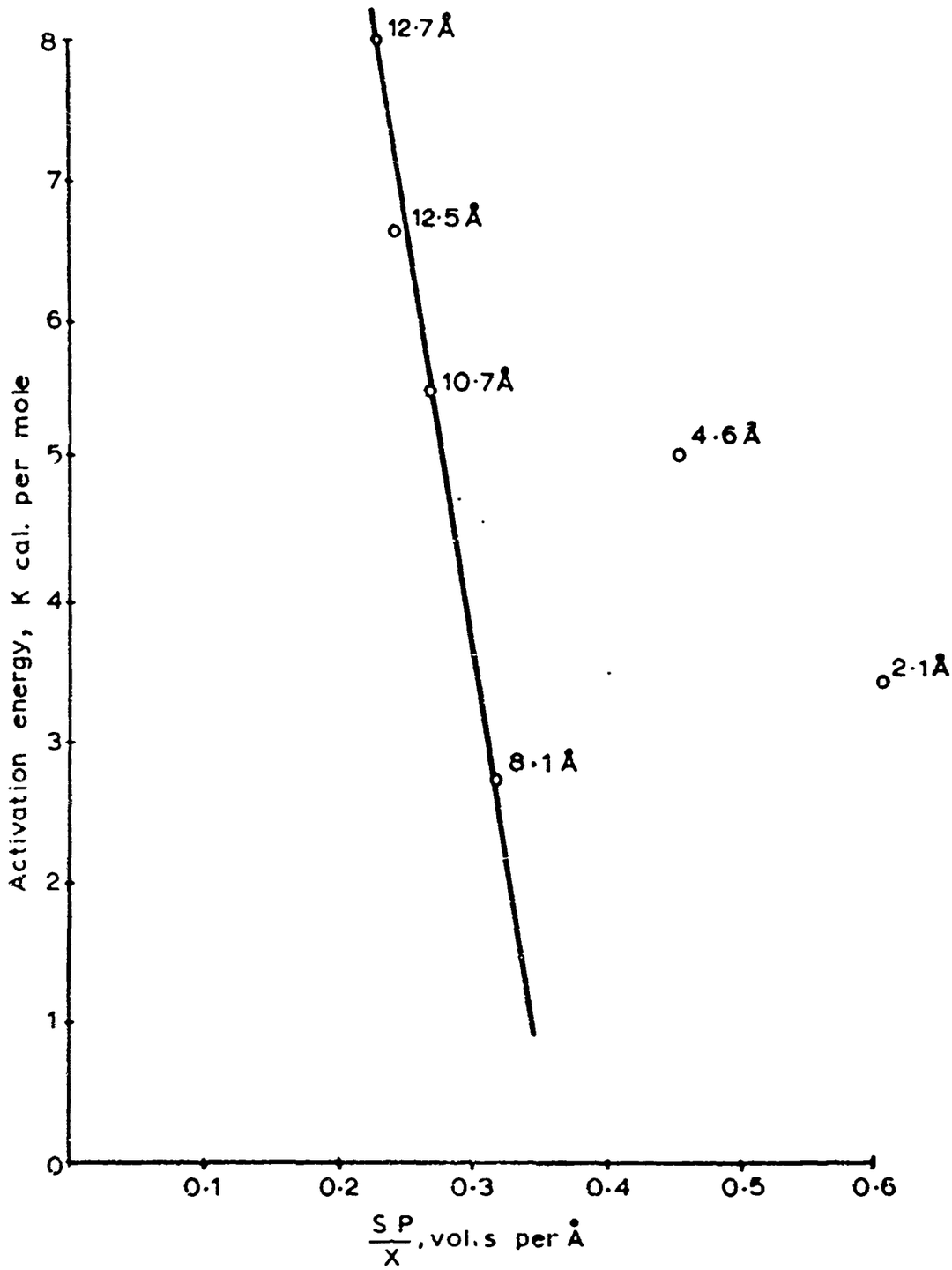

Fig.18 The Dependence of Activation Energy During Oxidation on the Field Across the Oxide as Measured by the Surface Potential Divided by the Oxide Thickness

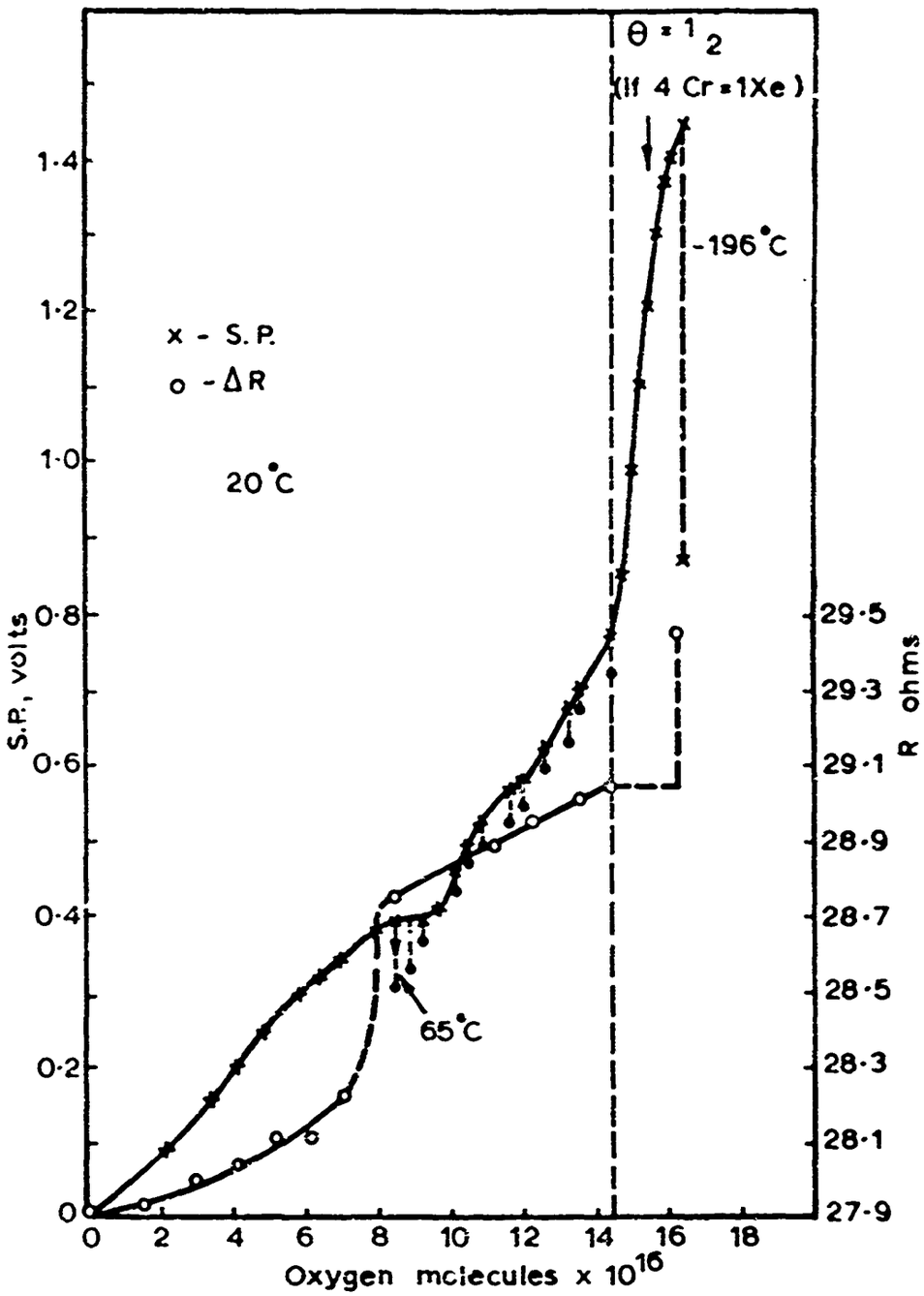

Fig.19. The Surface Potential and Resistance Changes Occurring During Chemisorption and Oxidation on a Chromium Film at Room Temperature and Sub-Monolayer Coverage. The Effects of Warming and Cooling are Shown

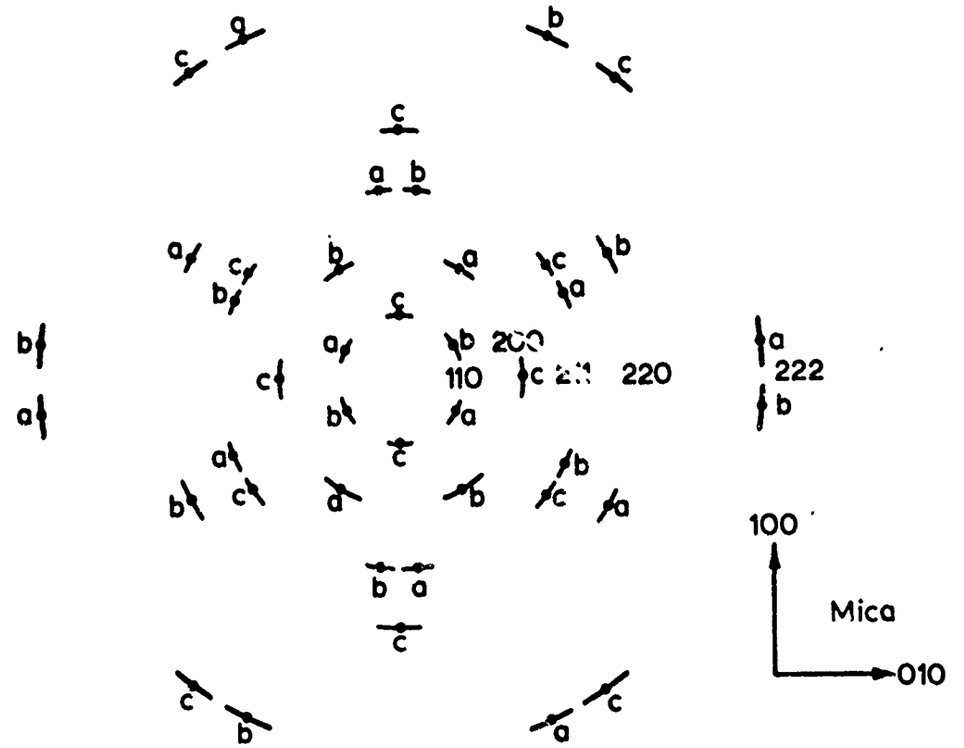

Fig.20. Diffraction Pattern Produced by Three Sets of {110} Nuclei (a,b,c,) at 60°

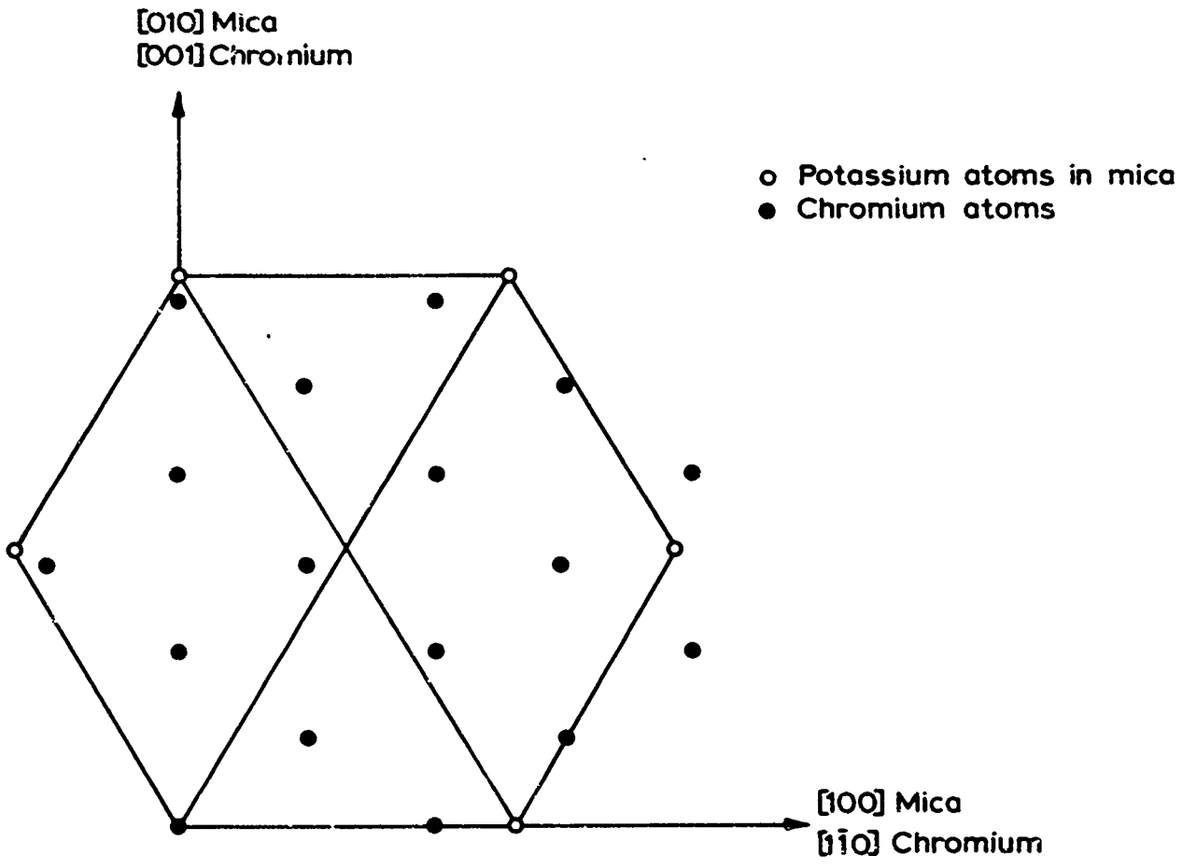

Fig.21. Atom Positions of (110) Chromium on (001) Mica

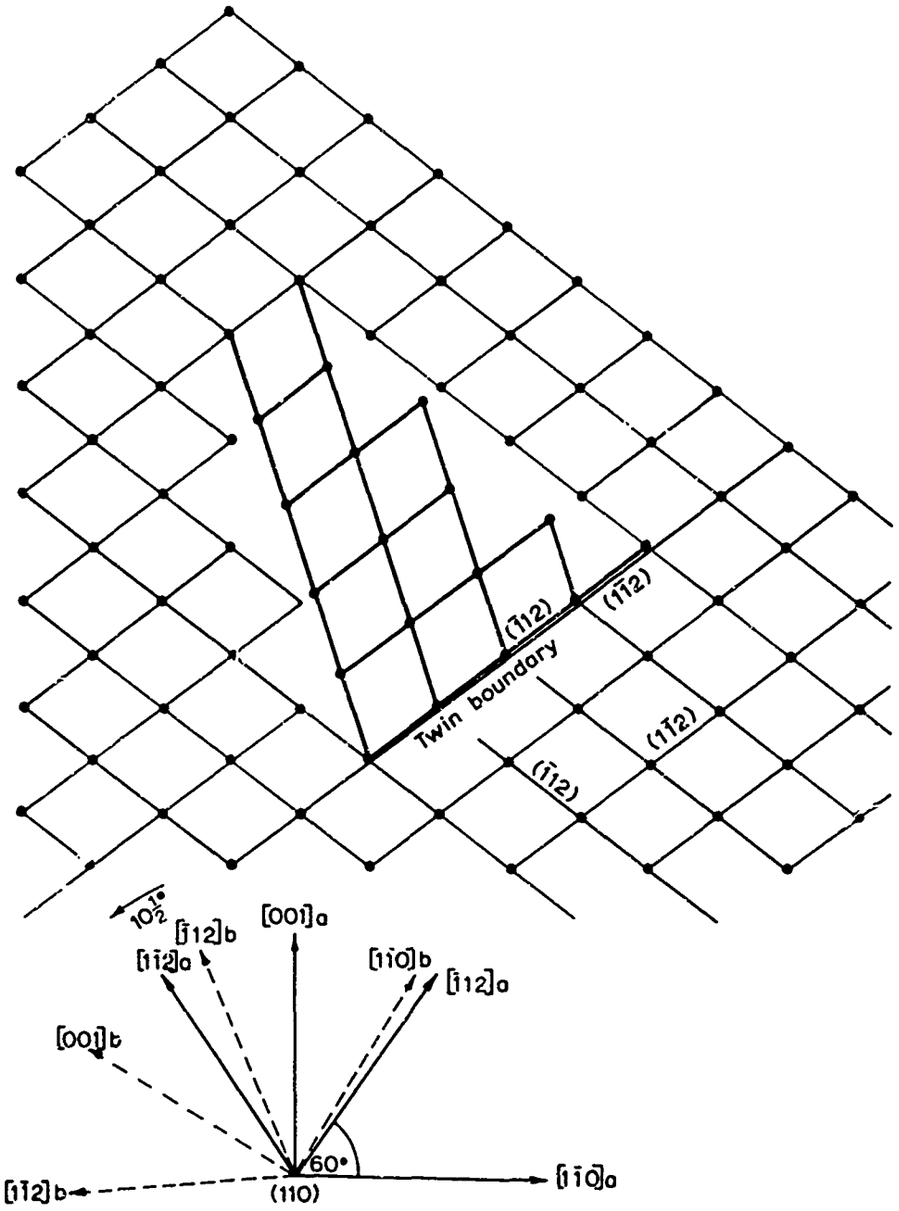

Fig.22. Twin Formation in Two {110} Nuclei (a,b) at 60° by a Total Rotation of $10\frac{1}{2}°$.

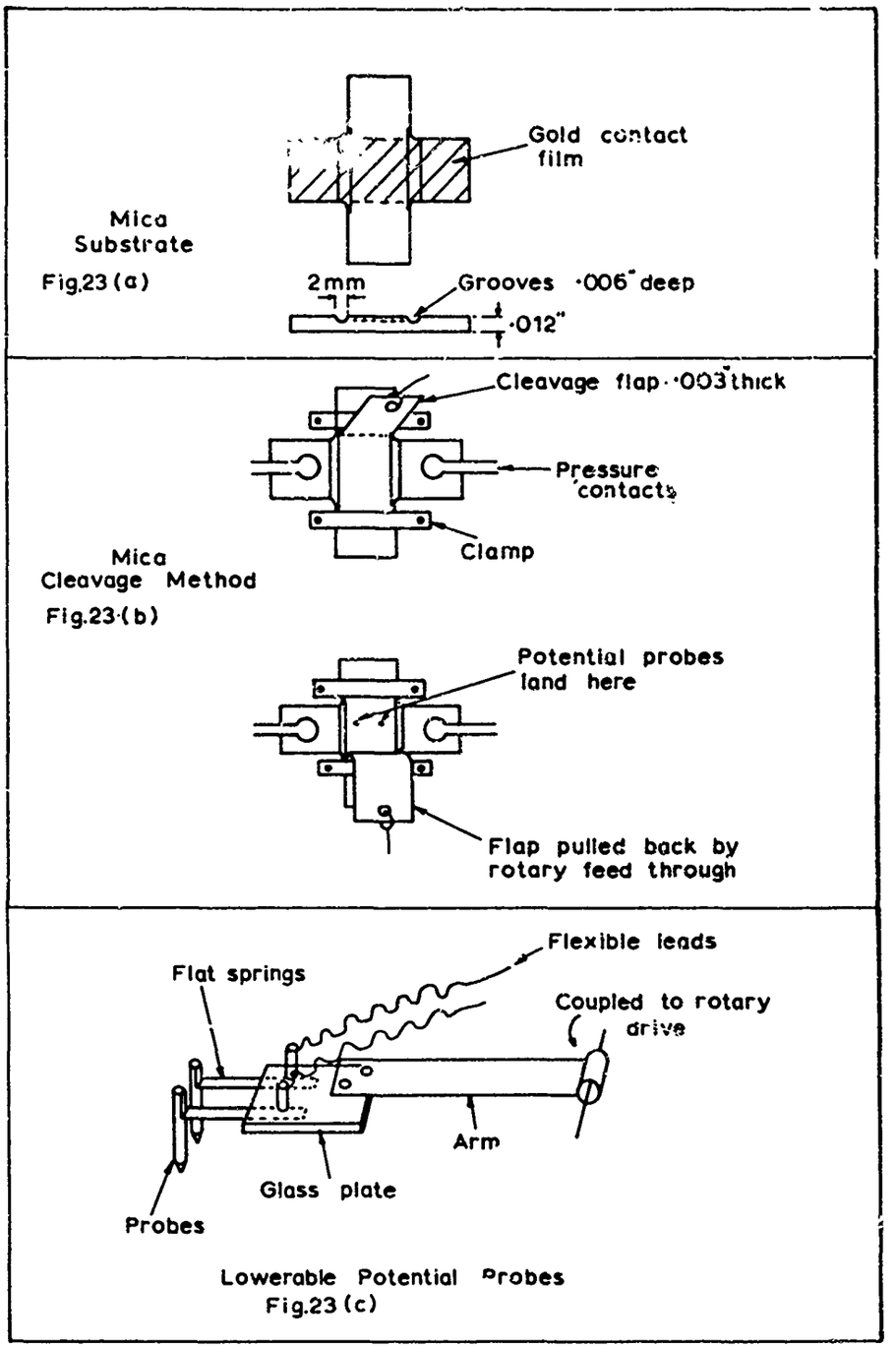
Gold contact film
Mica Substrate
Fig.23 (a)
2mm
Grooves ·006" deep
·012"
Cleavage flap ·003" thick
Pressure contacts
Clamp
Mica Cleavage Method
Fig.23 (b)
Potential probes land here
Flap pulled back by rotary feed through
Flexible leads
Flat springs
Coupled to rotary drive
Arm
Glass plate
Probes
Lowerable Potential Probes
Fig.23 (c)

Fig. 23

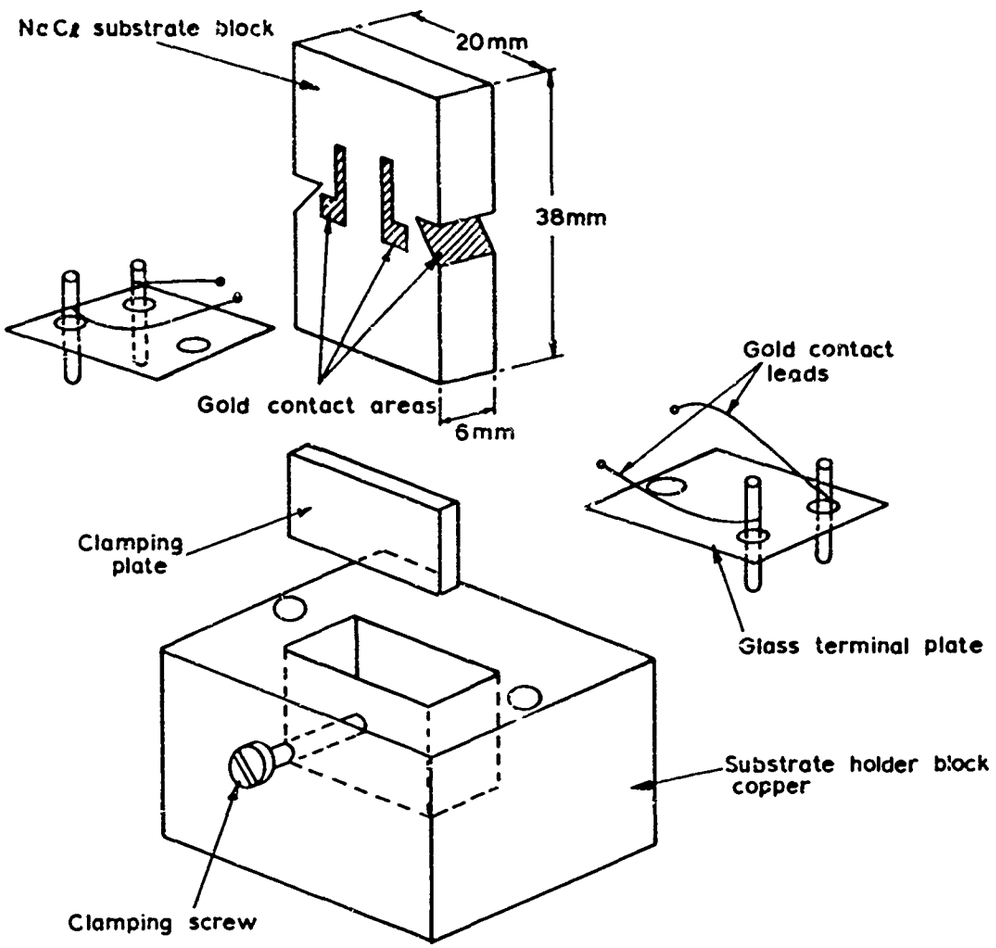

Fig.24. NaCℓ Substrate and Substrate Holder Assembly.

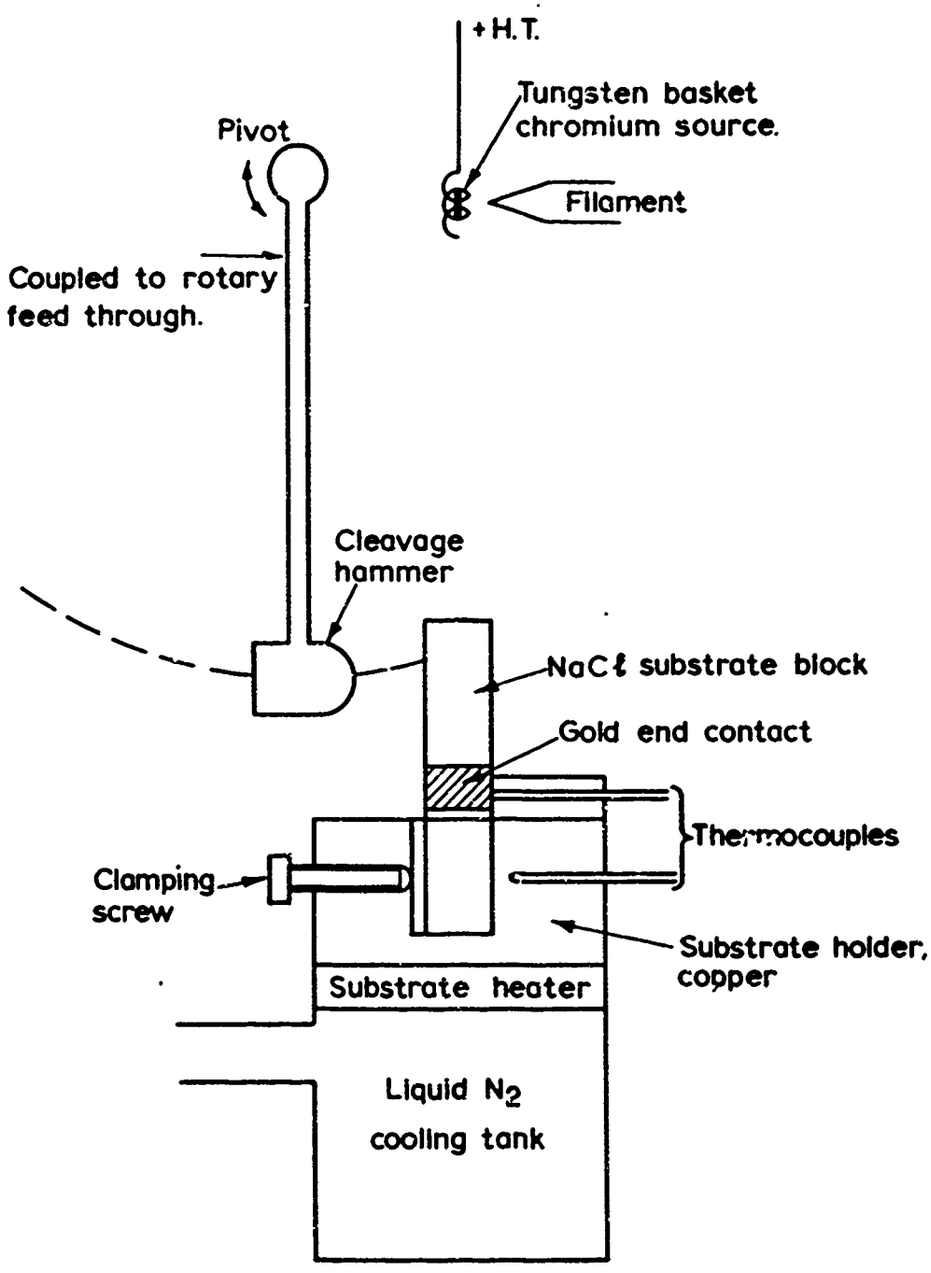

Fig.25. Chromium Deposition onto NaCℓ Substrate Cleaved in Vacuum.

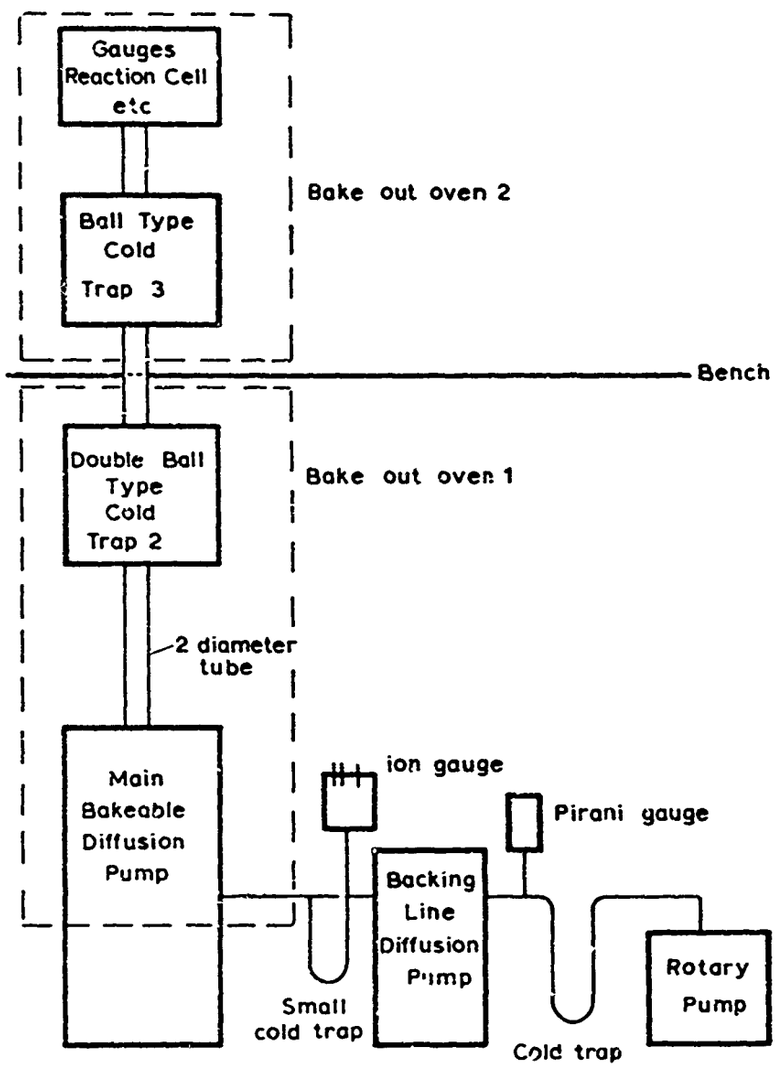

Fig.26. Schematic Dicgram of High Pumping Speed Mercury - Glass u.h.v System for Work Function Measurements on Single Crystal Film Surfaces

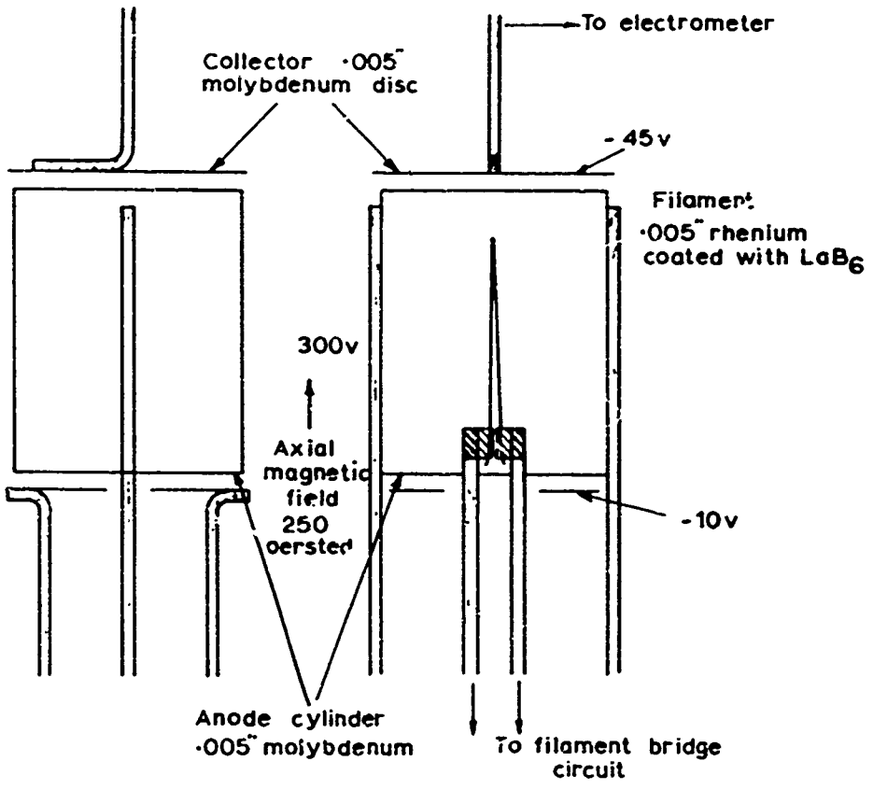

Fig.27. Electrode and Filament Arangement (Front and Side Views) of Hot Cathode Magnetron Gauge

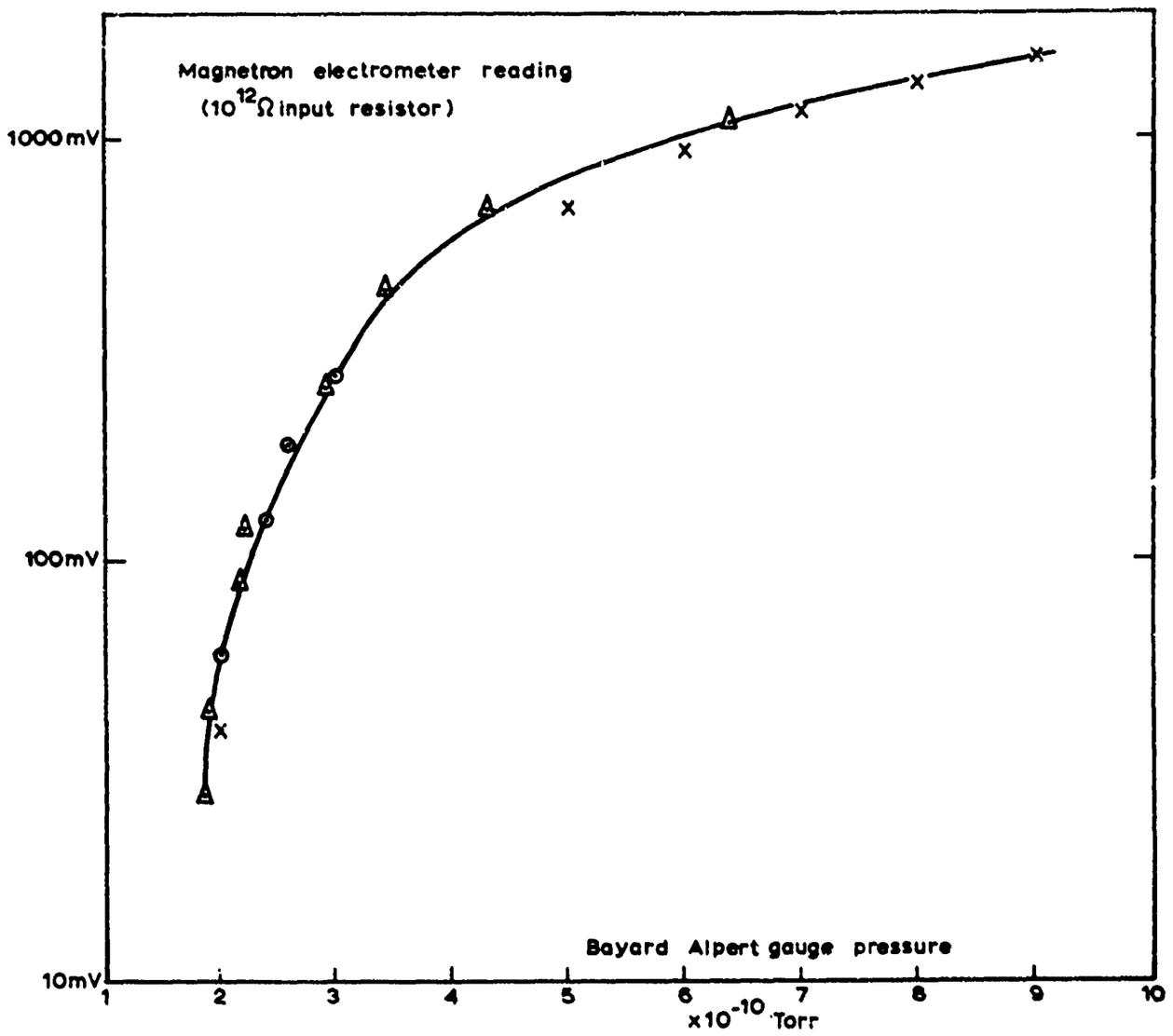

Fig.28 The Calibration of the Hot Cathode Magnetron Gauge Versus a Bayard Alpert Gauge in the 10^{-10} Torr Decade

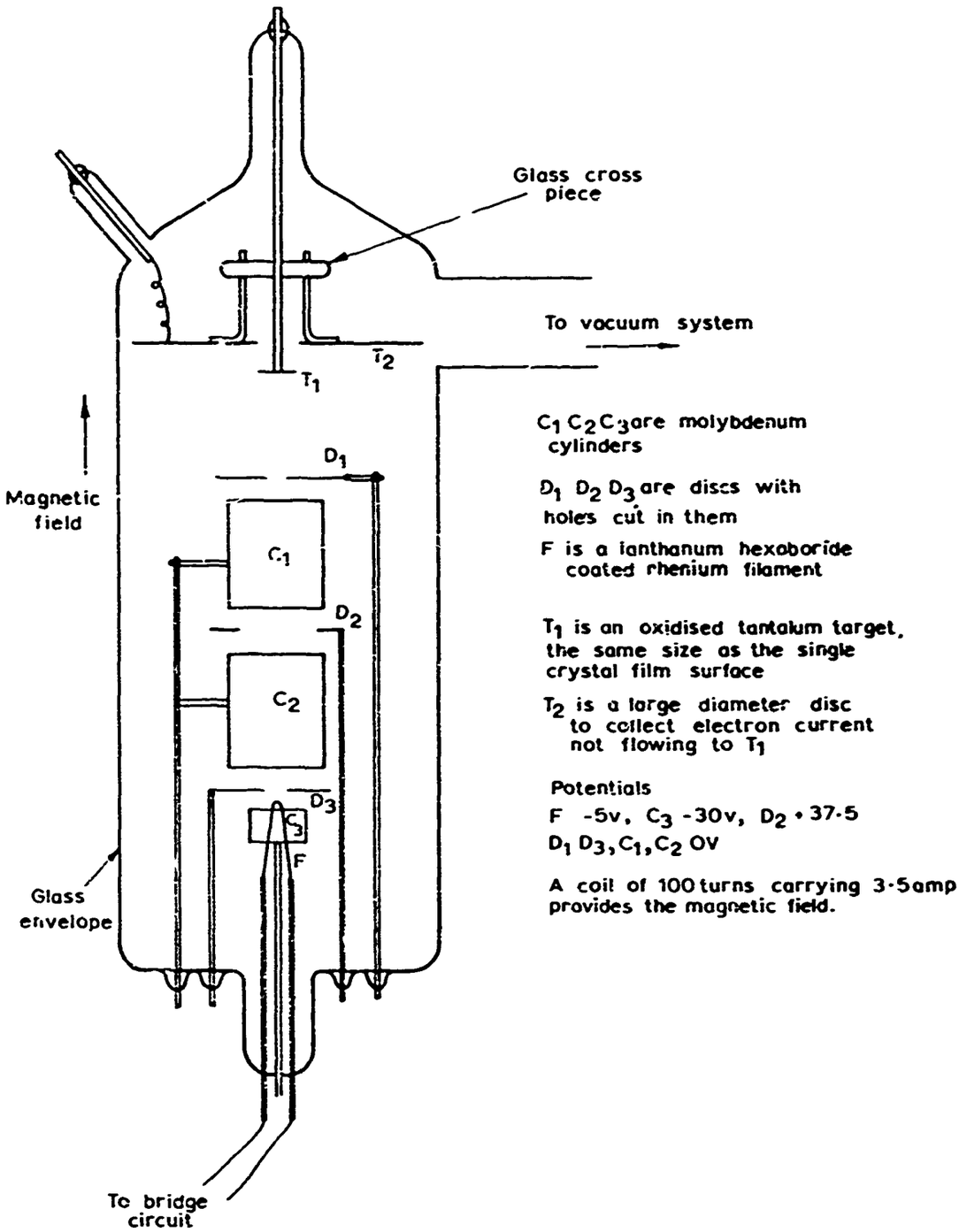

Fig. 29. The Arrangement Used to Test the Slow Electron Gun Diode.

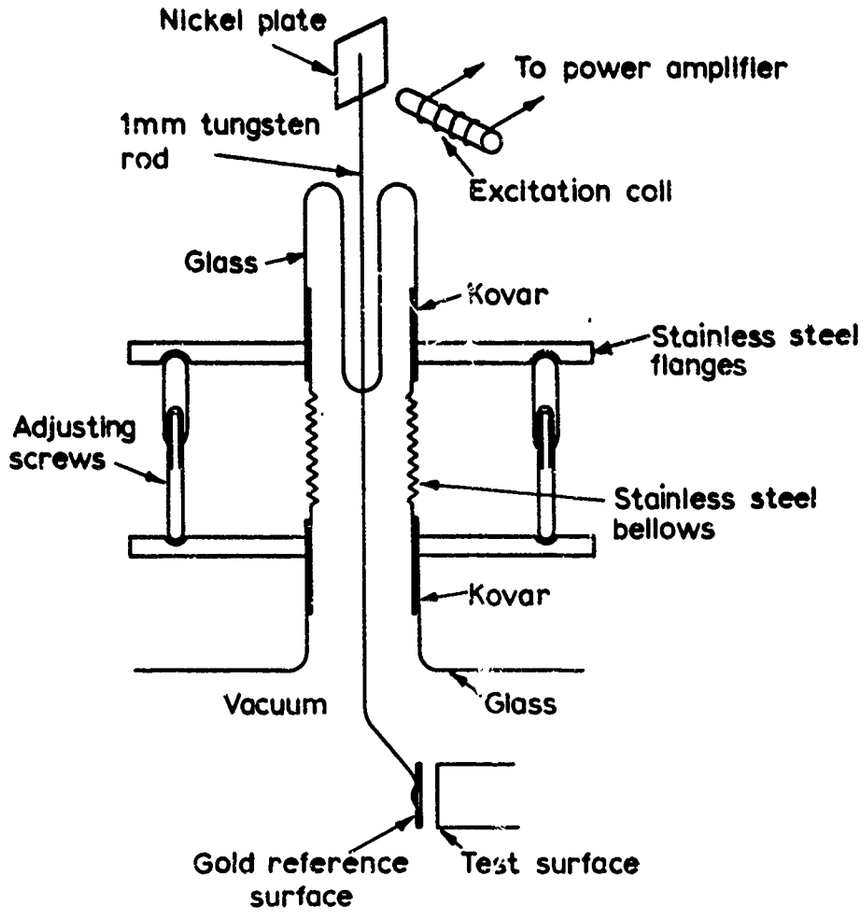

Fig.30. Vibrating Capacitor Test Arrangement.

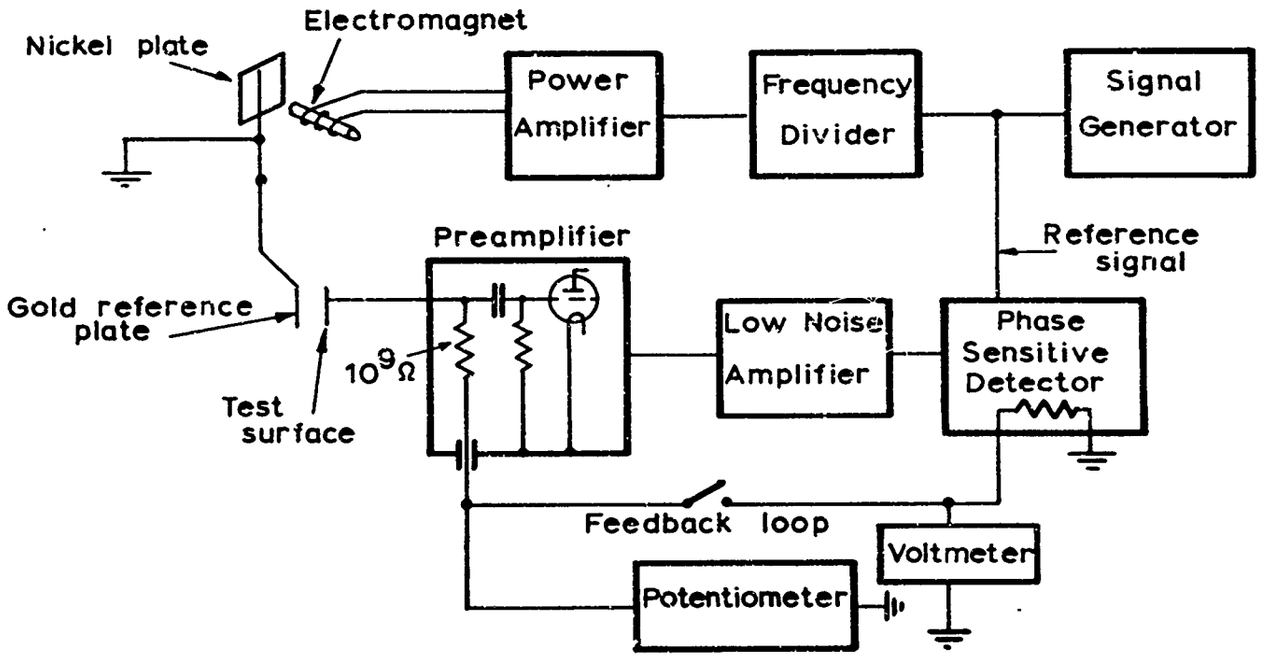

Fig.31. Circuitry Used with Vibrating Capacitor for Work Function Measurements.

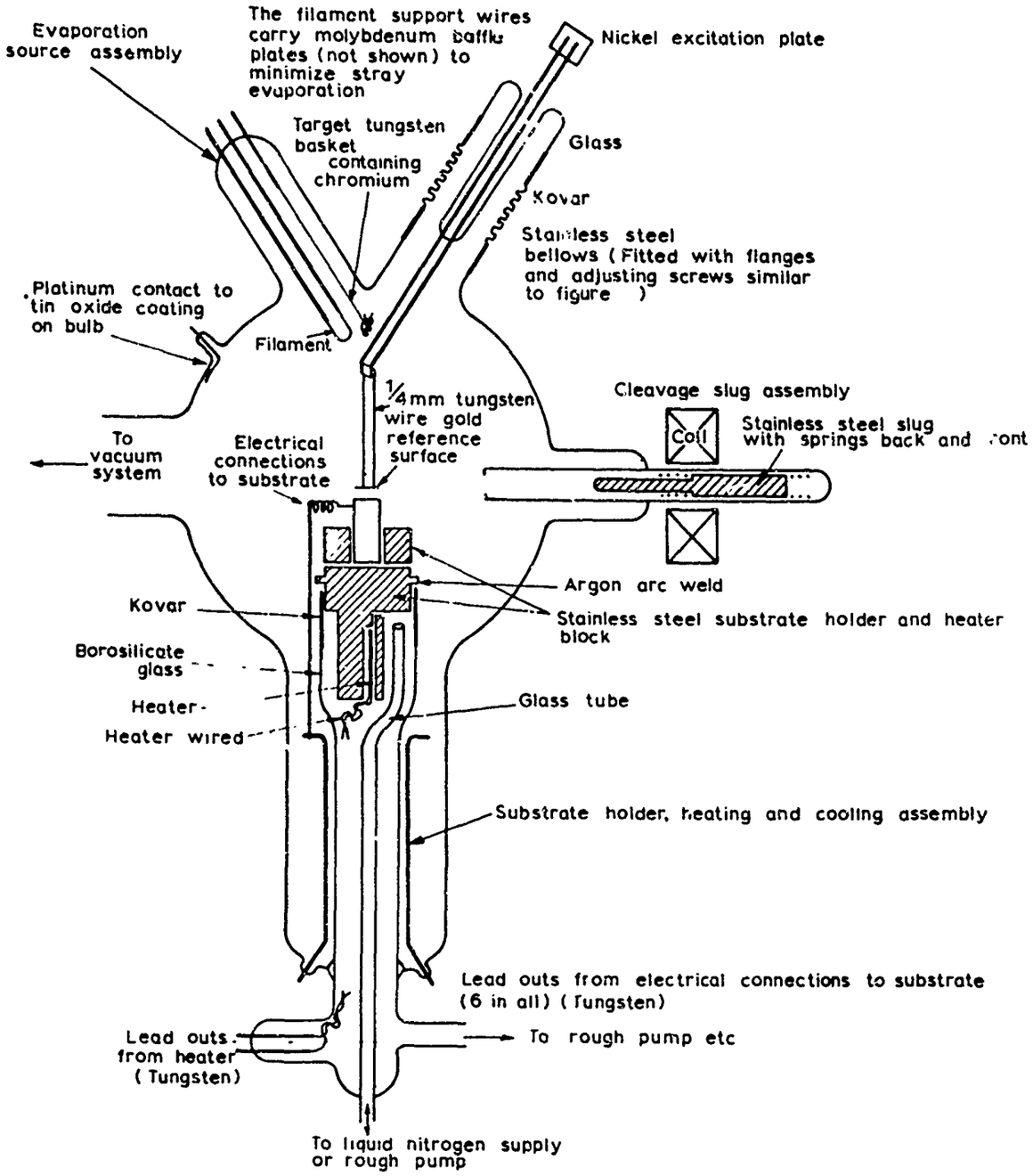

Fig. 32. Sketch to Show Layout of Vibrating Capacitor Reaction Cell for Single Crystal Films

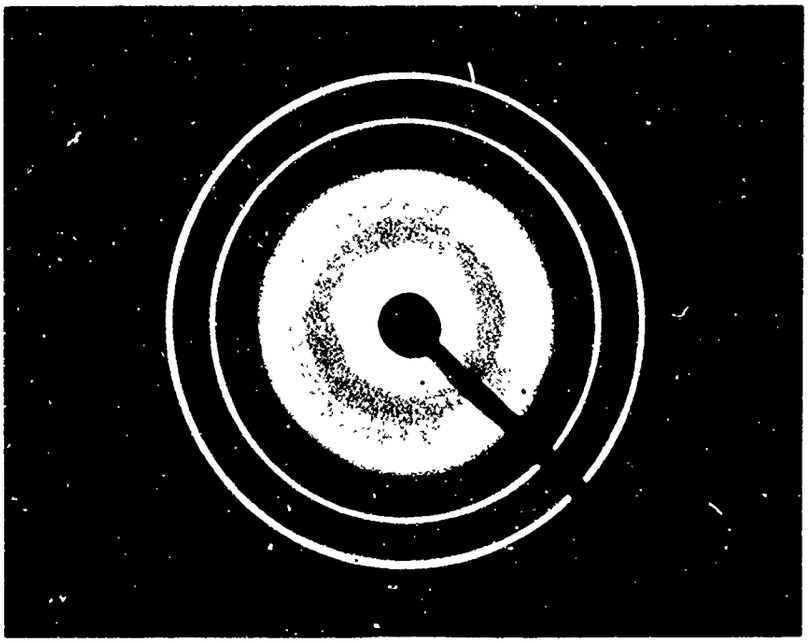

PLATE 1. Diffraction pattern of polycrystalline chromium film deposited on glass

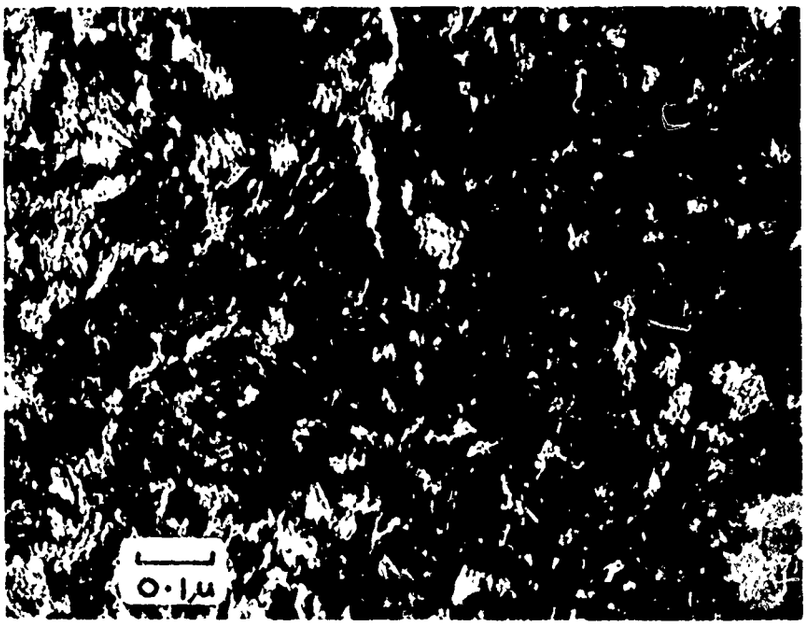

PLATE 2. Micrograph of polycrystalline chromium deposited on glass

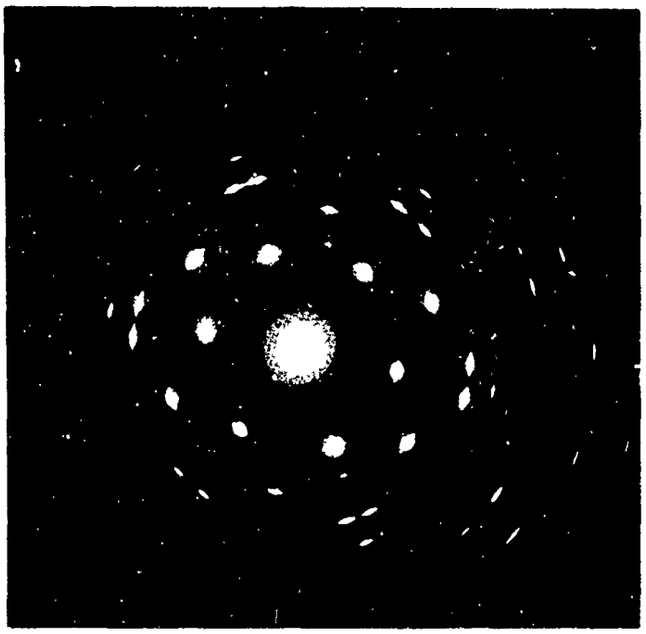

PLATE 3. Diffraction pattern of chromium film deposited on mica (110) orientation.

PLATE 4. Micrograph of chromium deposited on mica showing twin boundaries T.

PLATE 5. Micrograph of chromium deposited on mica showing low angle boundaries L

PLATE 6. Diffraction pattern of chromium deposited on air cleaved NaCl at 10^{-6} torr.

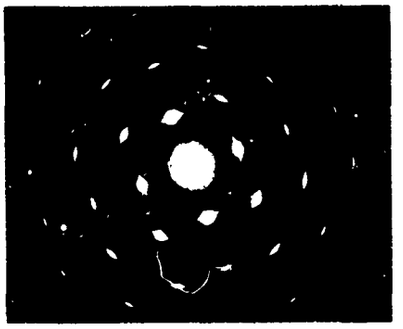

PLATE 7. Diffraction pattern of chromium deposited on vacuum cleaved NaCl at 10^{-6} torr.

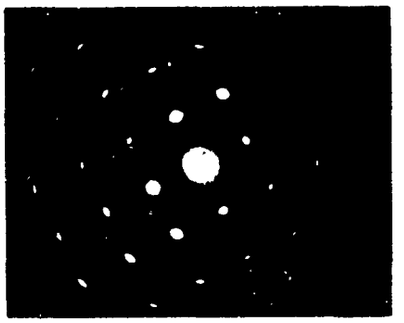

PLATE 8. Diffraction pattern of chromium deposited on air cleaved NaCl that had been heated to 480°C and then cooled to deposition temperature at 10^{-6} torr.

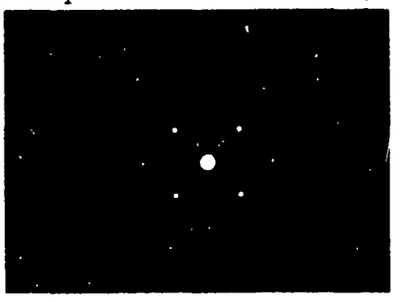

PLATE 9. Diffraction pattern of single crystal chromium film deposited on vacuum cleaved NaCl at 10^{-9} torr (100) orientation

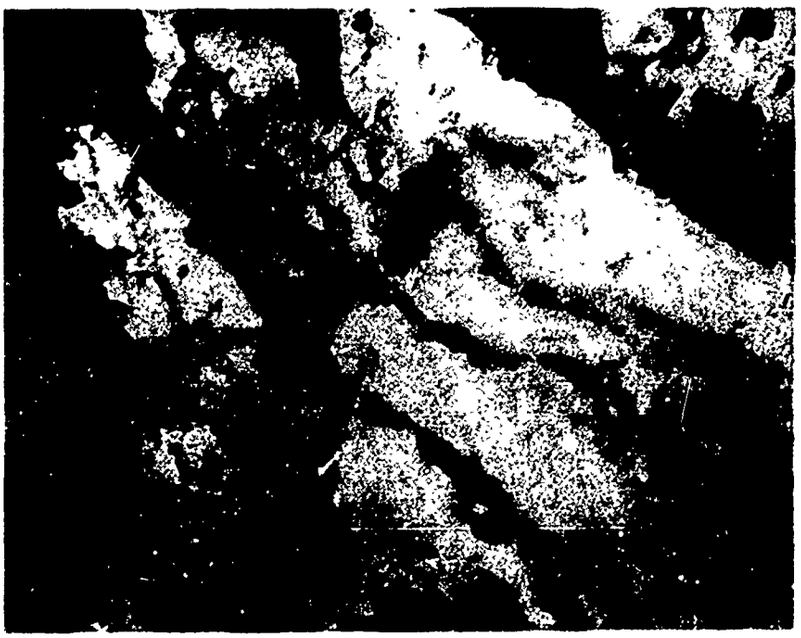

PLATE 10. Micrograph of single crystal chromium film deposited on vacuum cleaved NaCl at 10^{-9} torr.

PLATE 11. Micrograph of single crystal chromium film showing extinction contour pattern.

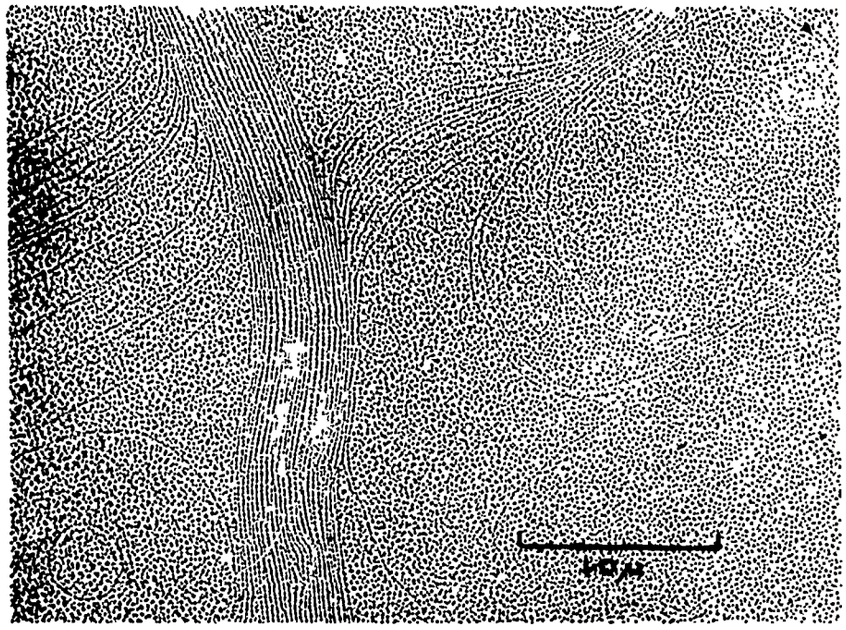

PLATE 12. Gold decoration replica of NaCl surface cleaved in air

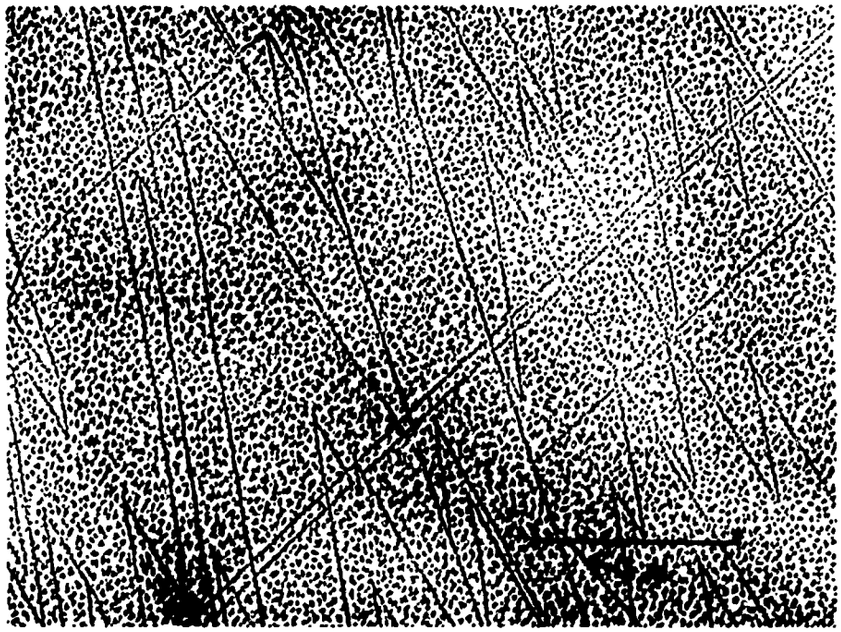

PLATE 13. Gold decoration replica of NaCl surface cleaved in vacuum

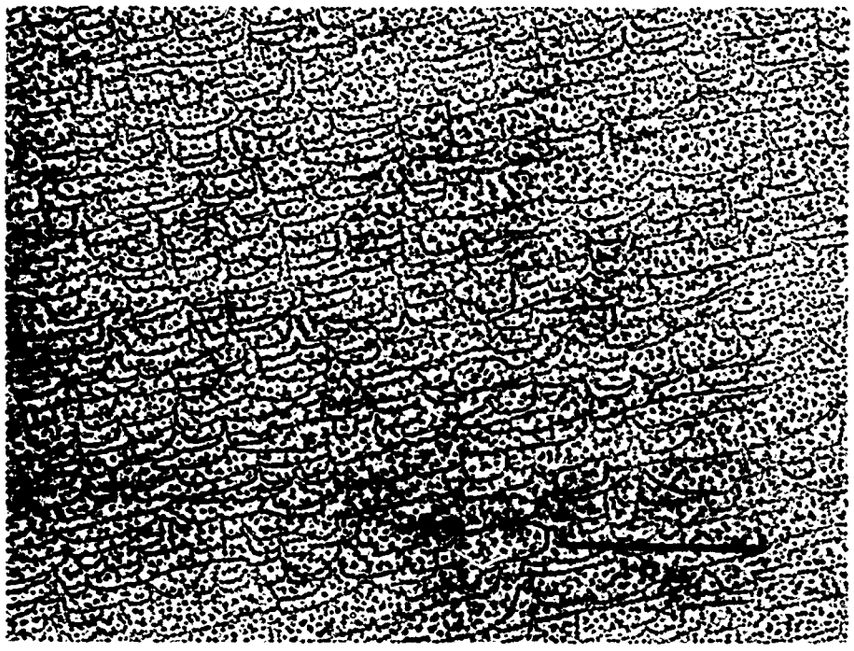

PLATE 14. Gold decoration replica of NaCl surface cleaved in air and heated to 480°C.

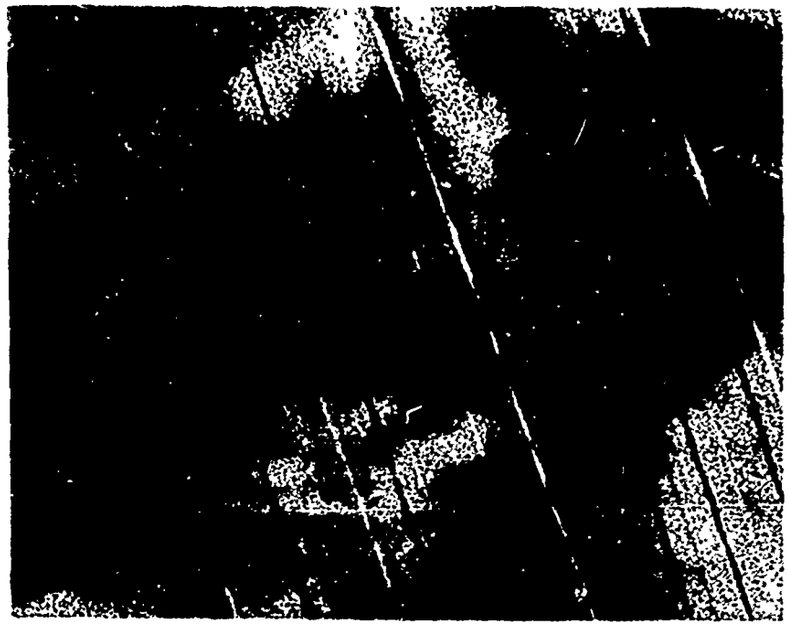

PLATE 15. Gold-palladium 45° shadow replica of typical NaCl cleavage surface.

PLATE 16. Typical NaCl cleavage steps revealed by polarization interferometry. One fringe displacement corresponds to 0.3μ height difference.

Unclassified

Security Classification

DOCUMENT CONTROL DATA - R&D

(Security classification of title, body of abstract and indexing annotation must be entered when the overall report is classified)

1 ORIGINATING ACTIVITY (Corporate author)	2a REPORT SECURITY CLASSIFICATION
Standard Telecommunication Laboratories, Harlow, Essex, England.	Unclassified
	2b GROUP

3 REPORT TITLE

Physics of Ageing in Thin Film Resistors : Oxidation of Clean Chromium Films

4 DESCRIPTIVE NOTES *(Type of report and inclusive dates)*

Final Scientific Report, February 1966 - January 1967

5 AUTHOR(S) *(Last name, first name, initial)*

Crossland, William A.
Marr, Collin A.
Roettgers, H. Theo

6 REPORT DATE	7a TOTAL NO OF PAGES	7b NO OF REFS
28th February 1967	148	53

8a CONTRACT OR GRANT NO.	9a ORIGINATOR'S REPORT NUMBER(S)
AF(052)-923	TM No.592
b PROJECT NO 1040	
c	9b OTHER REPORT NO(S) *(Any other numbers that may be assigned this report)*
d	

10 AVAILABILITY/LIMITATION NOTICES

The distribution of this document is unlimited

11 SUPPLEMENTARY NOTES	12. SPONSORING MILITARY ACTIVITY
	Rome Air Development Centre (EMERP) Griffiss Air Force Base, New York 13440

13 ABSTRACT

An attempt has been made to study the oxidation of thin film resistors and its impact on the electrical film properties as an isolated process. Polycrystalline and single crystal chromium films were deposited under extremely clean conditions thus leaving mainly the various gas-metal interactions as possible degradation process.

Simultaneous measurements of resistance and surface potential as functions of oxygen uptake from atomically clean polycrystalline films upto 20Å oxide thickness distinguished between the individual oxidation stages, and it was found that the kinetics of incorporation is consistent with the surface potential and the surface structure to be rate controlling. At oxides thicker than 6Å the oxidation is governed by the Mott-Cabrera mechanism over the temperature range from below -78°C to higher than +50°C. The oxidation appears to affect the resistance merely by the reduction of the cross section of the conductive path, the effective thickness being much less than the measured mass thickness.

Single crystal chromium films without detectable grain boundaries over the substrate area have been prepared on vacuum cleaved rocksalt. A reliable contacting technique has been developed and the rocksalt surface fine structure found to be compatible with meaningful electrical measurements. Preliminary measurements showed the TCR to be equal to the bulk value above room temperature.

Equipment for simultaneous surface potential and resistance measurements during oxidation of single crystal films has been designed and constructed.

DD FORM 1 JAN 64 1473

Security Classification